Università degli Studi di Napoli Federico II
Ph.D. Program in Industrial Products and Process Engineering
XXXVIII Cycle

THESIS FOR THE DEGREE OF DOCTOR OF PHILOSOPHY

CHRISTOS PSEVDOS

Effect of Chain Grafting on the Dispersion State of Polymer Nanocomposites

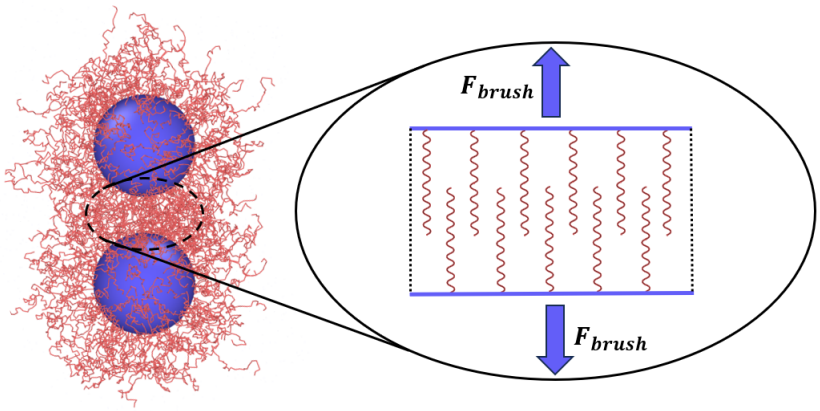

Scuola Politecnica e delle Scienze di Base
Dipartimento di Ingegneria Chimica, dei Materiali e della Produzione Industriale

Effect of Chain Grafting on the Dispersion State of Polymer Nanocomposites

Ph.D. Thesis presented
for the fulfillment of the Degree of Doctor of Philosophy
in Industrial Products and Process Engineering
by

Christos Psevdos

Approved as to style and content by

Advisors: Prof. Giovanni Ianniruberto

Co-advisors: Prof. Emeritus Giuseppe Marrucci

Università degli Studi di Napoli Federico II
Ph.D. Program in Industrial Products and Process Engineering
XXXVIII cycle - Chairman: Prof. Andrea D'Anna

Candidate's declaration

I hereby declare that this thesis submitted to obtain the academic degree of Philosophiæ Doctor (Ph.D.) in Industrial Products and Process Engineering is my own unaided work, that I have not used other than the sources indicated, and that all direct and indirect sources are acknowledged as references.
Parts of this dissertation have been published in international journals and/or conference articles (see list of the author's publications at the end of the thesis).

Napoli, December 8, 2025

_____

Christos Psevdos

Abstract

Polymer brushes alter the interactions between grafted surfaces, typically promoting repulsion through osmosis and excluded volume of the grafted chains. An exceptional case is that of brushes in a chemically identical polymeric matrix of equal or higher molecular weight and at relatively high grafting densities. Using a newly developed coarse-grained molecular dynamics methodolgy we present for the first time proof of the existence of attraction between flat brushes. The onset of favorable interbrush interactions are connected to the formation of a well defined brush-matrix interface due to autophobic dewetting. These insights are then used to capture the mesoscopic filler structure of polymer nanocomposites with grafted nanoparticles. Simulations are performed where the change in interparticle interactions due to grafting are accounted for implicitly by tuning a single-parameter pairwise hard-core potential. The desired morphology can only be obtained by setting up the particles in small rigid aggregates that represent their post-mixing configurations which act as the building blocks of larger agglomerates. Finally, the effect of grafting density on aggregate size during mixing is studied through simulation of opposing flat brushes under shear, showing a monotonic increase in shear stresses with grafting density that should aid in aggregate breakup.

Keywords: polymer nanocomposites, grafting, polymer brush, molecular dynamics, autophobic dewetting

AVGVSTVS FRIDERICVS ROMANORVM IMPERATOR SEMPER

Contents

Acknowledgements

As I'm beginning to write this I cannot help but think first of the people who made part of this work that represents my 3 years as a PhD student. At the top of the list there is none else but my supervisor Giovanni, who placed his trust in me and accepted me as his student even though I probably wasn't the ideal candidate for the position (foreshadowing!). From that point on he has always been following me closely, providing valuable help on both academic and extracurricular matters, his reassuring presence helping alleviate the inevitable stress that comes with the pursuit of the title of Doctor of Philosophy. It has also been a great pleasure having the chance to interact with Pino Marrucci, who frequently joined in our discussions and always managed to surprise us with his vast knowledge of the field, clarity of thought and fresh ideas. Coming from the industrial side, Christian has been following the project from the sidelines giving just the right "pushes" that helped shape the scope of this work towards an objective of practical interest without making discounts on the scientific rigor. During the course of this period I naturally had the chance to meet, discuss and work with many other researchers to whom I am grateful and I hope that they will recognize a small piece of themselves in this manuscript without me having to nominate them all. I would however like to make a special mention at Guilhem Baeza, who I was fortunate enough to meet during his sabbatical year in our department. Life had it that he had done his doctoral thesis on a closely — way too closely — related topic and now there he was, stationed at my department during the first year of my PhD with lots of time and willingness to explain. Can't complain. Last but not least, I couldn't not thank my colleagues, the ones who made everyday university life something to look forward to even when things seemed to not be going as planned. They know who they are.

Having said the above, it's time to finally move away from the work environment – for better or worse the PhD journey also takes up a significant space of the "life" part in the so-called "work-life balance". It can all start with a question that many people, especially Neapolitans, make when first meeting me: Why on earth did you choose Napoli? The story goes more or less like this: It is summer of 2022 and the world is still recovering from the collective shock of

COVID-19 but I am more concerned about what I am going to do after having interrupted a PhD course at the University of Patras, a city not too far from my hometown of Athens. I had been there for the last 2 years, working on a PhD project that I started just days after I finished my degree and things are not going well right from the start. Nevertheless, it only takes me 2 years to finally accept that sometimes it is okay to give up and I do just that. It is now my turn to leave behind academic research and get a "real" job, even though I have no serious motivation to do so. In fact, my motivation is so low that friends and (now ex-) colleagues cannot help but notice. Among them are Giancarlo and Antonio, the two first Neapolitans I ever met. We first became friends and passed time together in Patras, where they stayed for academic purposes. They were the ones to plant the idea of giving myself another chance and brought me in contact with professors of their department. While the rest is history, I cannot understate the support I received during that period from my friends, sisters and my then long-time partner Dioni, all of whom helped me regain my confidence and convinced me of being capable to take this second shot at glory. Support that continued after my departure for Napoli and goes on until today, even from my parents who were initially opposed to this endeavor. I think they still are, but you don't get to choose your son I guess.

Lastly, it would be a huge omission on my part to not dedicate a few words to the city that is currently hosting me and the people I met here (is there any difference?). Admittedly it was a rough beginning, language barrier and all, but I never felt or was made to feel like a passerby. In this new home I am not simply the n^{th} (in a typical italo-mathematical way of speaking) abroad student marked by the expiration date of his graduation. I *share* my life with my friends here and maybe they are the ones who taught me a bit more about that word. All the recognition I gave to my dearest ones from Greece also goes out to them.

List of Figures

Introduction

The second half of the 20^{th} century was marked by rapid advances in the development of polymeric materials, who went on to assume an irreplaceable role in modern industry. The combination of low density and ease of processing while retaining their durability, renders polymers perfect candidate materials for a wide range of applications. However, despite their well rounded set of properties, they may still lag behind when it comes to more specialized use cases where other materials, e.g. metals and ceramics, prevail due to their excellent mechanical and/or thermal properties. In the constant race of developing materials suitable for such applications that will simultaneously retain the generally low cost and high processability of polymers, engineers have experimented with diverse molecular chemistries and architectures as well as blends. It is this exploration that gave rise to the *polymer composites* (PCs), materials consisting of a usually inorganic phase — aptly named the "filler" or "reinforcement" — dispersed in a polymeric matrix in the form of particles, fibers, platelets or other desired shapes [1].

PCs are characterized by design flexibility, with their final properties depending on the matrix and filler details as well as their proportions in the mix. A typical example is the addition of hard inorganic particles in a polymeric matrix, leading to increased rigidity and durability. The level of property enhancement is strongly connected to the degree of interaction between the dispersed and continuous phase, which in turn is tied to the surface area of the interface between the components [2]. It is precisely this microscale impregnation of the matrix

with the filler that imparts to composite materials their attractive traits makes their separation arduous and impedes recyclability. Such is their value however, that demand is expected to remain high regardless of the increasing institutional push towards a more circular economy of materials [3].

Accordingly, composite materials have been developed with nanoscale filler units, coining the term *polymer nanocomposites* (PNCs). The proven improvement in performance obtained when the filler dimensions diminish dramatically makes PNCs highly desirable but also creates new technological challenges. A crucial aspect when it comes to optimizing a desired property is that of the dispersion state of the filler: When the degree of aggregation is high, nanoparticles (NPs) fuse into larger structures, drastically reducing their surface area and essentially transforming the PNC into a generic PC, which is why good filler dispersion is a typical requirement of PNC production [4].

A particular inspiration for the present thesis comes from the automotive industry, and specifically the silica reinforced rubber used during vehicle tire assembly. Since the 1990s precipitated silica filler has succeeded the originally used carbon black as it provides a better combination of rolling resistance, heat dissipation and overall resilience, increasing the tire lifetime and reducing fuel consumption [5]. The seemingly sole drawback of embedding silica in car tire rubber is its high polarity which promotes agglomeration, partly negating the benefits stemming from its usage. To counter this issue a variety of techniques has been tested, with the one of the most promising being chemically binding some of the matrix polymer chains to the NP surface [6]. The idea behind this modification is that the "halo" of surface grafted chains will act as a compatibilizer between the NP and the matrix and filler aggregation will be prevented [7].

There is a variety of PNCs where chain tethering is found to be an efficient method of improving dispersion, with various strategies being adopted for the realization of the desired grafted NPs. The grafting methods revolve around two philosophies, the "grafting to" and "grafting from" approach respectively. In the first case, the functionalized polymer is mixed with the NPs and surface attached through a suitable chemical reaction. This approach allows for complete freedom on the choice of the grafted chain architecture since it can be synthesized independently. An example is shown in fig. 2a, where reactive groups on the chain

end form permanent bonds with matching groups on the NP surface. The main challenge in this case is controlling the grafting density, that is the number of grafted chains per unit surface area. In order to bond with the NP surface, the polymer chain has to diffuse within a polymer melt or solution and assume the correct orientation, i.e. the functionalized part of the chain must face towards the nanoparticle surface in order for the coupling reaction to take place. This already challenging feat becomes even more unlikely as the grafting density increases. The area around the NP is now heavily populated by the tethered chains, further impeding the diffusion of polymer towards the surface. In the "grafting from" approach on the other hand the NPs are mixed with the polymer building blocks and the polymerization is performed starting from the NP surface (fig. 2b). As such, monomers diffuse in a low molecular weight medium until reaching the zone near the NP surface where polymerization takes place, alleviating the frustration relative to the notoriously slow polymer diffusion. The grafting density is essentially determined by the availability of polymerization initiators on the NP surface. However, the "grafting-from" polymerization process is not as easily controlled and imposes limitations on the types of grafted chains that can be synthesized. This stems directly from the fact that conditions in the zone adjacent to the NP surface are different from the bulk polymer [8]. For the simple linear end-grafted chains which are the exclusive focus of this work this drawback is not crucial, but could become more relevant in the future if a demand for finely tuned grafted chain properties arises in specific applications [9]. To avoid straying too far from the main scope of this work we also abstain from presenting in further detail variations of both grafting strategies which include coupling agents that may allow the polymer to tether at various points throughout the length of its backbone.

Regardless of the rapid advancements in the methods employed in the fabrication of the functionalized NPs, there is still limited understanding of the mechanisms promoting NP dispersion in PNCs in the presence of surface grafted chains. It is the objective of this thesis to hopefully paint a better picture of the changing NP-matrix interactions as a function of the properties of the population of the tethered chains. This exploration can easily become disorienting as systems of grafted PNCs are far from simple: Even for a given matrix and NP, one

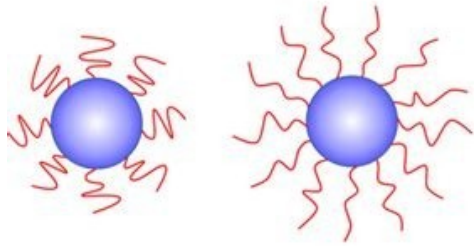

Figure 1. Schematic representation of polymer-grafted NPs at two different grafting densities, going from lower (left) to higher (right)

can vary all the properties regarding the grafted polymer, such as the grafting density, molecular weight, topology & chemical composition of the monomers. To add to the confusion, it has also been made possible to fabricate NPs with polydisperse or outright different types of grafted chains on the same particle [8]. To limit this vast parameter space we will focus on the the case of chemically identical linear matrix and graft polymers. This represents the most industrially relevant case, with significant work found in the research literature. This leaves us with two main parameters to worry about: i) The grafting density, which has a central role on the present study and ii) The ratio between the molecular weights of the grafted and matrix chains, for which we will mostly present preexisting work from the relevant literature. Accordingly, for the first part of this thesis we will delve into the details of *polymer brushes* — the structures that are formed by the grafted chains near the NP surface — and how their presence can alter the interparticle interactions in the context of the PNC. On the second part we will try to confirm whether or not the interactions induced by the brush are actually capable of bringing about the significant changes in dispersion that are observed experimentally, and on the third and final part some of the consequences of polymer grafting on the PNC rheology and potential secondary effects on dispersion due to flow will be examined.

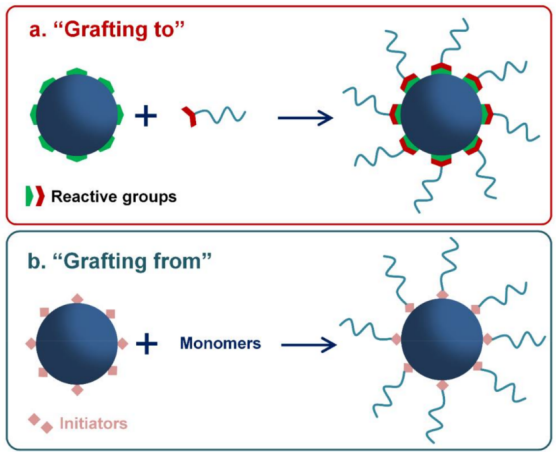

Figure 2. Schematic representation of the main grafting strategies: a) Grafting to (upper panel): Active sites on the NP surface bond with reactive groups on the polymer chain. b) Grafting from (lower panel): Initiator sites on the NP surface react with monomers and start the polymerization process. Adapted from [10]

AVGVSTVS FRIDERICVS ROMANORVM IMPERATOR SEMPER

Chapter 1

"Brushing up" the Polymer Brush

As anticipated in the introduction, a population of surface grafted polymer chains is referred to as a "brush" due to its likeness to the structure of everyday objects such as paintbrushes, which are made up of fibers extending from a flat or curved surface. This is illustrated in the sketch of fig. 1.1, drawn for our particular case where the grafted chains coexist with a melt of chemically identical free chains. It is also evident that the "hairs" in such a brush are not straight but take on the typical tortuous shape of polymer coils. Ignoring any particular properties of the NP surface, the brush system can be completely characterized by:

- The grafting density, σ
- The degree of polymerization of the grafted and free chains expressed as the number of Kuhn segments, N and P respectively
- The curvature of the surface, which can be expressed in terms of the brush height with respect to the NP radius

But how is it that these physical parameters affect the NP dispersion? A long held opinion is that when grafted NPs approach each other and the brushes

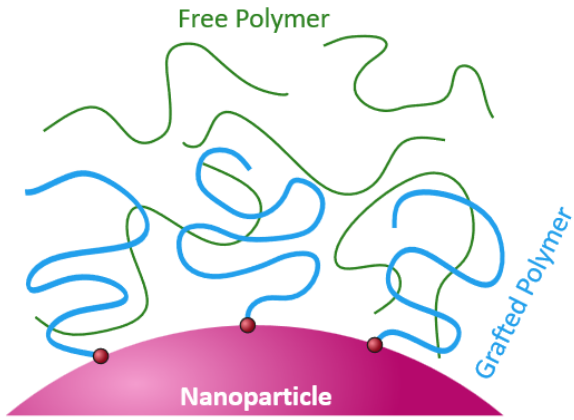

Figure 1.1. Schematic representation of a part of the grafted NP surface dispersed in a polymer melt.

on their surface begin to overlap repulsive interactions start developing, acting against the van-der-Waals or Coulomb-type interactions that typically lead to aggregation. The cause of the apparent repulsion could be as straightforward as a densely grafted brush acting as an obstacle that prevents NP contact, or more theoretically involved such as the grafted and free chains taking on entropically unfavorable configurations at the interface between approaching NPs. To get a better understanding of these possible explanations, we start from the examination of the literature on the heavily studied case of flat brushes, ignoring for the moment the influence of curvature.

1.1 Theory of Flat Brushes

1.1.1 Polymer Brushes in Good Solvent

Even though it is not directly related to our study, the vast majority of research on polymer brushes has been carried out for the case of brushes immersed in a good solvent. For a quick reminder, in polymer science a good solvent is one whose molecules interact more favorably with the monomers of the macromolecule than the monomers do among themselves. As a result the molecule

expands in size so that more monomer-solvent interactions are facilitated. This observation is closely tied to the description of the dependence of a polymer chain size on its molecular weight, which is typically expressed through a power law of the form $R_g \sim \alpha N^{\nu}$. R_g is the average chain radius of gyration while α represents the Kuhn segment length and ν is the scaling exponent. For a chain in a melt state, also known as ideal chain, the exponent is equal to $\nu = 1/2$, while for a good solvent ν is much closer to $3/5$, an important result that illustrates the swelling of polymer chains in the presence of a good solvent and will be useful in the following paragraphs.

The first theoretical description of polymer brushes on a flat surface and in a good solvent has been provided by Alexander & de Gennes [11, 12], who assumed a step function density profile, i.e., the brush density is uniform perpendicular to the wall. Starting from very low grafting density, the average minimum distance between grafted chains, $D \approx \sigma^{-\frac{1}{2}}$, is larger than R_g. This is the so-called *mushroom regime* (fig. 1.2a), named after the fact that the coils are far apart enough to not interact with one another and as such assume a spherical shape reminiscent of the free polymer in solution, mimicking isolated "mushrooms" growing on a surface. At this stage the brush — if it is even valid to call it one yet — height will be equal to the individual chain size. As the grafting density or chain size increase and D becomes smaller than R_g, the excluded volume interactions between the neighboring chains will force them to stretch in the vertical direction. If the overall concentration in the brush is in the semidilute regime[1], the chains can be represented as vertical stacks of blobs (fig. 1.3), each of size D. As a result, brush height will grow as:

$$\frac{h}{R_g} \approx \left(\frac{D}{R_g}\right)^{1-\frac{1}{\nu}} \tag{1.1}$$

An important insight of the above expression is that the degree of chain extension depends only on the average distance between chains in proportion to the coil size. By replacing the R_g and ν expected for a good solvent:

[1] The semidilute concentration requirement is automatically satisfied as soon as chain overlap occurs and should remain valid as long as the volume fraction of the polymer within the brush remains $\ll 1$

$$h \approx \alpha^{\frac{5}{3}} N \sigma^{\frac{1}{3}} \tag{1.2}$$

Note that the brush height grows faster than the size of the unperturbed coil with respect to N. The linear growth of h with N can also be understood intuitively, as increasing the molecular weight of the brush chains is equivalent to additional blobs being placed on top of the preexisting stack.

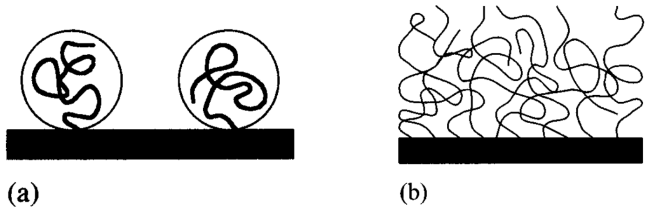

Figure 1.2. Polymer chains grafted on a flat surface in the mushroom (a) and brush (b) regimes. Taken from [13].

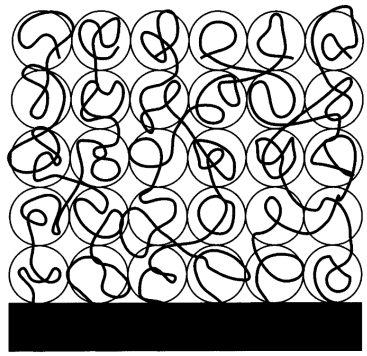

Figure 1.3. Polymer brush represented as a stack of blobs. Taken from [13].

By further increasing grafting density and moving from the semidilute to the concentrated regime, the blob-based approach no longer holds. Instead, invoking a Flory type mean-field argument by balancing the free energy cost of chain stretching with that of the excluded volume interactions results in a very similar expression:

$$h \approx N \left(\alpha^2 w \sigma\right)^{\frac{1}{3}} \tag{1.3}$$

with w being the excluded volume parameter of the Flory-Huggins theory. The scaling dependence of h on N and σ is the same as before, with the only difference now being that the effect of solvent quality is also accounted for through w.

The first evidence of the linear scaling of h with N come from the surface force apparatus (SFA) experiments of Hadziioannou et al. [14]. The brushes were formed by PV2P/PS diblock copolymers, with the PV2P side strongly adsorbing on an atomically flat mica surface. The idea behind the experimental setup, pictured in fig. 1.4, is that as the two grafted surfaces are brought closer, repulsive forces will develop between them due to the disturbance of the brush from its equilibrium configuration. Measurements in good (toluene) and almost theta[2] (cyclohexane at 38°C) solvents verified the onset of a repulsive force, and the brush height was considered as half the distance at which forces were first observed. For a bad solvent (cyclohexane at 21°C), attraction is observed at brush contact, since the brush chains interact more favorably with one another than with the solvent molecules. At smaller separations repulsion is restored as the solvent is almost completely expelled and the grafted layers get compressed. Later similar experiments [15, 16] observe a departure from the linear scaling and instead give $h \sim N^{0.6}$, which can be explained by accounting for the fact that in the experimental system grafting density drops as molecular weight increases due to the relatively weak grafting energy. More definitive proof of the linear height growth came from small-angle neutron scattering experiments that allowed for the direct measurement of brush height [17].

1.1.2 Interactions Between Opposing Brushes in Good Solvent

Besides estimating the brush height, SFA results can be used to directly study the grafted surface interactions. These measurements may then be compared to

[2]Theta solvents screen excluded volume interactions between chain monomers and cause it to assume ideal conformations as if it were in melt state

Figure 1.4. Schematic of surface force apparatus experimental setup. End-active polymer chains graft onto crossed mica cylinders and the force between them is measured at various separations. Taken from [15]

analytical expressions of the force developed between flat opposing brushes as obtained from the scaling and mean-field theories described previously. Assuming no interpenetration between the two layers, the force per unit area is given respectively by [18]:

$$F_{sc}(h) \approx \frac{kT}{D^3}\left[\left(\frac{h_0}{h}\right)^{\frac{9}{4}} - \left(\frac{h}{h_0}\right)^{\frac{3}{4}}\right] \tag{1.4a}$$

$$F_{mf}(h) \approx kT\left(\frac{w}{\alpha^4 D^8}\right)^{\frac{1}{3}}\left[\left(\frac{h_0}{h}\right)^{2} - \left(\frac{h}{h_0}\right)\right] \tag{1.4b}$$

where h_0 is the equilibrium brush height and h half the separation length between the grafted surfaces, which coincides with the compressed brush extent under the no interpenetration assumption. Obviously, the above relations are valid only for $h \leq h_0$. A similar relationship has been developed by Patel et al. [19], following the same scalings as eq.(1.4a) but is not presented here since it is algebraically more complex while not offering any further physical insight. Both expressions presented above give similar scaling of forces with compression, with the first term in the square brackets corresponding to the osmotic pressure which tends to swell the brush, while the second one to the entropic chain elasticity which acts to bring the elongated brush chains back to their equilibrium length. Figure 1.5 illustrates how eq. (1.4a) describes well the SFA force-separation profiles of [15, 16] up to an arbitrary vertical shift factor. Important discrepancies between data and theory are observed at high separations, that is near the initial

brush contact. A probable explanation is that the density profile near the brush edge deviates significantly from the step function initially assumed by Alexander and De Gennes.

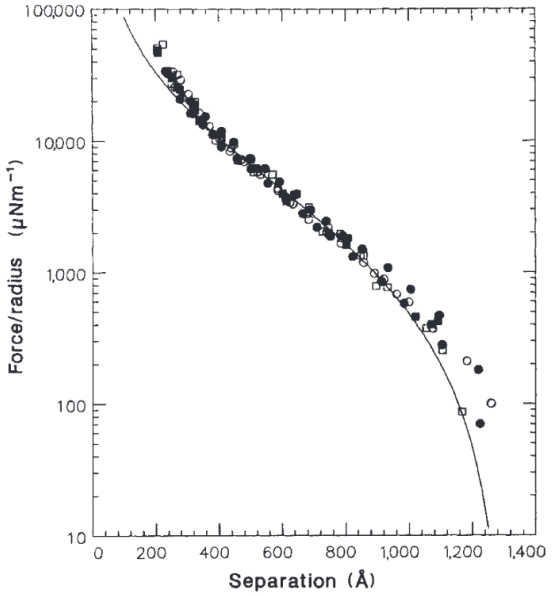

Figure 1.5. Force/Cylinder Radius profiles from the SFA experiments of [15]. Obtained with the setup of fig. 1.4, they are equivalent to energy per unit area between two flat plates as per the Derjaguin approximation [20]. The squares and circles represent the results of two separate experiments. Solid symbols show the forces measured on compression of the adsorbed layers, and open symbols the corresponding forces on rapid decompression. The solid line is the predicted energy per unit area between flat plates, as given by integrating eq. (1.4a)

.

To tackle the limitations of the scaling and mean-field approaches, Milner et al. [21] utilized a self-consistent field (SCF) theory and by making no assumptions about the form of the brush density profile showed that it is parabolic. At the limit of very long chains, $(N \to \infty)$, an analytical solution is available:

$$c(z) = \frac{\pi^2}{8N^2} \frac{\upsilon}{w} \left(h_0^2 - z^2\right) \tag{1.5}$$

where $c(z)$ is the number concentration of the brush segments at a distance z

from the grafting surface and υ is a parameter with dimensions [length]$^{-2}$. The equilibrium brush height for this case is given by:

$$h_0 = \left(\frac{12}{\pi^2}\frac{w}{\upsilon}\right)^{\frac{1}{3}} \sigma^{\frac{1}{3}} N \tag{1.6}$$

These expressions are valid at relatively high grafting densities, where the chains are substantially stretched in the vertical direction, and when the solvent is not too good[3]. Interestingly, the scaling exponents of brush height through the SCF approach are identical to those predicted by the scaling / mean-field theories, which is also true when the SCF approach is used for the case of a very good solvent and/or low grafting density. Neutron reflectivity [22, 23] and neutron scattering [24] experiments confirm the parabolic form of the density profile, with the exception of the zone near the brush maximum extension, where the profile is better approximated by an exponential decay. This can attributed to the finite size of the chains, which can be accounted for by performing direct numerical calculations for different degrees of brush polymerization [25], as shown on fig. 1.6. This picture is further reinforced by Monte Carlo (MC) [26] and coarse-grained molecular dynamics (MD) [27] simulations.

Through the SCF theory it is also possible to extract an expression for the force per unit area:

$$F(h) = \frac{kT}{2}\left(\frac{\pi}{12}\right)^{\frac{1}{3}} w^{\frac{2}{3}} \upsilon^{\frac{1}{3}} N \sigma^{\frac{5}{3}} \left[\left(\frac{h_0}{h}\right)^2 - 2\frac{h}{h_0} + \left(\frac{h}{h_0}\right)^4\right] \tag{1.7}$$

A re-examination of the data of [15] using eq.(1.7) has shown that SCF theory and experiment match very well without the need for any fitting parameters [29]. The agreement at high separations is still limited but can be significantly improved by extending the SCF theory to account for the polydispersity of the brush chains. Further experimental studies [30] showed a similar trend.

Theoretical predictions of the forces between overlapping brushes can also be evaluated through computational studies. Murat & Grest performed MD simulations of brushes in implicit good solvent [31], assuming that the interaction

[3]The criterion is that the thermal blob size must be larger than the distance between grafted points. For a more detailed explanation the interested reader can check the relevant chapters of any polymer physics textbook, such as the classic read of Rubinstein & Colby [28].

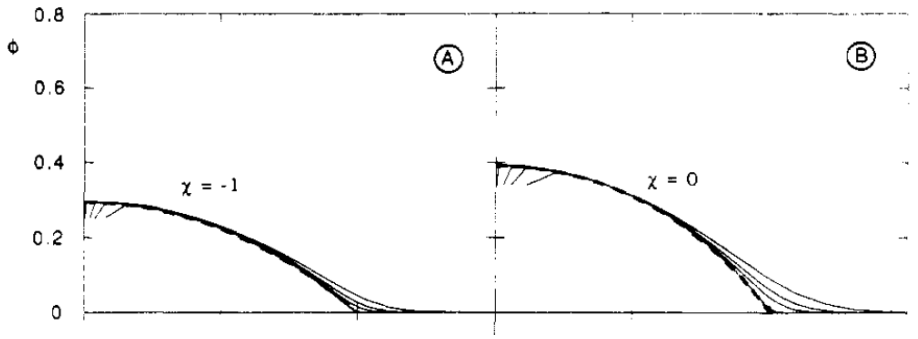

Figure 1.6. Volume fraction profiles of flat polymer brushes in good (A) and athermal (B) solvent. The dashed curve is the analytical prediction of SCF theory and solid curves correspond to degree of polymerization $N = 600, 100, 50, 25$ in order of increasing deviation from the dashed curve. Taken from [25]

force will be equal to just the force developing between the brush chains. The resulting force profiles were in agreement with the scaling theory only for low to medium compressions/grafting densities. Such a behavior is to be expected since at high brush concentrations the osmotic pressure, which is the leading contribution to the force, diverges logarithmically with $1 - \phi$, ϕ being the brush volume fraction. Another work treating the same system with a lattice Monte-Carlo method [32] found good agreement between the force profiles predicted by simulations and SCF theory, with deviations at low compressions, where chain finite-size effects are significant.

Performing these simulations with an explicit description of the solvent is not a trivial modification. In the SFA experiments the brush is immersed in bulk solvent reservoir that permits mass exchange between it and the brush zone. In terms of thermodynamics this means that the solvent within the brush will assume the chemical potential of the reservoir. That chemical potential is going to be the same at all compressions if the reservoir is kept at a constant temperature and pressure. Simulation studies with an explicit monomeric solvent have indeed been performed by setting the solvent chemical potential at a reference value for all separations [33, 34, 35]. In these simulations, performed in the so-called grand-canonical ensemble (GCE), the solvent chemical potential is

measured periodically through the Widom insertion method and adjusted by removing or adding particles using a feedback scheme. Results from [33] show good agreement between the GCE simulations and theoretical scaling laws.

1.1.3 Limit of High Compression

Regarding the discrepancy between theory and experiment/simulation at high compressions, it should be noted that in all presented theoretical approaches the scalings match at small separations, since in that limit the repulsive force is always approximated by the corresponding osmotic pressure of an ungrafted semidilute solution. At the high compression regime the energy per unit area scales with an exponent of -1 or -1.25, as predicted by integrating eqs. (1.4) and (1.7) and adapting them to the crossed cylinder geometry of the SFA setup through the Derjaguin approximation. Experimentally measured forces though increase faster than predicted, showing energy scalings as strong as $\sim h^{-3}$, which is expected as the mass density becomes too high for the osmotic mean field potential to be well approximated by a term proportional to the number density. This disparity has been addressed by assuming a quartic equation of state for the (osmotic) pressure of the polymer solution consisting of unthethered brush chains and using it to extend the SCF method [36]. Comparing the numerical solution of the resulting expression for interaction forces with further SFA experiments of double/single brush systems at strong compression validates the claim that at high brush densities interaction is dominated by the osmotic pressure of the equivalent polymer solution.

Another way to tackle the problem of force prediction at high compressions could be by accounting for the brush interpenetration. As mentioned previously, most theoretical treatments are performed under the assumption of no interpenetration, that is the chain monomers of each grafted layer are found at most a distance of half the overall separation away from their respective surface. While such a claim is valid at the limit of infinitely long chains, experimentally relevant systems do indeed demonstrate significant brush interpenetration. A typical way to quantify interpenetration is:

$$I = \frac{\int_h^{2h} \rho_1(z)dz}{\int_0^{2h} \rho_1(z)dz} \tag{1.8}$$

where ρ_1 is the number density of the brush monomers grafted on the $z = 0$ surface. Essentially the interpenetration as defined here is the fraction of the brush mass that is further than h, that is half the separation length, from the grafting surface.

The first scaling theory developed considering brush interpenetration predicts a scaling law of $\sim h^{-2.5}$ for the interaction energy, which gives good agreement with experiments at intermediate to high compressions, up to $h/h_0 \approx 0.1$ [37]. In the same study they also showed that the interaction energy is essentially proportional to the interpenetration width, as measured in MD simulations. While approaches based on brush interpenetration seem to aid in closing the gap between theory and experiment, there may still be significant discrepancies as grafting density increases beyond levels that are experimentally accessible. A more recent theoretical approach based on the density functional theory [38] reports that strongly compressing dense brushes leads to power law exponents at least as strong as -2.4, and up to -4.3 for higher grafting densities.

1.1.4 Effect of Solvent Quality

The above picture changes drastically as we move towards the theta and bad solvent regimes. By invoking eq.(1.1), the brush height scaling is:

$$h_{theta} \approx \alpha^2 \sigma^{\frac{1}{2}} N \tag{1.9}$$

$$h_{bad} \approx \alpha^3 \sigma N \tag{1.10}$$

The above scaling expressions are correct even though the blob picture is not valid for a bad solvent. Even in that case though the same logic works by just considering the volume occupied by a fully collapsed brush. Such brush collapse as the solvent quality worsens has been demonstrated by neutron scattering experiments [39], with the observed density profiles partially adhering to

the theoretical description of Zhulina et al. [40]. Simulation studies with implicit [41, 42] and explicit [43] description of the solvent confirm the density profile predictions. In addition, they showcase the formation of dimples for relatively low grafting densities, as the brush chains form clusters to avoid exposure to the bad solvent, leading to an inhomogeneous density profile (fig. 1.7). The appearance of lateral structure on a polymer brush in a bad solvent has also been confirmed by atomic force microscopy (AFM) [44], showing the characteristic formation of grafted polymer clusters on flat surfaces, as shown in fig. 1.8.

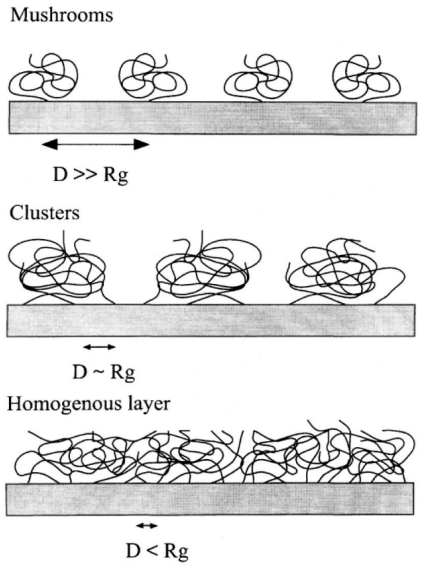

Figure 1.7. Observed structures of brush layers in a poor solvent. At low (top) and high (bottom) grafting density the chains form collapsed mushrooms or a homogeneous collapsed layer respectively. At intermediate grafting densities, $R_g \approx D$ (mid), bundling of the brush chains in localized clusters can be achieved.

1.1.5 Polymer Brushes in Polymeric Solvent

Switching the low molecular weight solvent for a polymeric one leads to a qualitatively different behavior. Assuming neutral interactions between the brush and matrix chains, the unperturbed radius of gyration of the brush chains scales

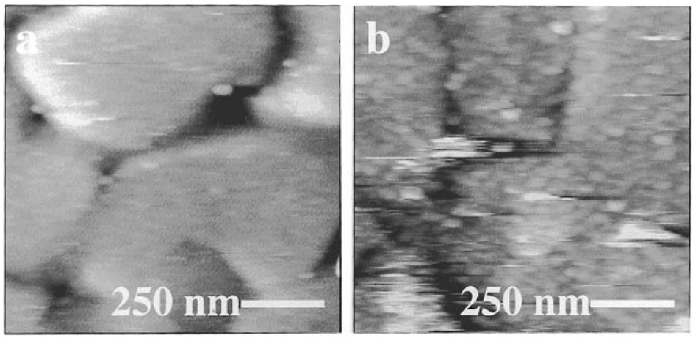

Figure 1.8. AFM scans of a dextran grafted surface immersed in water before (a) and after (b) the replacement of water with propanol. The grafted layer is initially smooth as the brush is swollen within the good solvent (water) but forms a globular morphology as it dehydrates under the presence of propanol. Taken from [44]

as:

$$R_g \approx \alpha N^{\frac{3}{5}} P^{-\frac{1}{5}} \tag{1.11}$$

The above expression is mentioned in other works [45, 46] without any citation and we have not been able to find an original source. It does however look reasonable as it gives the typical scaling of a chain in a good solvent for $P = 1$ and is valid up to $P = \sqrt{N}$, at which point the coil size scales as $\sim N^{\frac{1}{2}}$. For higher values of P the chains will retain the ideal statistics as if they were in melt state.

Following the above scalings, the mushroom regime for brushes in a chemically identical melt is defined by:

$$\sigma \leq \begin{cases} \alpha^{-2} N^{-\frac{6}{5}} P^{\frac{2}{5}}, & P < \sqrt{N} \\ \alpha^{-2} N^{-1}, & P \geq \sqrt{N} \end{cases} \tag{1.12}$$

Naturally, by increasing the grafting density above these thresholds we enter the brush regime. For $P < \sqrt{N}$ we have a picture similar to that of a brush in a good solvent, with a scaling of $h \sim \alpha \sigma^{\frac{1}{3}} N P^{-\frac{1}{3}}$. On the other hand, when $\sqrt{N} < P < N$, the brush will not start stretching immediately with increasing σ: Instead, the brush chains — following ideal statistics — will initially overlap

without stretching, up until the point where the entropic cost of preventing the matrix chains from mixing with the brush overcomes that of brush stretching. This is observed at $\sigma = \alpha^{-2} N^{-\frac{3}{2}} P$, above which the same "good solvent" scaling is recovered. This wet brush regime will dominate the brush behavior until high values of surface coverage, where once again the entropic cost of introducing matrix chains in the brush becomes prohibitive. The solvent will be essentially expelled from the brush and the height will scale as $h \sim \alpha \sigma N$. As expected, the crossover grafting density separating the wet from dry brush regime drops with the matrix chain size, following the line $\sigma = \alpha^{-2} P^{-\frac{1}{2}}$. Finally, for $P \geq N$, the stretched brush regime is completely bypassed. Instead there is a transition from the unstretched to the dry brush regime at $\sigma = \alpha^{-2} N^{-\frac{1}{2}}$, which signifies the point at which the unstretched chains completely occupy the brush volume. All of the above information is summarized on the phase diagram of fig. 1.9, taken from Aubouy et al. [46].

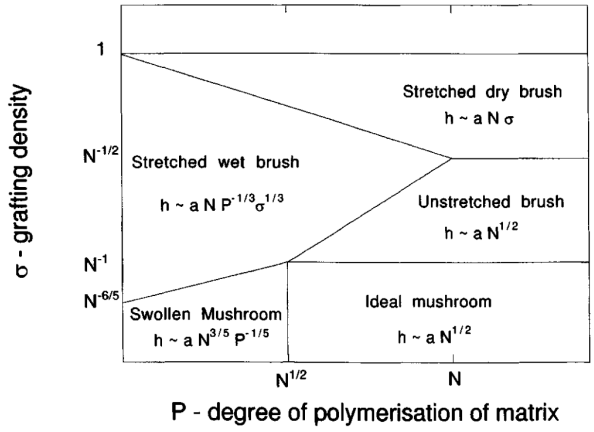

Figure 1.9. Various regimes for a brush formed of chains of degree of polymerisation N with a grafting density σ, exposed to a matrix of a chemically identical polymer melt with degree of polymerisation P. Taken from [46]

The effect of matrix molecular weight, responsible for the wet to dry brush transition, has been observed with direct measurement of the brush density profile through neutron reflectivity experiments [47]. The overall scaling picture has also been validated by numerical solution of the SCF equations [48] and coarse-grained

MD simulations [49] for the brush-in-melt system, with the added observation that the crossover between different scaling regimes is much more gradual than implied by the phase diagram borders.

When it comes to interactions between brushes coming in contact in a melt matrix, the brush regime is a defining factor. Wet brushes will behave qualitatively similar to the good solvent case, with repulsive forces developing upon brush contact. The picture is different at the dry brush regime: As the opposing brushes come in contact, the matrix polymer trapped between them will be forced into unfavorable conformations, leading to its expulsion from the gap. This creates a negative osmotic pressure which translates into an effective attraction between the two surfaces, as the brush chains interact preferentially with the brush chains grafted on the opposite surface. This attractive interaction is limited to a small range of separations as soon as brush contact is achieved and after full expulsion of the matrix material strong repulsive forces are restored. Numerical solutions using the SCF theory have shown that the magnitude of the attractive force increases with increasing P/N and grafting density, without indicating a specific functional dependence [48]. Experimental evidence have been provided by Hasegawa et al. [50], who checked the dispersion state of grafted NPs in a chemically identical matrix for increasing grafting densities. Going from nude to lightly grafted particles leads to improved nanoparticle dispersion due to the repulsive forces developing between the surface brushes that gradually screen the NP attractive interactions. Overcoming a critical grafting density dispersion gradually worsens, hinting at the onset of the dry brush regime and the development of attractive forces between the brushes. These results are accompanied by a theoretical treatment where the overall interaction potential between the grafted NPs was obtained as the sum between the interparticle Hamaker-type interaction and the and the interbrush potential resulting from mean field calculations. The critical grafting density is then chosen as the one that minimizes the depth of the attractive well, with the result being close to the experimentally observed one (fig. 1.10).

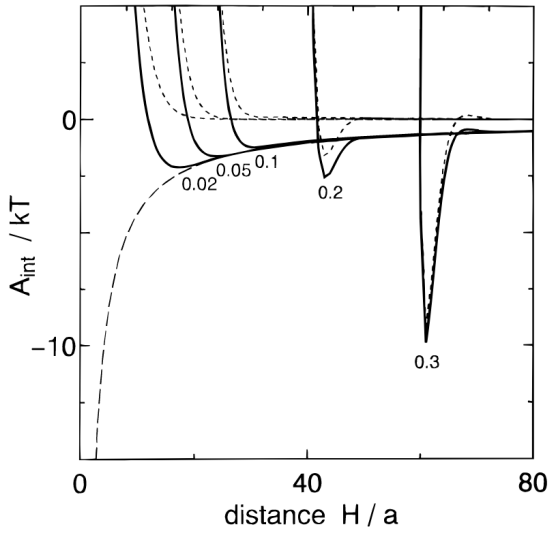

Figure 1.10. Interaction energy plotted against the separation between 400nm particle surfaces for $N = P = 100$. Each curve is labeled by the corresponding grafting density in units of nm^{-2}. Solid lines show the total interaction energy, dashed lines the polymer contribution, and the single broken line the van der Waals attraction between the particles. The depth of the attraction energy reaches its minimum around $\sigma = 0.1\mathrm{nm}^{-2}$. Adapted from [50].

1.2 Computer Simulation of Polymer Brushes in a Melt

Apart from the few theoretical works and scarse experimental evidence, there seems to be no computational approach dealing with the issue of interactions developing between brushes in a polymeric solvent. As a starting point in this direction, we open the discussion with the simulation study of the effect of a polymeric matrix on the static properties of brushes, which necessitates that the solvent molecules be explicitly present. We adopt the system of Grest [49], where brush and solvent molecules are represented by Kremer-Grest coarse-grained bead-spring chains [51]. With all species being chemically identical, beads on the same and different chains interact with a purely repulsive Lennard-Jones

(LJ) potential truncated at the minimum and shifted so that it only takes positive values:

$$U_{LJ}(r) = 4\varepsilon \left[\left(\frac{\sigma_{LJ}}{r} \right)^{12} - \left(\frac{\sigma_{LJ}}{r} \right)^{6} \right] + \varepsilon, \quad r \leq r_{min} = 2^{\frac{1}{6}} \sigma_{LJ} \tag{1.13}$$

with r being the euclidean distance between bead centers, ε the depth of the potential well before the shift, and σ_{LJ} the "size" of the bead. Neighboring beads in the chain are held together by FENE bonds:

$$U_{FENE}(r) = -0.5 K R_{max}^2 \ln \left[1 - \left(\frac{r}{R_{max}} \right)^2 \right]$$

where K is stiffness parameter of the bond and R_{max} its maximum extent. Brush chains are attached by immobilizing a chain end bead on one of the z-surfaces of the simulation box (randomly or in a hexagonal pattern), while the surfaces themselves act as hard impenetrable walls interacting with all beads through the aforementioned Lennard Jones potential, which must be expressed in terms of distance of the bead center from the wall surface, z_w:

$$U_{wall}(z_w) = 4\varepsilon \left[\left(\frac{\sigma_{LJ}}{z_w + z_w^{min}} \right)^{12} - \left(\frac{\sigma_{LJ}}{z_w + z_w^{min}} \right)^{6} \right] + \varepsilon, \quad z_w \leq z_w^{min} = 2^{-\frac{5}{6}} \sigma_{LJ}$$

The position vector, $\boldsymbol{r}_i$, of the beads (except for the grafted ends which remain fixed) at each timestep is updated by numerically integrating the Langevin equation of motion:

$$m \frac{\mathrm{d}^2 \boldsymbol{r}_i}{\mathrm{d}t^2} = -\nabla U - \zeta \frac{\mathrm{d}\boldsymbol{r}_i}{\mathrm{d}t} + \boldsymbol{W}_i(t) \tag{1.14}$$

where m is the bead mass and U the sum of the potentials acting on the bead. The system is thermostatted by coupling the bead movement to a heat bath through the damping coefficient ζ and the white noise term $\boldsymbol{W}_i$ which satisfies the fluctuation-dissipation theorem. As such, at each timestep each component of $\boldsymbol{W}_i$ has to be picked randomly from a Gaussian distribution with variance

$2m\zeta k_BT/\Delta t$ (or for computational savings from a uniform distribution of range $\pm\sqrt{6m\zeta k_BT/\Delta t}$ [52]) where k_B is the Boltzmann constant and T the desired temperature. Simulations are performed in LJ units with $m = \sigma_{LJ} = \varepsilon = 1$, with the FENE parameters being $R_{max} = 1.5$ and $K = 30$, rendering chain crossing energetically prohibitive [51] at the chosen temperature $T = 1$ with a damping coefficient of $\zeta = 0.5$. Time integration is performed with the velocity-Verlet algorithm using a timestep of $\Delta t = 0.005$.

To setup the simulation system, polymer chains are placed one by one and constructed successively from the first bead. The first bead of brush chains is placed on the wall surface following the chosen grafting pattern while the first bead of solvent chains is placed randomly at a point in the simulation box. All bead centers must be at a minimum distance z_w^{min} from the walls, while successively added beads are placed at a distance r_{min} from the previously added bead by selecting a random angle. An additional restriction is placed on back folding, that is the distance between second neighbors in a chain must be larger than a set minimum, $|\boldsymbol{r}_{i-2} - \boldsymbol{r}_i| \geq 1.02$. Brush chains are inserted first, followed by the addition of solvent chains, up until the desired total monomer number density $\rho = 0.85$ is achieved, the typical value for a Kremer-Grest melt. The resulting setup is that of two opposing brushes extending in the z direction, as illustrated in fig. 1.11. At this stage the individual beads are strongly overlapping with each other but these overlaps are broken up by replacing the diverging LJ potential with a soft sinusoidal and performing a preliminary MD run. The form of the soft potential is:

$$U_{soft} = A\left[1 + \cos\left(\frac{\pi r}{r_{min}}\right)\right], \quad r \leq r_{min}$$

its value decreasing monotonically with bead separation from $2A$ at $r = 0$ to 0 at $r = r_{min}$. The value of the prefactor A is not held constant, instead increasing linearly with time from 0 to 60 for the duration of the preliminary run. Once finished, beads are well-separated, the hard-core potential can be reinstated and canonical ensemble (NVT) MD may be performed.

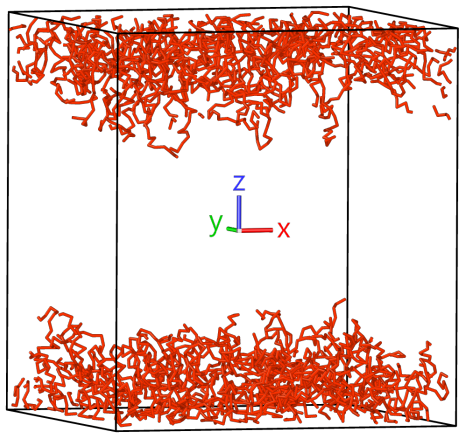

Figure 1.11. Simulation box of two opposing brushes ($\sigma = 0.05$, $N = 30$) in explicit monomeric solvent, only the bonds of the brush chains are visualized for clarity. Borders are periodic in the x and y directions while flat walls block the passage of beads through the z direction borders.

1.2.1 The Reservoir Concept

The above setup is useful for extracting configurational and dynamic properties of the brush but cannot be used for the accurate measurement of interaction forces. That would require that the chemical potential of the solvent remains constant between runs at different separations, as in the case of [33, 34, 35] for a monomeric explicit solvent. Unfortunately, such approach is not feasible as the method used for the measurement of the solvent chemical potential is not readily applicable for non-rigid solvent molecules. To circumvent this issue we introduce a solvent reservoir, by extending the simulation box in one horizontal direction (fig. 1.12). The reservoir essentially operates as a tank of bulk solvent that can exchange mass with the brush zone. Being a single component bulk phase, it can be maintained at the desired chemical potential simply by maintaining it at the same temperature and pressure at all separations, thus indirectly controlling the chemical potential in the brush area, which has to match that of the reservoir. The separation between the grafted surfaces can be easily adjusted by moving the walls that are limited to the brush area closer, without confining the reservoir

material that must always correspond to a bulk state. Temperature control is achieved by the Langevin thermostat without extra modifications, while pressure can be set by implementing a Berendsen barostat. Since the barostat will only operate by changing the box boundaries in the expanded direction — let's assume along the x-axis — then the simulation box size in that direction, L_x, changes during the simulation as:

$$\frac{\mathrm{d}L_x}{\mathrm{d}t} = \frac{L_x}{\tau_B}\left(P_r(t) - P_r^*\right)$$

where P_r is the current pressure in the reservoir zone, which will be clearly defined in the following paragraphs, P_r^* is the set point, e.g. the desired reservoir pressure, and τ_B is the damping parameter of the barostat. Larger τ_B values will lead to a slower approach towards the set point and vice versa. $\tau_B = 10$ has been chosen for all subsequent simulations, allowing for reasonably responsive pressure control without excessive fluctuations. P_r, as well as all other pressures/stresses presented in this work, is calculated using the virial theorem:

$$P_{ij} = \frac{1}{V}\sum_{k=1}^{N_V} m_k u_{k_i} u_{k_j} + r_{k_i} f_{k_j} \tag{1.15}$$

The above expression calculates the components of the pressure tensor, P_{ij} in a region of volume V by summing the contributions of the beads inside that region, u_{k_i}, r_{k_i} and f_{k_i} being the i^{th} component of the velocity / position / force vector corresponding to the k^{th} bead. The hydrostatic pressure in a bulk region may then be taken as the average of the normal components of the pressure tensor, $P = \left(P_{xx} + P_{yy} + P_{zz}\right)/3$.

Introducing the reservoir solves the chemical potential measurement problem but presents a new one: The existence of a brush-bulk border means that the brush chains near it will have fewer neighboring grafted chains, leading them to take on significantly different configurations from their counterparts in the interior part of the brush. To ensure that only the desired states are sampled, all presented quantities will be measured at that central part of the brush where such "edge effects" should be negligible. To define the measurement region, the brush area is separated into vertical bins at different distances from the brush

centerpoint and the density profile of the grafted chains in each bin is extracted. Figure 1.13 presents such an example, where the density profiles of the bins overlap up to a distance of 10.4 from the brush area center. It is then assumed that measurements can be safely made up to that point since chain configurations are not affected, thus signifying the limits of the "Inner Brush Zone" of fig. 1.12. In the same spirit, properties in the reservoir zone will be sampled only after a distance away from the brush zone at which no brush chain segments are detected.

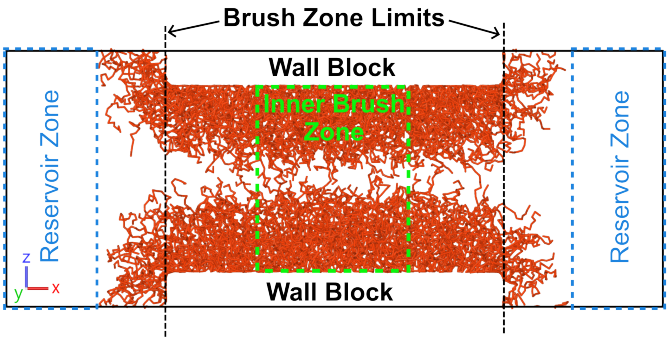

Figure 1.12. Simulation box of opposing brushes ($\sigma = 0.2$, $N = 30$) in explicit monomeric solvent, including a solvent reservoir along the x-axis. Only the bonds of the brush chains are visualized for clarity. The various regions of interest are highlighted with dashed lines. Measurements of reservoir pressure for barostatting purposes are performed in the "Reservoir Zone" region while all brush properties are extracted from the "Inner Brush Zone" region, where the density profile of the brush is stabilized.

The workflow up to now can be summarized as: Obtain an initial setup of non-interacting opposing brushes, break overlaps between beads using the soft potential, bring the brushes at the desired separation and equilibrate the system while using the barostat, and finally perform the production run. The Berendsen barostat however does not correctly sample from the isothermal-isobaric (NPT) ensemble, and is thus not suitable for the production run. An additional intermediate step is needed after equilibration, where the average L_x is tracked and then imposed for the production run, which is subsequently performed in the NVT ensemble.

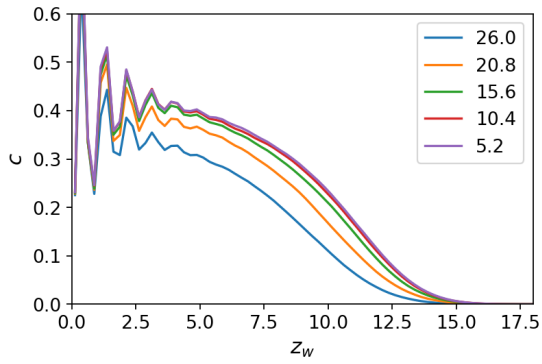

Figure 1.13. Number density profile of brush beads at various bins taken along the x direction. Extracted from the system of fig. 1.12, with the separation between brushes increased to the full box length in the z direction so that they are fully separated. Different lines correspond to different bins, with the bin maximum distance from the brush area center listed in the legend.

1.3 Model Validation with Good (monomeric) Solvent

Opposing polymer brushes are setup from chains of $N = 30$ segments, with their ends placed in a hexagonal grid and adding the monomeric solvent. The low degree of polymerization of the brush chains will lead to significant differences from theoretical predictions but is a necessary compromise: Increasing the number of chain segments will eventually bring the system to the entangled regime, drastically slowing down the dynamics and thus calling for exponentially longer simulation time. The grafting density of the brush is $\sigma = 0.2$, which is high when compared to real-life scenarios but necessary to reach the strongly stretched regime when the number of segments is this low. To get an idea of the degree of stretching of the brush chains we determine their unperturbed radius of gyration by performing simulations of a dilute solution of $N = 30$ free chains in a monomeric solvent. This gives $R_g \approx 3$ which results in $D/2R_g \approx 0.4$, ensuring that the distance between grafting points is significantly smaller than the coil size, leading to it stretching in the vertical direction.

To make comparisons between the normal forces extracted from simulation runs and the scaling laws proposed in eqs. (1.4) and (1.7), an estimate of unperturbed the brush height is needed. An examination of the density profile from the simulation system on fig. 1.14, reveals that it has a parabolic shape near the wall, as predicted by the SCF theory, but gradually turns into an exponential decay near the brush end due to the finite size of the chains, dropping to zero at a distance from the wall of about 17.5. To make a direct comparison with the analytical profile of the SCF theory we have to estimate the w and υ parameters, which can be obtained from the solution osmotic pressure, Π, and the chain end-to-end distance, R_e respectively [29]:

$$\Pi = \frac{1}{2} w c^2$$

$$R_e^2 = 3N/\upsilon$$

Simulations of the polymer solution give $w \approx 1.2$ for c from 0.2 to 0.5 and $\upsilon \approx 1.5$ at the dilute regime. This value of w means that the the thermal blob size is significantly smaller than the average distance between grafting points, placing the studied system outside the validity of eqs. (1.5) and (1.6), which is evident when the two profiles are superimposed in fig. 1.14 and significant discrepancies are observed between them. Still, the maximum extent of the brush seems to be essentially the same for both cases and for that reason the unperturbed brush height predicted by the SCF theory, $h_0 = 17.4$ will be used for the rest of this section.

The osmotic pressure of the system of opposing brushes is measured at different separations starting from non interacting brushes. The target pressure at the reservoir is set at $P_r^* = 8.19$, which is the bulk pressure of the Kremer-Grest monomer contained in it. Obtaining the z-component of the normal stress within the brush is not as simple, as the existence of the immobilized chain ends may lead to underestimation of the pressure if eq. (1.15) is applied directly on the overall inner brush volume. In addition, the presence of walls and the high grafting density lead to an oscillating pressure profile at their vicinity due to bead layering. Consequently, the pressure calculation must be performed in a subvol-

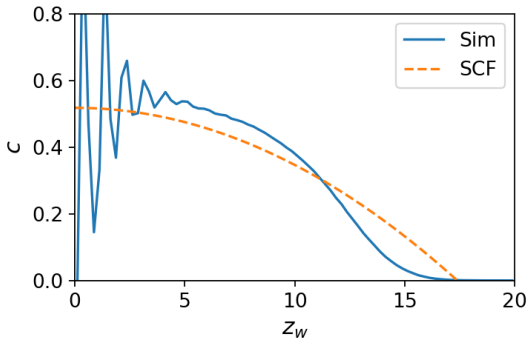

Figure 1.14. Density profile of single brush with $N = 30$, $\sigma = 0.2$ in a monomeric solvent (blue line), superimposed with the analytical prediction of the SCF theory for that system (orange dash).

ume that does not include the immobilized beads and is also outside the range of pressure oscillations which could lead to inconsistencies in the measurement. To this end, the inner brush region is separated along orthogonal bins in the vertical direction and the pressure profile is drawn by applying eq. (1.15) at each bin. Since mechanical equilibrium dictates that P_{zz} be constant within the bulk along the z direction, we can estimate it by taking its average from the bins that are placed in the "flat" zone of the profile. An example is shown in fig. 1.15, where the pressure profile of the system of fig. 1.14 is presented. The pressure oscillations have fully decayed after $z_w = 10$ and taking the average for all $z_w > 10$ we find that $P_{zz} = 8.19$, equal to the reservoir pressure. This is the expected behavior, since the brushes are not yet interacting at this separation and as a result no osmotic pressure develops between the brush zone and the reservoir.

Following the procedure described above, we obtain the osmotic pressure within the brush at various separations. Due to the high grafting density of the brush we observe that already at intermediate compressions the repulsive force scales with an exponent of ≈ -4 (fig. 1.16b), which is significantly higher than theoretical predictions. This can be explained by looking at fig. 1.16a, where the osmotic pressure is plotted against the concentration. Choosing the concentration corresponding at each separation is not trivial as the brush system is inhomogeneous in the z direction. It is reasonable to assume that osmotic pres-

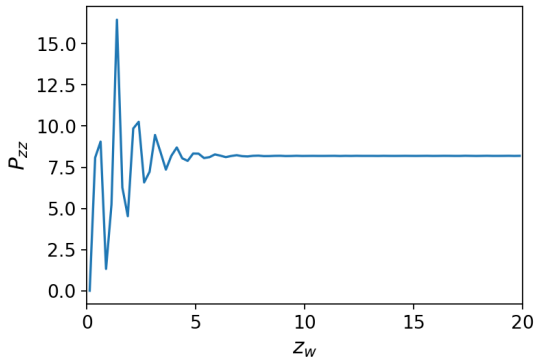

Figure 1.15. Profile of the zz component of the pressure tensor along the z-direction within the "Inner Brush Zone" for the system of fig. 1.14.

sure will be determined by the minimum concentration observed at the midpoint of the density profile between opposing brushes, corresponding to $z_w/h = 1$ on fig. 1.17a. Using that value, we see that starting from a concentration of ≈ 0.2, the osmotic pressure scales as $\sim c^3$. Simulations of a bulk polymer solution at this concentration range show a similar scaling, confirming that the osmotic contribution to the repulsive force is dominated by three-body interactions, in contrast to the analytical laws that only consider pair interactions. Furthermore, brush osmotic forces seem to always be slightly higher than the osmotic pressure of the equivalent bulk solution. Similar observations have been made in [30] and may be related to the confinement of the polymer chains between the flat walls. It has been shown through MD simulations that confining polymer melts between flat repulsive surfaces leads to the onset of increasingly repulsive forces as wall separation decreases [53]. This can be explained in terms of the loss of entropy of the confined chains or through the onset of the so-called anti-Casimir effect, as described in [54]. In both cases, an effective repulsion is observed starting at ranges of the order of the coil size.

Another interesting observation has to do with the inconsistency between fig. 1.16a and b. Since concentration typically scales as $\sim h^{-1}$, a scaling exponent close to -3 should be expected at high compressions. However, by plotting the effective brush concentration c_{mid} (as defined in the previous paragraph) against

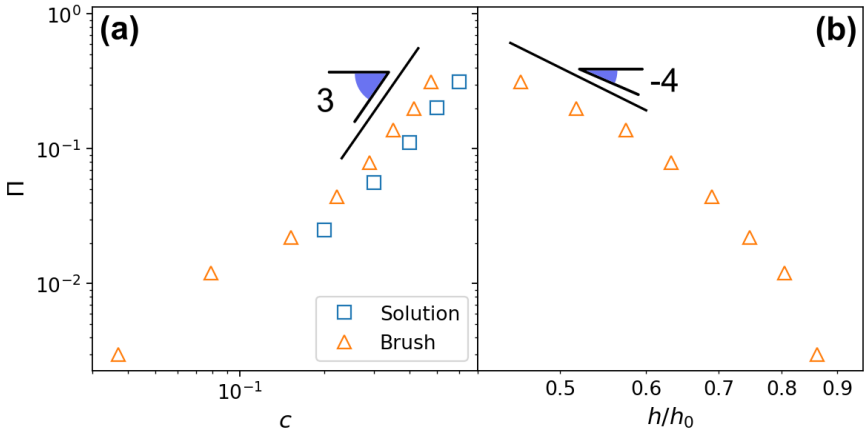

Figure 1.16. Osmotic pressure as a function of concentration (a) and separation distance normalized by the unperturbed brush height (b). The concentration of the brush monomers in (a) is determined by the value of the density profile at the midpoint and the osmotic pressure of a polymer solution at similar concentrations is provided for comparison (blue squares). Black lines are drawn as guides to estimate the pressure scaling at high compressions.

h_0/h (fig. 1.17b) we notice that the two quantities do not scale linearly, with a minimum exponent of ≈ 1.5 at high compressions, a direct consequence of the inhomogeneous brush density profile. It is therefore expected that the force will increase faster when considered a function of separation instead of concentration.

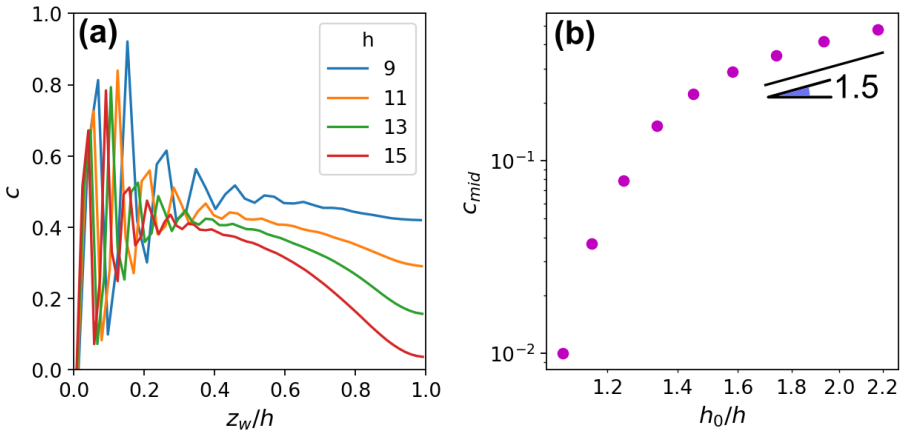

Figure 1.17. (a): Opposing brush density profiles at different separations. Distance from the wall is normalized by half the overall separation, h. (b): Brush concentration at midpoint ($z_w/h = 1$) plotted against h_0/h. Black line is drawn as a guide to estimate the scaling between these quantities at high compressions. System of $N = 30$, $\sigma = 0.2$ in a monomeric solvent

1.4 Brush in Polymeric Matrix: Results & Discussion

The same procedure can be followed to measure the interactions between brushes immersed in a polymeric solvent with a number of segments equal to that of the brush chains $P = N = 30$, the only other difference being that the set point of the barostat is now set to the bulk pressure of a Kremer-Grest 30-mer, $P_r^* = 4.99$. For the given grafting density, $\sigma = 0.2$, the system is just within the "Stretched Dry Brush" regime of fig. 1.9. Since the transition between the various regimes is not abrupt and the degree of polymerization is relatively low, we do not actually expect a fully collapsed brush. This is evident in fig. 1.18 where the density profile of the noninteracting brush is presented. While the brush is now more concentrated towards the wall and its height is significantly reduced with respect to its counterpart immersed in a monomeric solvent, there is still clear interpenetration between the brush and solvent chains while no clustering

is observed thanks to the high grafting density. In lack of a theoretical expression that can be used to estimate the brush height, like for the case of a good solvent, we take as maximum brush extent the distance from the wall at which the brush concentration drops below 1% of the bulk density, which occurs at $z_w = 12.2$

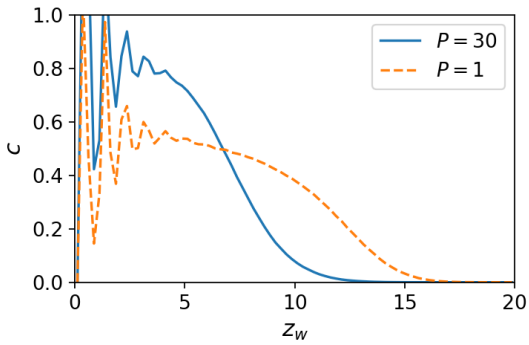

Figure 1.18. Density profile of brush with $N = 30$, $\sigma = 0.2$ in monomeric (dashed line) and polymeric solvent with degree of polymerization $P = 30$ (continuous line).

The net normal pressure between the opposing brushes at different separations is presented in fig. 1.19b. The situation is qualitatively different compared to the good solvent case: At high separations the interaction is slightly repulsive but right after after the initial brush contact — at h/h_0 between 0.8 and 0.9 — a weak attraction is observed in the form of negative osmotic pressure. This observation is in agreement with the theoretical treatments of systems of collapsed brushes that predict the onset of weak attraction due to the significant restrictions on the matrix chain conformations that lead to their expulsion from the brush. Further compression leads once again to repulsion as osmosis overcomes the entropically motivated attractive interaction between the brushes. Furthermore, from comparing the data of figs. 1.16 and 1.19 at high compressions, the presence of the polymeric matrix leads to significantly lower disjoining force for similar monomer concentrations, which is not surprising given that osmotic pressure is a colligative property.

One cannot help but notice the absence of results for other (lower or higher) values of the grafting density as well as longer chains. Considering the signifi-

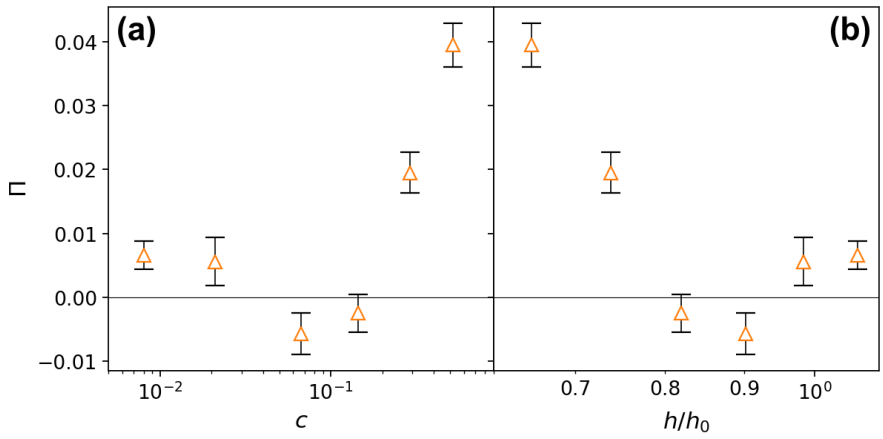

Figure 1.19. Osmotic pressure as a function of concentration (a) and separation distance normalized by the unperturbed brush height (b) for a system of $N = 30$, $\sigma = 0.2$ and $P = 30$. The concentration of the brush monomers in (a) is determined by the value of the density profile at the midpoint. Errorbars denote 95% confidence intervals.

cantly increased size of the system with the inclusion of the reservoir, the large relaxation times characteristic of polymers and the fact that each data point presented in fig. 1.19 corresponds to 3 distinct stages (equilibration, barostatting, production run), we have unfortunately not been able able to fully explore this topic due to time and computational power limits. These issues are only amplified by the inherently weak nature of the interactions that we are trying to observe, requiring even longer runs to obtain a satisfactory statistical accuracy, as evidenced by the relatively large errorbars on fig. 1.19. In any case, the developed methodology, initially validated on a good solvent system, has been invaluable in reinforcing the theoretically established connection between the dewetting of the brush and the appearance of weak attractive forces upon brush contact.

AVGVSTVS FRIDERICVS ROMANORVM IMPERATOR SEMPER

Chapter 2

Effect of Grafting on Nanofiller Structure

On the previous chapter we zoomed in on the interface between NPs and examined how the presence of polymer brushes can alter the interaction between opposing grafted surfaces. We focused on the case of flat brushes, for which there is a rich literature and should provide useful insights even for curved brushes. It is now time to move up on the size scale and try to elicit how the changes due to the chain grafting correspond to different dispersion states, always with respect to non-grafted, "nude", NPs. This topic has already been mentioned on the fly when discussing the work of Hasegawa et al. [50], who tested the effect of varying the grafting density. Recapping, they made the interesting observation that starting from nude NPs and increasing the grafting density initially improves dispersion. The dispersion gets progressively better until a critical value of the grafting density is reached, after which NPs begin to flocculate, forming increasingly bigger structures. Even more interestingly, the critical grafting density did not seem to be affected by the NP size and volume fraction. This however is not conclusive as both tested sizes of NPs (170 and 350nm) are much larger than the unperturbed size of the grafted chains, whose end-to-end distance is estimated to be around 25nm, meaning that in both cases the curvature is low enough for the brushes to be considered practically flat. In any case, the experimental re-

sults have been accompanied by numerical SCF calculations which show a strong correlation between the dispersion state of the NPs and the wetting state of the brush. It has already been shown that when opposing brushes transition from the wet to the dry regime, attractive forces develop between them, which can be responsible for the NP aggregation. It is therefore intuitive to assume that the best dispersion is achieved when the brushes on the NP surface are well wetted by the matrix, whereas flocculation is promoted when the matrix material is fully expelled from the brush.

2.1 NP Dispersion State & Brush Wetting

Other evidence connecting brush wetting with the nanofiller structure come from Green & Mewis [55]. As a basis of comparison they used the phase diagram of Maas et al. [56], which has been constructed from tracking the wetting behavior of a drop of polymer on a surface grafted with chemically identical chains. Molecular weight of the polymer drop and grafting density of the plate are varied, producing the phase diagram of fig. 2.1. The phase diagram reveals three distinct wetting zones: At low grafting densities we encounter the allophobic regime. The plate is not wetted by the droplet because of the interfacial tension between the plate and the polymer, which is not diminished significantly by the few tethered chains. As grafting density increases the surface gets compatibilized and eventually fully wetted by the droplet. This transition is characterized by a discontinuous change of the contact angle from finite values to zero, marking it as a first-order transition. The critical grafting density required to achieve complete wetting (σ^*) increases with the droplet polymer size, as longer matrix chains interact even more unfavorably with the flat surface. Adding even more grafted chains eventually leads to a gradual second-order phase transition towards autophobic dewetting. At this stage the droplet is only in contact with the brush chains, from which it has been fully expelled, forming two separate layers. Looking back at the flat brush theory, we remember that increasing the matrix chain length leads to quicker brush collapse, it is therefore of no surprise that the critical grafting density required to reach the autophobic regime (σ^{**}) decreases with the matrix polymerization degree. At $P = N$ the first and second

order curves intersect and there is a direct transition from the allophobic to the autophobic regime.

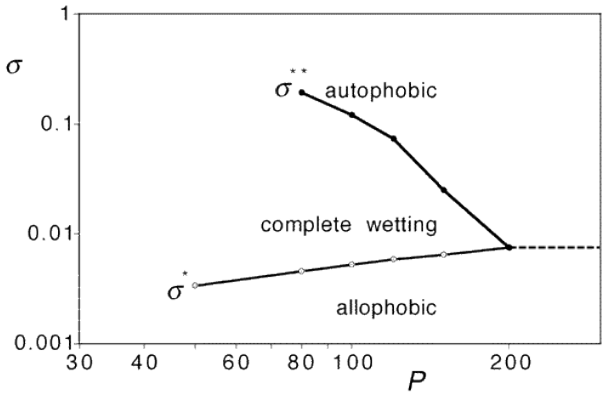

Figure 2.1. Wetting phase diagram in terms of the grafting density, σ, and the length of the chains of the polymer melt, P, for $N = 200$. The curve marked as σ^* passing through the open symbols represents the first order wetting transition at low grafting densities, whereas σ^{**} (filled symbols) corresponds to the second order transition at high grafting densities. Adapted from [56].

Green & Mewis [55] attempted to relate this phase diagram to the dispersion states of PDMS-grafted silica NPs in a PDMS matrix. For increasing matrix chain lengths they observed a transition from an agglomerated to a well dispersed state for increasing grafting densities (fig. 2.2). The parameter values at these transition points correspond to the first-order transition, while a second-order transition is never observed, probably because the grafting density required is not achieved in the experimental conditions, combined with the fact that $P/N < 1$ for all studied setups. A further confirmation of these observations comes from the experiments of Hart et al. [57], who also used scaling theory to identify that this first order transition closely coincides with the transition from the mushroom to stretched brush scaling regimes of the grafted chains. Such transition from a phase separated to well dispersed state with increasing grafting density has also been observed by coarse grained MD simulations of grafted particles [58], without any comment on the brush configuration. Interestingly, there is also the mention of an intermediate state of string-like aggregates, implying that this so-called

first-order phase transition may not be as abrupt as previously thought.

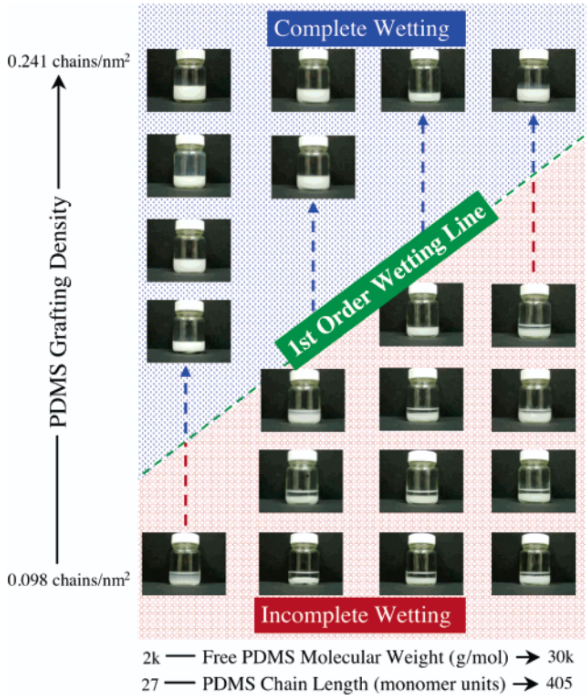

Figure 2.2. Wetting phase diagram of PDMS grafted silica spheres in PDMS melts. Silica volume fraction is 3% and grafted PDMS molecular weight is 36kg/mol. Taken from [55].

Further experimental studies have managed to capture the supposed wet to autophobic transition by increasing P/N to values significantly larger than 1 [59, 60, 61, 62, 63, 64, 65], leading to the formation of aggregates. Across the literature the critical values of P/N reported range from 2.5 [63] to 5 [64, 65], much higher than the theoretically predicted maximum of $P/N = 1$ for flat brushes. This departure from flat brush theory is linked to the much smaller NPs (diameter in the range of $10 - 20$nm) used in these experiments, which introduce the effect of curvature, with the general trend being that smaller grafted NP suspensions remain stable at higher matrix molecular weight. The mean-field theoretical study of Harton & Kumar [66] attempts to combine this observation

with the brush wetting, justifying the increased stability of smaller NPs with the fact that brushes on highly curved surfaces experience much less crowding with respect to their flat counterparts when moving towards the brush edge. This effect is illustrated in fig. 2.3 and can be thought of as an effective decrease of the grafting density at high curvature, which promotes brush wetting and thus NP dispersion. This interpretation however is somewhat lacking: Decrease of grafting density of a flat brush corresponds to a vertical downwards movement on the phase diagram of fig. 2.1, which for $P/N > 1$ can only lead to a transition from the autophobic to the allophobic regime, both of which are related to NP flocculation. It is therefore still unclear if the curvature has a more complex impact on the wetting behavior than just an apparent decrease of the grafting density or if, on a more fundamental level, the brush wetting behavior and NP dispersion state do not coincide.

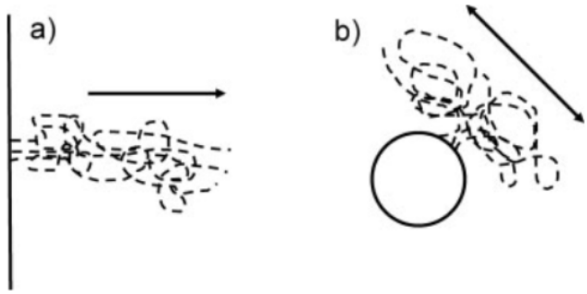

Figure 2.3. Sketch of polymer brush chain structure on (a) planar and (b) spherical surfaces. The arrow in (a) indicates the stretching normal to the surface due to steric repulsion with the neighboring (not visualized) brush chains, while the arrow in (b) shows the tangential spreading of the chains as the distance from the surface increases. Taken from [66].

Direct measurements of the brush height on the NP surface can aid in clearing up this issue. Neutron scattering experiments have demonstrated that the NP aggregation is closely associated with a significant collapse of the brushes [63]. On the same work, the individual spherical NPs are replaced with linear aggregates. This effectively decreases the curvature and results in the phase transition threshold shifting towards $P/N = 1$, highlighting the importance of

curvature as the main control parameter of the phase transition point while at the same time supporting the connection between wetting and NP dispersion. A similar relationship between wetting and dispersion is observed by implicit measurements of brush size from scattering spectra of grafted PNCs [62]. As for the big discrepancy between their observed transition point and $P/N = 1$, apart from curvature the authors propose as possible explanations the brush polydispersity and processing effects, e.g. the "entrapment" of the grafted NPs in a metastable dispersed state due to the dramatic decrease in their diffusivity induced by the interaction between grafted and free chains. They also highlight the gradual nature of the wet to dry brush transition, meaning that for P/N slightly larger than 1 the brushes are only partially collapsed and maintain a small degree of matrix interpenetration that could promote NP dispersion. This reinforces the idea that the wet to dry brush transition is closely related to the dispersion-aggregation one, with just a "delay" separating them given that the brush collapse precedes NP aggregation. Simulation studies of grafted spherical particles whose diameter is just 5 times that of the brush monomer unit [58] do not show any sign of of phase separation due to autophobic dewetting for values of P/N as high as 10, clearly demonstrating the crucial effect of curvature. The above points are nicely summarized by Sunday et al. [65], who managed to recreate the phase diagram of fig. 2.1 by checking the dispersion states of polystyrene grafted silica NPs. Dispersion regimes on fig. 2.4 qualitatively match those of fig. 2.1, with the main difference being that the maximum P/N value required to exit the wetting/well dispersed zone is around 5, essentially corresponding to a horizontal shift of the flat brush phase diagram towards the right.

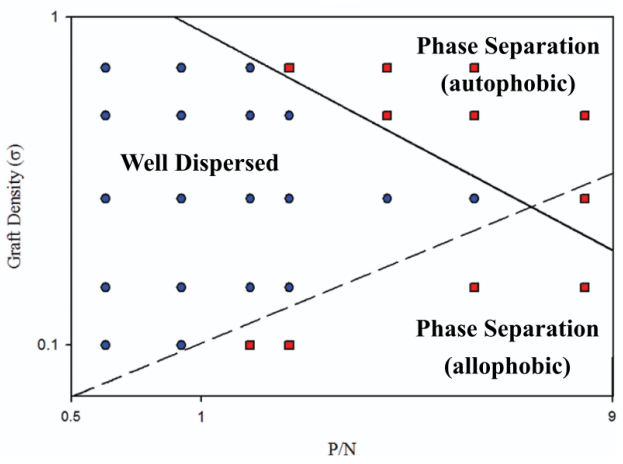

Figure 2.4. NP stability phase diagram with fits of the scaling lines for the (supposedly) autophobic (solid line) and allophobic (dashed line) phase transitions. The power law slope for the autophobic and allophobic transitions are -0.71 ± 0.04 and 0.54 ± 0.08 respectively. Adapted from [65].

2.2 Interactions between Grafted NPs

The relationship between brush properties and PNC phase behavior may also be examined indirectly by probing the interactions between individual NPs, pretty much following the example of the interactions between opposing brushes in the previous chapter. Due to technical limitations, studies of this type are limited either to simulations [67, 68, 69, 70] or other numerical approaches based on theory [71, 72]. In both cases, the main objective is to correctly predict the forces developing between grafted entities as a function of their separation, or equivalently, extract the potential of the mean force. Starting from the structure of the brush on a small spherical NP surface, coarse-grained MD simulations of NP pairs grafted with relatively short chains [68, 69] lead to the surprising finding that for P/N beyond 1 there are no significant changes in the brush density profile, with only a very slight extra expulsion of matrix material being observed for P/N taking values as high as 14. Even though the brush structure seems unaltered, the same cannot be said for the interactions between the grafted particles. Results

show categorically that at intermediate grafting densities increasing the length of matrix chains reduces the efficacy of grafting by reducing the range of the repulsive forces that are due to the brush interaction. At higher grafting density the effect is even more pronounced, eventually giving its place to the appearance of an attractive well. There seems to be a "critical" grafting density at which the onset of attractive interactions is achievable for reasonable P/N values, and that critical value seems to coincide with the point at which the grafted chains create a sort of "impenetrable" layer around the NP core, preventing it from interacting directly with the matrix (fig. 2.5). This paradoxical situation of the interactions changing without any apparent effect on the isolated brush structure is tackled by the numerical work of Trombly & Ganesan [72], who demonstrated that increasing P/N leads to slight decrease in the average penetration length of matrix within the brush, termed the "wetting length". By testing various values of P/N and particle sizes, wetting length comes up as the parameter dominating interbrush interactions. Starting from high wetting lengths, that is at low P/N and high curvatures, the interaction is purely repulsive. Increasing P/N and/or decreasing the curvature results in smaller wetting lengths which lead to the appearance of an attractive well, whose depth increases as wetting length drops.

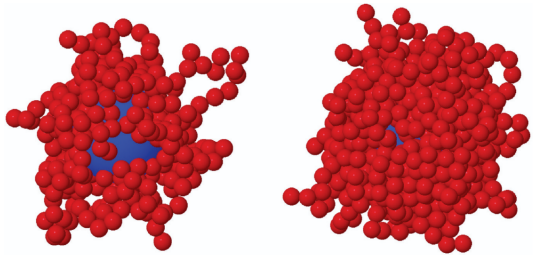

Figure 2.5. Snapshots of single particles at low (left) and high (right) grafting densities. The grafted particle diameter is 5 times the polymer bead diameter and chain lengths are $N = 10$ & $P = 70$. Matrix chains are not shown for clarity. Taken from [68].

Based on what has been mentioned up to now, high grafting densities should be avoided as they can lead to attraction between the brushes belonging to nearby NPs. At the sime time however, numerical results dictate that the coverage of

the grafted particle with a thick brush layer is fundamental in screening out the short range attractive interactions between NPs [71]. This inevitably creates a dilemma: Good coverage of the particle can lead to attraction due to Asakura-Oosawa depletion-like interactions between the dense brushes of the approaching particles, but on the other hand a lower grafting density may not be enough to prevent particle adhesion due to van der Waals or electrostatic forces. The solution to this conundrum becomes obvious by pointing out that all the aforementioned studies were performed for short grafted chains. By increasing grafting chain length while keeping the grafting density high it is possible to obtain both a very good coverage near the core while further away from the particle surface the particle curvature leads to a less dense brush that will interact more favorably with the matrix. Other ideas that can create a similar setup, such as using a mix of short and long chains for the brush, could prove beneficial but are beyond the scope of this study.

The results presented so far in this section are obtained through generic bead-spring type polymer models. A different approach is presented in the more recent computational work of Munaó et al. [70], where silica NPs, nude or grafted with polystyrene chains, are placed in a polystyrene matrix. Using a coarse-grained but realistic model that accounts for the chemical detail of the various species, they extracted the mean force potentials for various degrees of grafting and graft/free polymer lengths. Nude particles demonstrate strong attraction which is attributed not only on the dispersion and Coulomb interactions of the silica, but also on the depletion effect induced by the heavily deformed matrix chains that are found between the approaching particle surfaces, as illustrated in fig. 2.6a. The introduction of tethered chains of increasing length and at increasing grafting density dampens the attraction and eventually leads to effective repulsion between the particles. The interpretation of this result is based once again on the conformation of the polymer chains on the interface. With the addition of more and longer grafted chains, less free chains penetrate the interparticle zone, leading to weaker depletion forces (fig. 2.6b). This explanation is not in line with the state of the art presented in the previous paragraphs and does not provide a clear mechanism for the repulsive forces developing at high grafting densities and brush chain length. Comparison with previous works is made even

more difficult by the lack of (in silico) experiments on the effect of matrix length. As such, no conclusions can be drawn for that case and no instances of attraction due to autophobic dewetting are mentioned.

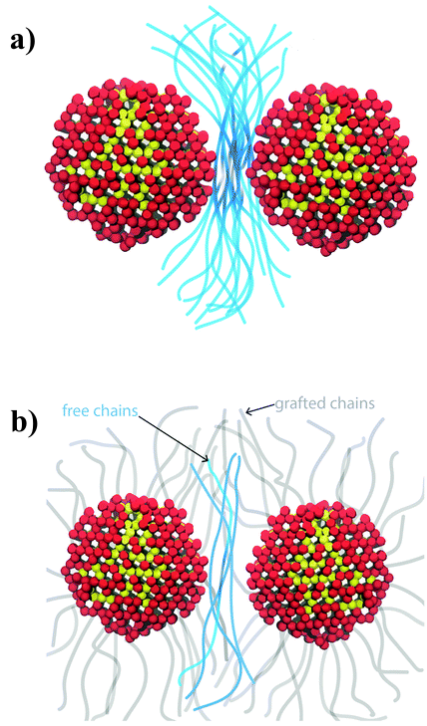

Figure 2.6. Snapshots showing confinement of free polymer chains between two nude (a) or grafted (b) NPs. Grafted and a subset of the free chains are illustrated in grey and blue, respectively. Taken from [70].

Apart from isolated pairs, the same researchers extracted the interaction potentials between particles in the vicinity of a third neighboring particle. For nude particles this leads to stronger attraction with respect to the 2-body case as the presence of the nearby third particle forces the matrix chains into even more entropically unfavorable conformations, as is seen on fig. 2.7. The situation is reversed when all three particles are grafted, as now the presence of grafted chains of the neighboring third particle displaces even more matrix chains from

the interface. Of special interest are the cases where the isolated pair exhibits attraction, but the introduction of the third particle leads to repulsion at all interparticle distances. It is thus clear that that the 3-body interactions can have a crucial effect on the overall dispersion state of a PNC and should be taken into account. This extra consideration steeply increases the complexity of the studied system, as the functional form of the 3-body potential will change unpredictably depending on the relative positions of the particles. This means that some approach directions may favor particle adhesion more than others, potentially giving rise to preferential aggregate geometries. The emergence of diverse filler structures owing to such phenomena will be discussed in the next section.

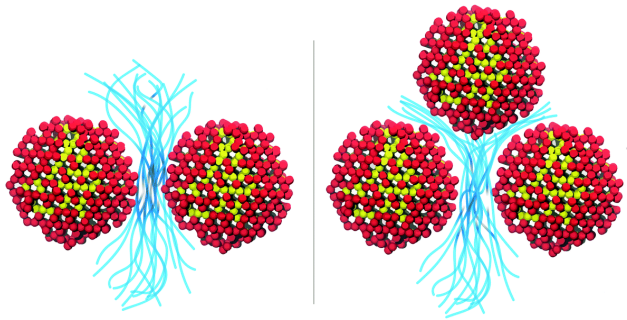

Figure 2.7. Snapshots showing confinement of free polymer chains between two (a) and three (b) NPs. Only a subset of the free chains is illustrated in blue. Taken from [70].

2.3 Anisotropic Assembly of Grafted NPs

As anticipated in the previous section, grafted PNCs carefully produced in a in a lab environment will result a multitude of organization states of the filler NPs, depending on the brush parameters of the composite. Most of these experimentally observed morphologies are also achievable by simulation and numerical studies and follow a similar distribution on the parameter space [73, 74, 75]. The general trend brought forward by these works is that as grafting density and/or grafted chain length increase, the filler transitions from forming spherical aggregates, to tetrahedral or hexagonal sheets, to strings, and finally to well-dispersed

individual NPs [73]. The role of curvature, even though not usually mentioned as a morphology defining parameter, is crucial. For successful reproduction of these complex structures NP size has to be comparable to the radius of gyration of the polymer brush chains. A rule of thumb is that smaller particles will produce uniform particle dispersions while larger particles will form amorphous agglomerates [74].

As is usually the case, real life is not as simple. The phase diagram of filler morphologies constructed by Kumar et al. [8] using available experimental data from third sources (fig. 2.8) shows that the various anisotropic filler structure regimes are not following a clear succession with respect to the mentioned parameters. In addition, an extra state of "small clusters" is observed. It must however be mentioned that the distinction between the different regimes is not always very clear, especially on the border between the "well dispersed" and "phase separated" zones, with many data points corresponding to different dispersion states sharing the same graph area. This is most likely due to the different materials and NP sizes used between collected data, highlighting once again the important role of curvature and polymer-NP interactions on the final filler dispersion state. The various methods used to measure grafting density between different studies introduce another source of uncertainty. On the other hand, it should be noted that in all but one cases silica NPs have been used, which means that the resulting phase diagram may be specific to the enthalpic interactions of silica. Comparison with numerical approaches should thus be done with caution.

By all accounts, the physical aspect responsible for the emergence of the aforementioned morphologies is the deformation of the brushes when two NPs are in close vicinity of each other. This effect is evident on fig. 2.9b, that shows an example of the brush density in the space surrounding two grafted NPs in contact. By taking one of the two NPs as a frame of reference, it is clear that the density profile is not homogeneous in the azimuthal direction. This is expected, as NP approach will lead to expulsion of the grafted chains from the zone near the contact area and towards the sides. The local increase in grafted chain monomer density will lead to further stretching of the brush in the surrounding area, with the effect being more pronounced near the point of contact. Instead, on the diametrically opposite point the effect will be minimal, as evidenced by

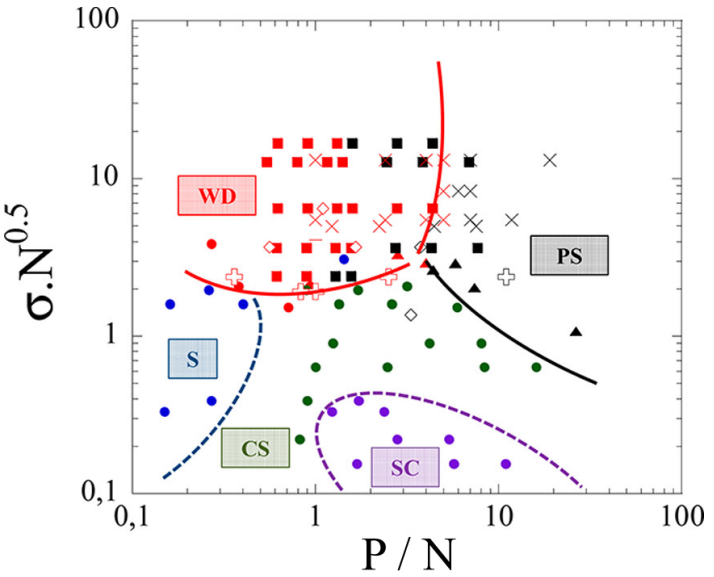

Figure 2.8. PNC morphology diagram with data coming from various experimental studies: Red points correspond to well dispersed (WD) particles; black to phase separated (PS) samples; blue to strings (S); green to connected sheets (CS) and purple to small clusters (SC). The color-coded lines are an attempt at classifying the data into regions in the plot where different morphologies occur. Square symbols are for 18nm PS-g-SiO_2 NPs [65], saltires for 10nm PEO-g-SiO_2 [64], rhombi for 17nm PS-g-SiO_2 [59], circles for 14nm PS-g-SiO_2 [73], triangles for 28nm PS-g-SiO_2 [62], dash for 12nm PBA-g-SiO_2 [76], and greek crosses for 8nm PS-g-γ-Fe_2O_3 [63]. Taken from [8].

the complete overlap of the red and blue curves in fig. 2.9e. We can now easily imagine that a third approaching NP will be more likely to adhere to or around that point where the "shielding" is thinner and less dense. The same is true for more approaching particles, thus promoting the formation of a string-like aggregate. If the grafting is not particularly dense, adhesion may be possible at angles closer to the contact point. Then, addition of a third particle defines a plane where brush density is lower, promoting the emergence of sheet-like structures. At even weaker coverage, there is not a particularly preferred direction anymore, leading to aggregates without a specific form. To put it simply, increasing the grafting efficacy leads to a decrease in the fractal dimension of the aggregates,

up until good dispersion is achieved, an interpretation that is fully supported by the computational and theoretical studies mentioned earlier.

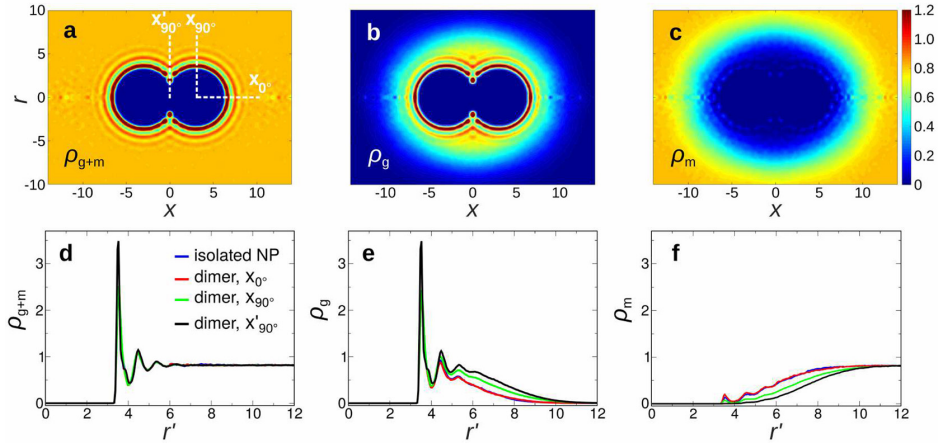

Figure 2.9. 2D contour maps of dimensionless monomer number density of the material surrounding two fused NPs. Cylindrical coordinates are used, with the $r = 0$ axis passing through both NP centers. Results are from coarse-grained MD simulations with $N = 20$, $P = 40$, $\sigma = 0.4$ and NP diameter 6 times larger than that of the chain monomer. (a) shows the overall density ρ_{g+m}, (b) the monomer density of the grafted chains ρ_g, and (c) the matrix chain monomer density ρ_m. The plots (d), (e) & (f) below each contour map show the corresponding 1D density profile along the traces drawn on (a). Taken from [77].

2.4 Structure Control of Industrial PNCs

The rich phase behavior of grafted PNCs that was presented in the previous section is characteristic of materials developed under strictly controlled laboratory conditions. Large scale industrial processes are generally more crude and such degree of fine-tuning is not usually achievable. A typical example is the reinforced rubber used in car tire manufacturing which results from mechanical mixing of the pre-vulcanized polymer with silica NPs that come in the form of pellets. These industrially used NPs may be added at volume fractions that can be as high as 30% and tend to exhibit significantly higher degrees of shape inhomogeneity and size polydispersity with respect to their lab-grown counterparts.

The filler structure of such materials has been explored in depth by Baeza et al. [78], who used a combination of scattering and imaging techniques on samples of simplified industrial PNCs consisting only of silica NPs and styrene-butadiene linear polymer chains. The possibility of grafting was introduced by using a 50-50 mix of unmodified and end-functionalized polymer that can attach to the silica through a silanol condensation reaction. Samples at silica volume fractions ranging from $8-21\%$ reveal a fractal filler network made up of highly polydisperse aggregates consisting on average of $40-50$ NPs each. The fact that the aggregate size remains pretty much the same for all silica volume fractions sparks curiosity, as higher filler content results in more available NP surface and less total functionalized chains. Assuming that all modified polymers do indeed attach to a NP, an increase in filler volume fraction should then be accompanied by a decrease in grafting density which can alter filler structure.

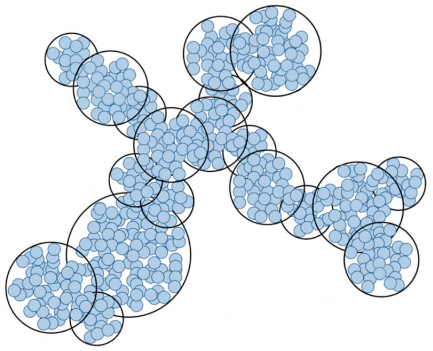

Figure 2.10. Schematic representation of the multiscale structure of an industrial PNC. The small blue spheres correspond to individual NPs while the black circles roughly represent the aggregates, which in turn organize into a fractal network. Adapted from [78].

To better understand the effect of grafting on the filler structure, further experiments were performed for different unmodified/functionalized chain ratios at constant filler volume fractions of 8.5 and 16.7% respectively [79]. Transmission electron microscopy (TEM) imaging of the sample slices reveal a gradual decomposition of the large-scale fractal structure into isolated aggregates as the

functionalized chain fraction increases from 0 to 100% (fig. 2.11). In addition, reduction of the aggregate size is confirmed through small angle X-ray scattering (SAXS). High (16.7%) volume fraction samples show a steady decrease of aggregate size with increasing functionalized chain fraction, whereas saturation is observed on the low volume fraction samples, with the aggregate size remaining practically the same for functionalized chain fractions above 25%. Our first instinct would be to relate the saturation of the aggregate size to the saturation of the number of grafted chains, but such an explanation is not acceptable. The increase of grafting density has been confirmed by measurement of the bound rubber and its effect is evident from the changes in the large-scale structure. Another seemingly paradoxical result also calls for an alternative mechanism: The high volume fraction samples consistently result in smaller aggregates [80], even though logic would dictate that the NPs in low volume fraction samples are more densely grafted. Once again, the breakup of the percolated fractal structure excludes the case of clustering due to brush autophobicity, that would instead lead to worse dispersion across all length scales. Instead, the answer more likely lies in the mechanics of nanocomposite mixing, as will be discussed in the next paragraph.

In the beginning of this section it was briefly mentioned that the industrially used NPs are usually added to the polymer matrix in the form of dust or pellets and then broken up during mixing. At this stage, the NP aggregates will assume their minimum size, which for a given mixing velocity will be determined by the viscosity of the material. Higher filler content does indeed increase the PNC viscosity and leads to improved aggregate breakup. After mixing stops these aggregates may or may not reagglomerate into larger structures and whether or not and up to what point that occurs can depend on various factors, including grafting. Indeed, for the simplified PNC described in this section, nominal grafting density has been identified as the sole deciding parameter of the final aggregate size [81]. Without getting into the details of its calculation in the experimental setup, it is defined as:

$$\rho_{D3} = \frac{\#\text{ of functionalized chains per unit volume}}{\text{total NP surface area per unit volume}}$$

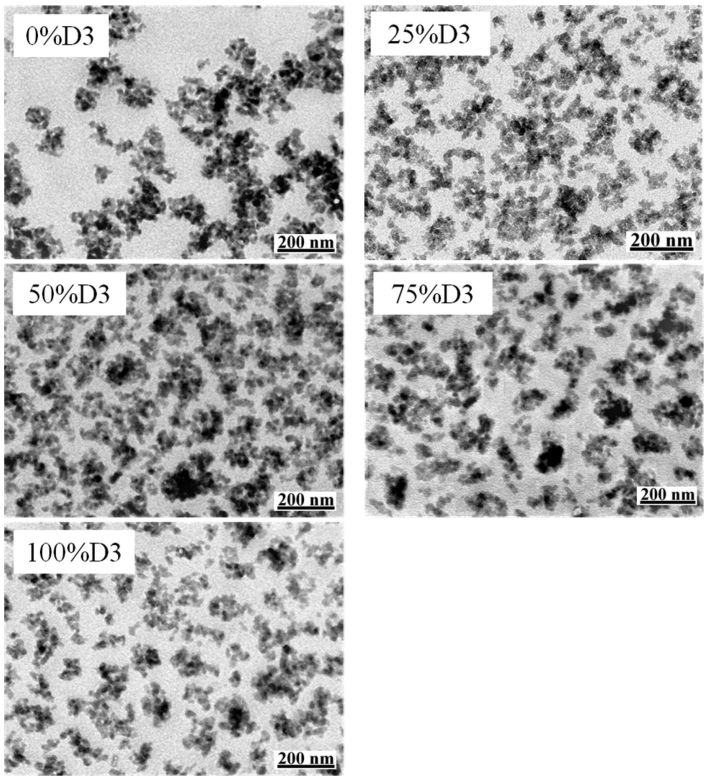

Figure 2.11. TEM pictures of silica/styrene-butadiene nanocomposites at 8.5% filler volume fraction. The D3 percentage listed on each panel corresponds to the ratio of functionalized chains in the polymeric matrix. Taken from [79].

This definition is equivalent to the actual grafting density if all functionalized chains homogeneously graft on the surface of the silica NPs. In the aforementioned studies they get into great pains to determine that the percentage of functionalized chains that actually graft is very high, ranging from practically 100% for low functionalization rations and approaching 80% even when all chains are functionalized! The culprit that actually makes real grafting density deviate from the above definition, that not all of the NP surface is available for grafting due to aggregate formation. Still, since the aggregates are generally small, typically consisting of 40-50 particles, it means that almost 80% of NPs will be on the

outer layer of the aggregate and thus most of their surface grafting sites will be available. As a result, if the condition that (almost) all active chains attach on the silica surface holds, the above definition should provide a fairly accurate estimate of the actual grafting density. Modifications that take into account the effect of aggregate properties on the reduction of available surface have been developed in later works, resulting in the "aggregate" grafting density, ρ_{D3}^{agg}. There exists then a critical ρ_{D3}^{agg} above which reagglomeration is suppressed [80]. This opens the way to two possible scenarios:

1. The critical grafting density is achieved during the mixing stage. Reagglomeration is suppressed and aggregates retain the size achieved during mixing, which is considered independent from grafting.

2. Aggregate size during mixing is too small to reach critical grafting density. As soon as mixing stops aggregates will start agglomerating. Agglomeration further reduces available surface, effectively increasing ρ_{D3}^{agg}. As soon as the critical value is achieved agglomeration will stop.

This proposed mechanism explains the results of [79], where aggregate size saturation is observed at low filler volume fractions, indicating that critical grafting density is already achieved at a functionalized chain fraction in the range of 25-50%. This is nicely illustrated in fig. 2.12, where aggregate size at two different volume fractions is plotted with respect to ρ_{D3}. Initially, aggregate size drops with increasing ρ_{D3} but it finally stabilizes at higher values. This means that critical grafting density is achieved for the minimum aggregate size and increasing it any further is pointless. This minimum size only depends on filler volume fraction, which is why smaller aggregates are recorded for higher filler content in that plateau region. A nice detail is that for both volume fractions the plateau is reached at similar ρ_{D3}, providing further support for this mechanism.

Although providing a very enlightening perspective on the factors affecting filler structure in industrial PNCs, the presented results also leave an open issue that could be the subject of future studies. An unexpected conclusion of the work performed on industrial NPs is that of ρ_{D3}^{agg} seemingly being the sole parameter affecting filler dispersion. This goes against experimental and theoretical evidence from sections 2.2 and 2.3 that show a strong dependence of the

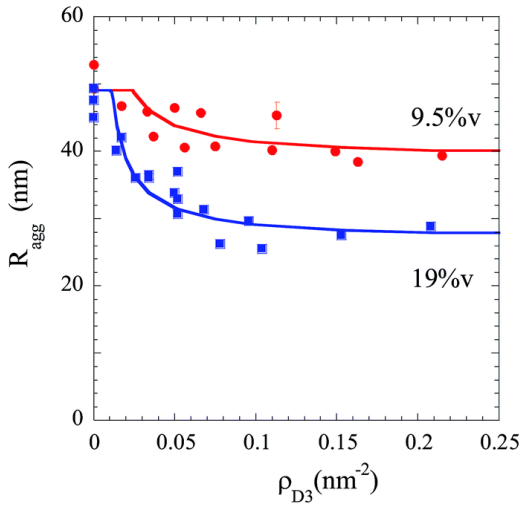

Figure 2.12. Average aggregate radius, R_{agg}, as a function of the nominal grafting density, ρ_{D3}, at two different volume fractions. Taken from [80].

interparticle interactions, and by extension their dispersion state, on the length of the grafted chains even when P/N remains fixed at 1, as is the case for all experiments discussed here. It could be that when the functionalized chains are longer, a decreasing fraction of them manages to bond with the silica surface due to steric obstruction provided by already grafted chains. That would lead to an overestimation of the actual ρ_{D3}^{agg} and might give the false impression that NP dispersion is independent of chain length.

2.5 PNC Filler Structure Emerges Solely from Interactions (?)

The results of the previous section point to an interesting implication: If NP aggregates are successfully broken up during mixing, the final filler morphology will be obtained solely as a result of post-mixing flocculation, which in turn is governed by the grafted brush properties. In sections 2.2 and 2.3 the connection between grafted NP dispersion state and brush-induced interactions has been

discussed in depth and significant proof have been presented in support of this relationship, reinforced by the fact that in all cases the grafting density of the industrial PNCs was much lower than the theoretically achievable maximum, excluding any saturation effects. We wish to explore this hypothesis for the particular case of industrial PNCs so as to provide useful guidelines that can aid in optimizing the fabrication process of these materials.

2.5.1 Simulation Methodology

In simulations studying the assembly of polymer-grafted NPs that have been performed so far, grafted and matrix chains were represented in a coarse-grained form, but always explicitly present [73]. Such an approach makes sense when just a small population of NPs is needed to obtain the simple structures observed in research-based model PNCs. For the case of industrial PNCs however, the filler structure is characterized by significant inhomogeneity which expands up to the micrometric scale. The amount of material that has to be simulated in order to capture these large-scale structures makes a fully explicit approach computationally prohibitive. Our only option is an implicit description of the matrix and grafted polymer, whose effect will be accounted for through the interparticle interactions. Since we already have a very good idea of the brush structure-interaction relationship, we only need the interaction-filler morphology connection in order to complete that conceptual series and make the jump from the microscopic scale of the brush to the mesoscopic scale of NP agglomerates. Considering the silica NPs as Brownian particles, their equation of motion may be obtained by ignoring the inertial term of eq. (1.14), giving:

$$\zeta \frac{\mathrm{d}\boldsymbol{r}_i}{\mathrm{d}t} = -\nabla U + \boldsymbol{W}_i(t) \tag{2.1}$$

All variables are equivalent to those described in section 1.2, with $\boldsymbol{r}_i$ now corresponding to the position vector of the NPs. It should also be noted that while ζ here has the same effect as in eq. (1.14), its role is conceptually different. While in the Langevin equation it acts as a damping parameter regulating the action of the thermostat, in Brownian dynamics it quantifies the friction the particle experiences when moving through the implicit solvent, the matrix polymer in

our case. In fact it is closely related to the viscosity of a Newtonian solvent through the fluctuation-dissipation theorem. The fluctuation-dissipation theorem can be modified to account for non-Newtonian viscoelastic solvents, such as the matrix polymer, whose relaxation can be described by the Maxwell model, e.g. a sum of exponential decay terms [82]. While important when studying the rheological properties of the composite, in the present work we are interested in the quiescent assembly of NPs, which happens at time scales large enough to render the viscoelastic character of the matrix irrelevant.

The interactions between NPs are modeled with the Hamaker potential, which is suitable for spherical particles made up of smaller Lennard-Jones particles [83]. A particle of radius a will interact with its neighbors with a potential U_H, defined as the sum of an attractive (U_A) and a repulsive (U_R) part:

$$U_A(r) = -\frac{A_{cc}}{6}\left[\frac{2a^2}{r^2-4a^2} + \frac{2a^2}{r^2} + \ln\left(\frac{r^2-4a^2}{r^2}\right)\right]$$

$$U_R(r) = \frac{A_{cc}}{37800}\frac{\sigma_{LJ}^6}{r}\left[\frac{r^2-14ar+54a^2}{(r-2a)^7} + \frac{r^2+14ar+54a^2}{(r+2a)^7} + 2\frac{r^2-30a^2}{r^2}\right]$$

$$U_H(r) = U_A(r) + U_R(r), \quad 2a < r \leq r_c$$

where similar to eq. (1.13), r is the euclidean distance between particle centers and & σ_{LJ} is the size of smaller the Lennard-Jones particles that the NP is supposedly made up of, meaning that σ_{LJ} must always be smaller than $2a$. A_{cc}, known as the Hamaker constant can also be defined through the Lennard-Jones parameters as $A_{cc} = 4\pi^2\varepsilon_{LJ}$, with ε_{LJ} being the attractive well depth of the Lennard-Jones potential. Our simulations are performed in reduced units where we set $2a = k_BT = m = 1$, k_B being the Boltzmann constant. The mass of a single colloidal particle, m, does not appear in eq. (2.1) and therefore does not affect particle dynamics but is given a value anyway in order to allow for the definition of a characteristic time scale. The cutoff distance of the Hamaker interaction, r_c, is taken equal to $6a$, the constituting Lennard-Jones particle diameter $\sigma_{LJ} = a/5$, and the friction constant ζ is set to 1.

We can now study the effects of brush induced interactions by simulating systems of particles for different values of ε_{LJ} or by directly changing A_{cc}, which is the more relevant energy scale for this system. Lower A_{cc} values correspond to better screening of the interparticle attractions due to grafting, whereas increasing A_{cc} is equivalent to decreased grafting efficacy in preventing NP adhesion. If we were to go ahead and perform simulations in a system of individual monodisperse particles with fully symmetric interactions we would be certainly disappointed, as it would only be possible to obtain neat small-scale aggregate geometries akin to those mentioned in section 2.3. As seen in the previous section however, industrial PNCs are instead characterized by the presence of highly polydisperse and unevenly shaped aggregates even after intense mixing, which are responsible for the formation of the inhomogeneous large-scale fractals during the post-mixing flocculation stage. It is therefore imperative to find a way to introduce these pre-aggregated entities into our computational model.

2.5.2 Aggregate Construction & Initial Configuration

Realistic aggregate geometries can be produced in an automated way by using simplified models coming from physics. The most commonly used one is the so-called random aggregation, which describes the formation of particle clusters by the addition of one particle at a time. The general strategy, known as a growth model, consists of the following steps [84]:

1. The new "aggregate" starts as a single particle
2. A new particle is released at a random point in the aggregate vicinity and starts executing a random walk
3. When it comes in contact with a particle already making part of the aggregate, there is a chance that it will "stick", joining it and increasing its aggregation number by 1
4. If it doesn't stick, it will continue its random walk in a legal (i.e. avoiding further overlap with the encountered particle) direction, bringing it back to step 3. If it sticks, the process restarts from step 2 unless the desired aggregation number is achieved, marking the end of the process.

Of course there are many modifications that can be made to accelerate this process. For example, if the roaming particle travels too far from the aggregate it can be "teleported" back in a closer location without changing the overall aggregation statistics. The main factor affecting the final aggregate characteristics is the probability of sticking during an encounter. In the extreme case of that probability being equal to 1, the particle will stick on the first encounter. This favors the growth of the outer parts of the aggregate that are more likely to be encountered first by the diffusing particle, which is why this scenario is named "diffusion limited cluster aggregation (DLCA)". The resulting aggregates are rather sparse and characterized by fractal branch-like structures, the "Brownian trees". On the other extreme, when the sticking probability approaches 0, the particle gets the chance to explore the interior zones of the aggregate, having essentially the same probability of adhering to any particle on the aggregate surface. This situation is referred to as "reaction limited cluster aggregation (RLCA)" and leads to more compact aggregates [85], as shown in fig. 2.13.

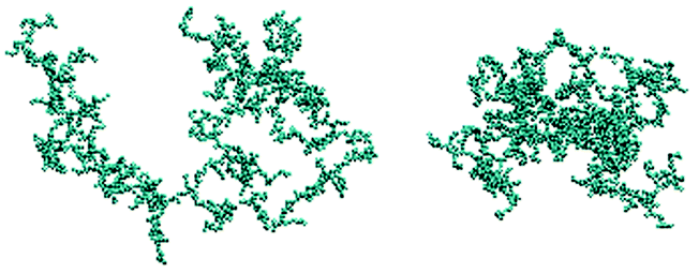

Figure 2.13. Typical examples of aggregates resulting from DLCA (left) and RLCA (right) processes.

For the small aggregates needed for our purposes, both DLCA and RLCA will produce similar shapes so we choose the computationally lighter RLCA [86]. This may look like a mistake at first, since the very low sticking probability means that each new particle addition will take much more time compared to DLCA. It is however the fact that in RLCA the particle has an equal chance to stick to any exposed point on the aggregate that we can take advantage of. Instead of simulating the whole random walk, a particle on the aggregate is chosen randomly

and a new "candidate" particle is placed adjacent to it at a random angle. If the candidate has a legal position, it unites itself to the rest of the aggregate and the process is repeated until the desired aggregation number. Figure 2.14 lays out this process in a clear manner.

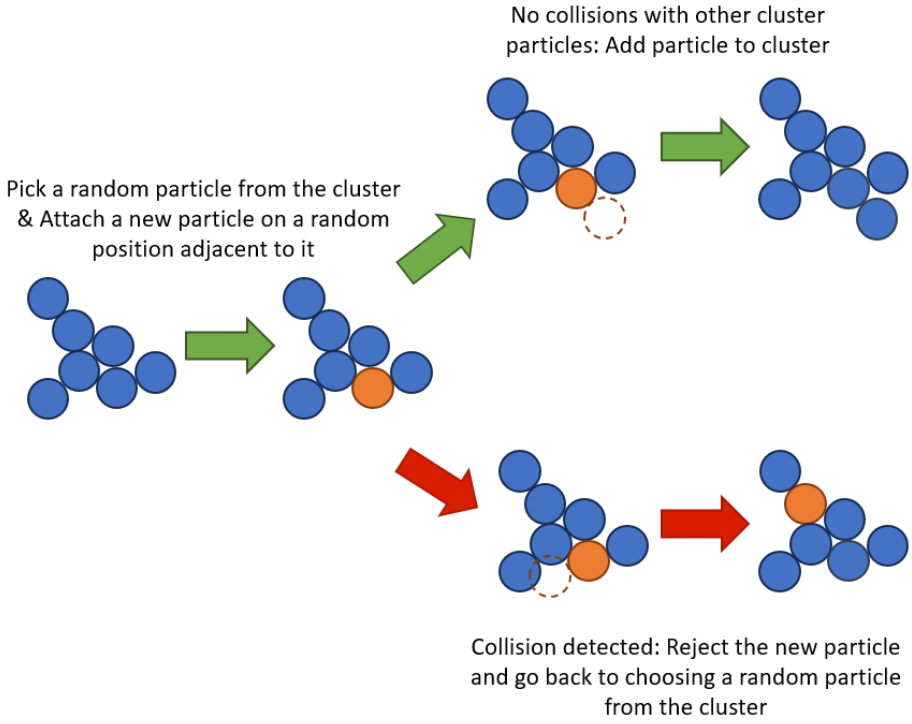

Figure 2.14. Schematic representation of the RLCA growth algorithm in 2D

The only input required for the construction of the aggregates is the aggregation number and of course how many of them we want in total. Since the aggregates discussed in section 2.4 are highly polydisperse, the aggregation number must also change on a per aggregate basis. Available data show that the aggregate radius of a reference system, R_{agg} follows a log-normal distribution with parameters $R_0 = 38.4$nm and $\sigma = 0.3$ [78]. Before assembling each aggregate we sample a radius from the distribution and calculate the aggregation

number from the ratio of the overall aggregate volume to the individual silica NP volume:

$$N_{agg} = \kappa \left(\frac{R_{agg}}{R_{\mathrm{Si}}} \right)^3$$

where for the silica NP radius we use the measured average $R_{\mathrm{Si}} = 8.9\mathrm{nm}$ and for the compacity (fraction of aggregate volume occupied by silica) a typical value of $\kappa = 0.35$ [78]. The resulting N_{agg} is then rounded to the immediately larger integer and the aggregate is constructed. It should be noted that this aggregate construction approach does not account for the the so-called *lacunarity*, i.e. a degree of overlap between the silica beads due to them fusing together on prolonged contact, which is typically present in these types of systems [87].

The growth model provides us with the aggregate shape, but we also have to come up with a way to retain it during the simulation run. To guarantee the rigidity of a 3D shape of this type from a topological point of view, each spherical NP acting as a building block has to be connected with a rigid beam to at least 3 other beads of the same aggregate [88]. Instead of rigid beams which are hard to implement in a Brownian dynamics setting, we use harmonic bonds. The potential between bonded particles is given by:

$$U_b(r) = \frac{k}{2} (r - r_0)^2$$

where r_0 is the original distance between the bonded particles and k the harmonic spring stiffness. The rule of thumb is that springs have to be stiff enough to prevent significant deformation of the aggregates but not to the point that the forces grow very fast even at small spring deformations, necessitating very small timesteps or risking the premature termination of the simulation due to floating point errors. We have found that $k = 100$ works well with a reasonable timestep choice of $\Delta t = 0.01$ and use these values for our simulations. Finally, the choice of the bonded neighbors also presents us with a dilemma: Choosing to bond together the nearest neighbors can significantly reduce computational costs, especially when running the simulations in parallel subdomains, but the resulting bond network is heavily localized and can lead to significant deformations of the overall aggregate. Increasing k within reasonable values results in at best

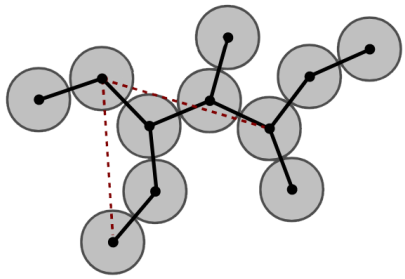

Figure 2.15. Schematic of aggregate connectivity. The springs between nearest neighbors are drawn in black solid lines. The springs placed on randomly chosen neighbors are shown in red dashed lines for just one particle. Taken from [82].

questionable improvement of the overall aggregate rigidity. Instead, we opt for a hybrid approach, where each bead is connected to its nearest neighbor to preserve the original aggregate connectivity and the other two bonded beads are chosen at random, as shown on fig. 2.15.

With stable aggregates available we can finally go on to perform our simulations. To prevent any overlaps before the beginning of the simulation, the aggregates are initially placed in a large cubic and fully periodic simulation box at distances that guarantee no interaction between them. A preliminary run is then performed, during which the box size in each dimension is reduced at a constant strain rate. If the box dimension initial size is L_0 and a final size of L_f has to be achieved within a preliminary run of total duration t_{pre} (in simulation time units), the size of the box side at each time instant is given by:

$$\frac{L(t)}{L_0} = \left(\frac{L_f}{L_0}\right)^{\frac{t}{t_{pre}}}$$

Finally, L_f is chosen based on the desired NP volume fraction, ϕ_{np}. For a system containing N_{np} NPs in total and once again ignoring lacunarity, the two quantities are related through:

$$\phi_{np} = \frac{4\pi a^3 N_{np}}{3L_f^3}$$

After the preliminary run the box size is kept constant and the system is

allowed to equilibrate, at which point the particle structure can be sampled. To obtain the results of the following section we constructed 8000 aggregates, totaling around 10^5 particles, and performed simulations at a final volume fraction $\phi_{np} = 0.167$.

2.5.3 Results & Discussion

Simulations have been performed for different values of ε_{LJ}, corresponding to increasing attractive strength between the NPs. To perform a visual inspection we have taken slices of the simulation box and present them in fig. 2.16. Comparing them with the TEM images of fig. 2.11 we notice an inverse relationship between ε_{LJ} and D3 percentage. Images at high %D3 show a well dispersed filler forming small aggregates, similar to what is observed at low ε_{LJ} in the simulations. On the other hand, at low %D3 the filler agglomerates into larger branches, which is also the case for the simulations performed at $\varepsilon_{LJ} = 2$. These comparisons reinforce the idea that increasing grafting density is effectively promoting dispersion by screening the attractive van der Waals and electrostatic forces between the NPs.

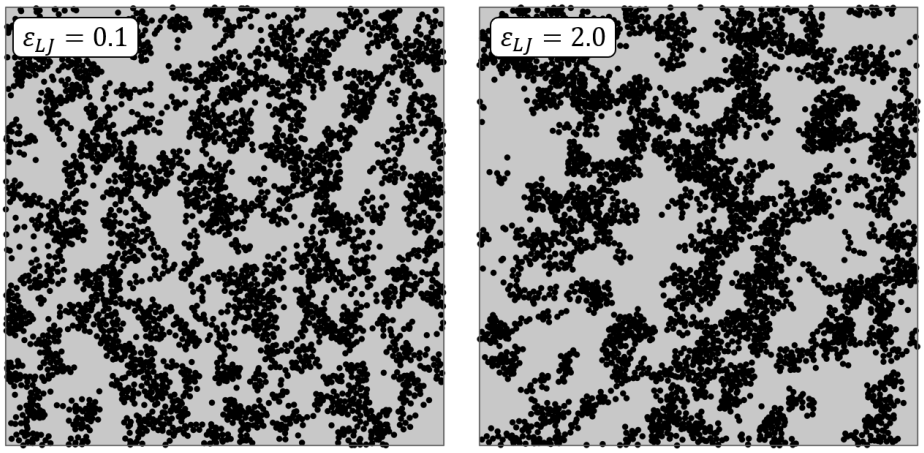

Figure 2.16. Snapshots from simulations performed at two different values of ε_{LJ}, listed on the top right of each panel. Left panel corresponds to less and right to more efficient grafting scenarios. Each panel is obtained by taking a slice of thickness $5a$ vertical to the viewing direction.

Despite providing useful insight, simulation snapshots do not constitute a quantitative measure of relative particle dispersion. Uniform systems, like the ones under scrutiny, are typically characterized by their radial distribution function (RDF), commonly symbolized as $g(r)$. The RDF of a simulated system is typically obtained numerically by separating the area around each particle into spherical bins and calculating the number density in each one, with a neighboring particle belonging at a given bin only if its center is found in it. The calculated per bin density is then averaged out over all particles and normalized with respect to the overall number density of the system, such that:

$$\lim_{r\to\infty} g(r) = 1 \tag{2.3}$$

Of course in a periodic simulation box the RDF can be determined for r no larger than half the system size, $l_f/2$. After that point no new information is added as the periodic image of the system is being sampled. While the RDF is informative of the small scale system structure and can be calculated with relative ease in simulations, it usually isn't an experimentally accessible quantity and is not really usable when trying to distinguish larger scale structure characteristics. It does however contain all the structural information of the system for $r \leq l_f/2$, information which can be rendered more accessible when viewed in the frequency domain by taking its Fourier transform. The resulting function is the static structure factor, $S(q)$ [89]:

$$S(q) = 1 + 4\pi\rho \int_0^\infty r^2(g(r) - 1)\frac{\sin(qr)}{qr}dr \tag{2.4}$$

where ρ is the overall system number density and the wavevector q is related to the real-space variable r through $q = 2\pi/r$. The minimum q is therefore achieved for the maximum value of r, giving $q \geq 4\pi/L_f$. The integration to infinity that is present in eq. (2.4) should not cause any worries as the second term in the integral drops towards zero relatively quickly, as implied by eq. (2.3). The numerical integration may therefore be truncated at the maximum value of r without any significant harm to the obtained result.

Still, the structure factor is not always directly accessible. SAXS experiments provide us with the scattering intensity, $I(q)$, which is "polluted" by the form

factor, $P(q)$, that describes the contribution of the particle shape and size on the scattering intensity [90]:

$$I(q) = I_0 P(q) S(q)$$

where I_0 is a constant prefactor. The form factor depends on the shape and size of the individual particles of the dispersed phase and as such may be difficult to determine for a real material characterized by size polydispersity and shape inhomogeneity. On the other hand, for the monodisperse spherical particles of our simulation we can use the theoretically predicted form factor [90]:

$$P(q) = \left(3\frac{\sin(qa) - qa\cos(qa)}{(qa)^3}\right)^2$$

By multiplying this with the structure factor we finally get a function proportional to the scattering intensity. Scattering intensities are calculated by averaging out the RDF over many simulation snapshots and performing the Fourier transform to obtain the structure factor. Our results are juxtaposed to experimentally obtained scattering intensities of silica/styrene-butadiene PNCs at the same volume fraction in fig. 2.17. There is qualitative agreement in the common region of the two graphs, with higher ε_{LJ} (lower %D3) corresponding to less aggregates of sizes ranging from approximately 80 to 200nm, as evidenced by the decreasing scattering intensity. Simulation data does not manage to capture the low-q upturn due to the large scale fractal structure of the filler, even though it should technically be detectable in the probed simulation length scales. This failure could be attributed to wrong conversion from the simulation to real units, meaning that the dotted lines should be shifted towards the left of the bottom panel of fig. 2.17. Other possibilities include degradation of the data near the lowest attainable q, as can be seen from the disordered oscillations of the curves on the top panel of fig. 2.17 or even the fact the low-q upturn in SAXS may be due to unbroken silica pellets in the experiments which are not reliably detected by TEM imaging [91].

Despite the aforementioned shortcomings, our results strongly support the proposed connection between chain grafting and NP interactions. We have been able to capture the complex filler structure of industrial PNCs with just a simple

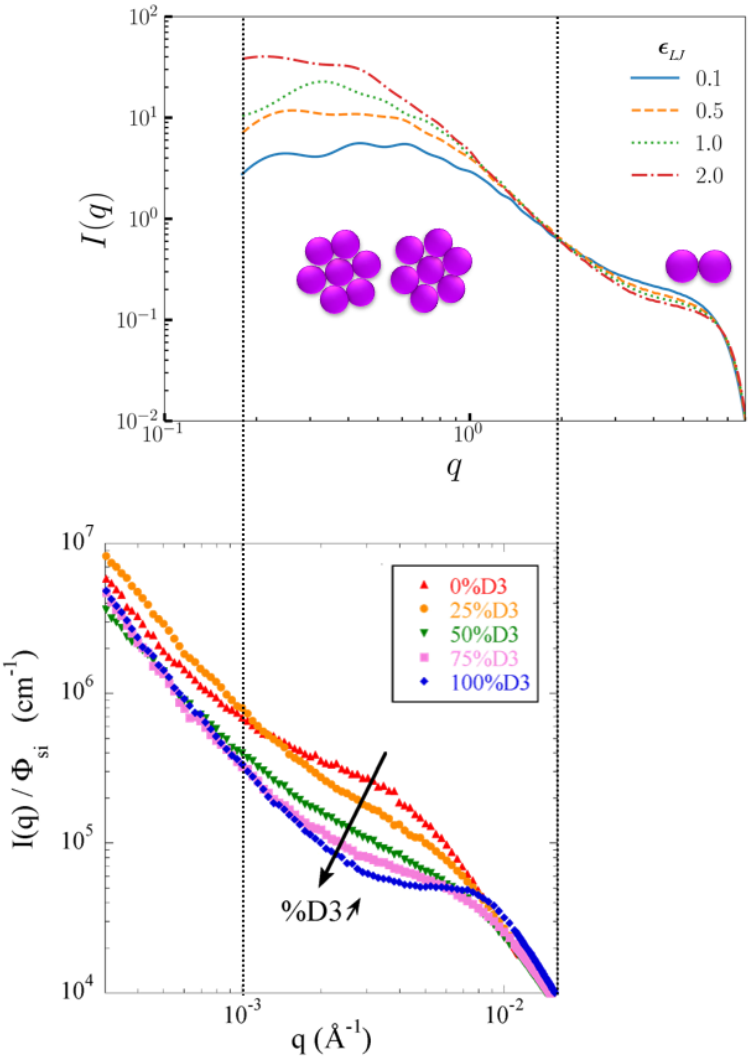

Figure 2.17. Scattering intensity as obtained from simulations (top) and SAXS measurements on a simplified industrial PNC [79] (bottom). Each curve corresponds to a different ε_{LJ} (top) or %D3 (bottom). Vertical dotted lines match the limits between the horizontal axes. The conversion from simulation to real length units was made by assuming that the simulation particles have a radius of 8.55nm. The cartoons drawn on the top panel show the typical structures probed at the corresponding length scales.

tunable pairwise potential acting between the particles without having to rely on complex many-body potentials that have been developed for the modeling of grafted NP assembly into organized structures [92]. We believe that it is the presence of the the highly disorganized aggregates that overshadows the more "sophisticated" interactions that develop between individual grafted NPs. As a result, instead of the well defined defined structures encountered in section 2.3 we observe highly heterogeneous agglomerates that can organize in large scale fractal geometries. Finally, and perhaps most importantly, we should note that the evolution in filler structure has been obtained with just a very simple change of the NP interaction strength. This goes along with the hypothesis that under good mixing conditions, i.e. optimized breakup of the initially aggregated NPs, the filler structure in the final product will only depend on the grafting parameters.

AVGVSTVS FRIDERICVS ROMANORVM IMPERATOR SEMPER

Chapter 3

Sheared Polymer Brushes

In the previous chapters we mainly dealt with the behavior of brushes and grafted NPs in static or quasistatic conditions. Only in section 2.5 there have been mentions of the interplay between the dynamic mixing conditions and the post-mixing quiescent stage when it comes to industrially relevant PNCs. To recap, it is during the mixing stage that the NP pellets/grains are broken up and the minimum aggregate sizes are obtained. As soon as mixing stops, reagglomeration may be observed. Whether or not and at what degree that happens depends on the efficacy of grafting. In that same section we studied that behavior by assuming that mixing is optimized and results in the smallest possible aggregates, effectively taking it out of the equation. We will now move to the other extreme scenario, where grafting is efficient enough to prevent any reagglomeration. This means that mixing is now the defining step during which the final filler structure emerges.

Mixing of industrial PNCs is characterized by temperature constraints. Irregardless of the sample formulation, the same final temperature has to be reached to promote grafting-to reactions during mixing, typically achieved by a combination of controlling the speed of the mixer rotor and preheating the mixer at a desired temperature. On the other hand, the determining factor of aggregate breakup is the mixture viscosity. A higher viscosity at the same mixing temperature will lead to bigger shear stresses that can fragment the aggregates into progressively smaller clusters. Linear viscoelastic data of PNCs obtained

at various grafting densities [79] provide an overview of the effect of the degree of functionalization on rheological properties. At low frequencies the exponents of both viscoelastic moduli decrease with %D3 as grafted chains cannot reptate. Viscosity increases and the sample becomes more gel-like. One should not however forget that these samples have gone through the post-mixing reagglomeration stage and the differences in their rheological response are also due to the differences in filler structure caused by altering the proportion of functionalized chains. In the linear regime this change is visible at higher frequencies, allowing for the isolation of the two effects [91].

Nonetheless, it is still not clear how grafted chain presence will exactly affect the material behavior during the strongly nonlinear flow conditions encountered during nanocomposite mixing that heavily alter filler structure with respect to the linear regime. The only indication we have so far comes from the thermomechanical characterization of the process. Tracking of the mixing process reveals that grafted PNCs are thicker and more torque is required for their mixing with respect to their ungrafted counterparts [79, 93]. This behavior can be explained intuitively by imagining the brush and matrix chains interpenetrating and promoting the transmission of stresses across the bulk of the material. The simplest model to test this and other hypotheses is to place a flat brush under a sheared matrix, mimicking the surface of an individual grafted aggregate in a bulk material that undergoes shear mixing. Another option is that of two flat brushes sliding past each other, a situation that can be encountered at the interface of two nearby NPs or aggregates constrained to relative movement due to mixing, as shown in fig. 3.1.

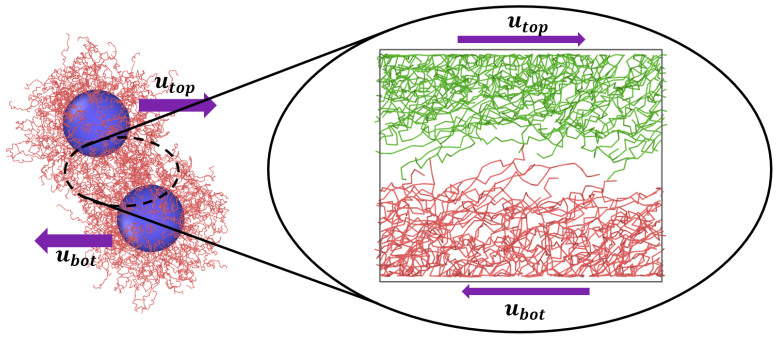

Figure 3.1. Schematic of two grafted NPs moving past each other at with velocities u_{top} and u_{bot} (left). The interface between them may be approximated by two grafted flat plates sliding past each other in opposite directions at the prescribed speed (right). Chains grafted on the top surface are painted green, while those on the bottom are red.

3.1 Sheared Polymer Brushes in Good Solvent

Imposing a shear flow on the solvent surrounding a polymer brush will alter its structure, given that the flow is strong enough. The vast majority of the early theoretical works on single polymer brushes in a good solvent at the semi-dilute regime and under shear flow utilize the scaling theory and predict a significant increase of the brush height [94, 95, 96] with increasing shear rate, the only exception being the work of Rabin & Alexander, where no dependence of brush height on shear rate is found [97]. The SFA experiments of Klein et al. [98] also hinted at the onset of brush swelling, with a sudden increase in normal forces detected above a critical shear rate between initially uncompressed brushes. This effect has been tested computationally with simulations using implicit [99, 100, 101, 102, 103, 104] and explicit [105, 106] solvent and no brush swelling has been observed. Instead, the brush chains are indeed being stretched above a critical shear rate but they also tilt in the flow direction, leading to the brush height remaining essentially constant or even decreasing significantly at high shear rates, as illustrated in fig. 3.2. The same picture is provided by the experiments of Webber et al. [107], who found that the hydrodynamic thickness — and by extension the height — of the brush does not depend on shear. Even direct

measurements through neutron reflectometry [108, 109] show no alterations of the brush density profile with changing shear, although these studies should not be considered definitive as the explored range of shear rates falls significantly below the supposed critical value required for swelling.

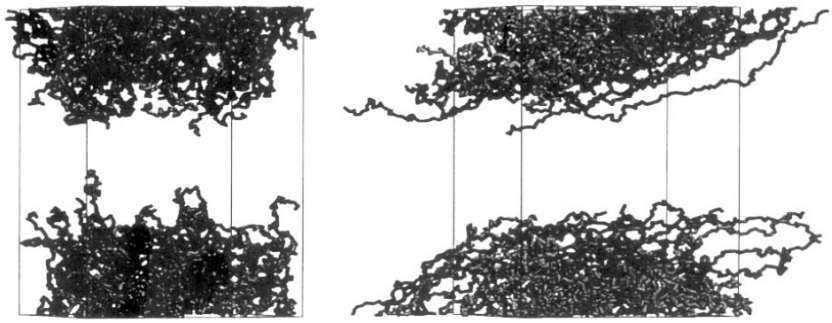

Figure 3.2. Snapshots from simulations of noninteracting brushes in implicit solvent. At low shear rates (a) the brush is still in the linear regime and no deviation from the equilibrium structure is observed. At shear rates deep within the nonlinear regime (b) there is significant stretching accompanied with tilting of the chains. Taken from [106]

Apart from the structure of isolated brushes, the tribological properties of compressed brushes are of special interest due to their possible applications as lubricants between sliding surfaces, particularly in biological systems such as the mammalian joints [110]. SFA experiments confirm the excellent lubrication properties of brushes in a good solvent [111], with the shear forces between them being undetectable up to high compressions. The measured normal forces are always higher by at least an order of magnitude, even though a direct comparison is not possible since the measurements have been normalized using the Derjaguin approximation, which has no clear physical interpretation for the shear forces. In any case, one can safely infer that the friction coefficient, defined as the ratio of shear to normal force, will steadily increase as the brushes get progressively compressed. Further experiments by Schorr et al. [112] reinforce this idea and also record a sublinear increase of shear stress at high apparent shear rates, effectively separating the brush response in a linear "Newtonian" and a shear-

thinning "non-Newtonian" regime. Simulation studies on the friction between sheared flat grafted surfaces [106, 103, 112, 113] have shown a qualitatively similar evolution of normal and shear stresses with separation and wall velocity, the main difference being that experiments mainly capture the linear regime whereas simulations are much easier to perform in the non-Newtonian regime since the very low shear rates required to probe linear behavior do not permit the accurate measurement of the shear force. The shear-thinning behavior is explained on the basis of the decreasing interpenetration as the relative velocity between the two brushes increases, and the chains tilt and orient in the flow direction [114]. The reduction of the friction between the opposing brushes is also mediated by the solvent which acts as a lubricating fluid layer. As for the lubricating properties of such systems, that is the relationship between normal and shear stresses developed during shear, one has to rely on simulations performed with explicitly present solvent molecules [106, 113] for accurate results. These studies affirm the increase of the friction coefficient as the gap size decreases, with an interesting observation being that normal stresses depend weakly on shear rate, remaining essentially just a function of separation with no substantial difference from the case of static brushes. The only qualitative difference between experiment and simulation is the nonmonotonic behavior of the friction coefficient for the simulated system, which slightly decreases as the compression overcomes a critical value. From a physical point of view such nonmonotonic behavior makes sense since the normal stress has been shown to diverge as the volume fraction of the brush within the pore approaches unity. On the other hand, the brush chains in the experimental system will eventually reach a glassy state as their concentration increases, leading to a solid-like behavior that will dramatically increase friction [111]. Such transition to the glassy state is not achievable in the computational description of the brush setup which is typically based around purely repulsive coarse-grained chains. That could be the reason behind the discrepancy in the functional dependence of the experimental and computational friction coefficients at high compressions.

A first attempt at modeling the linear response of sheared compressed brush bilayers in a good solvent was made by Klein [115], who provided explicit expressions for the shear stress and friction coefficient for sheared brushes at intermedi-

ate compressions[4] as a function of the brush and solvent properties, separation, and sliding velocity. A scaling relation for the viscosity of highly compressed molten brushes as a function of sliding speed at constant gap width was developed by Semenov [116], giving $\eta \sim u^{-0.5}$ in the nonlinear regime, u being the relative sliding speed. This exponent is very close to those presented in later works [117, 118], in which relevant scaling laws for the chain stretch and shear rate in the semidilute and melt states were extracted. In their approach, the linear to nonlinear transition is dictated by the brush Weissenberg number, defined as the product of the apparent shear rate with a characteristic relaxation time, $Wi = \dot{\gamma}\tau_s$. MD simulations were performed in the same works and τ_s was set as the inverse of the shear rate at which brush chain elongation in the form of a significant increase of their end to end distance is first observed, such that τ_s conceptionally corresponds to the terminal relaxation time of the brush chains. When chain stretching and shear stress data from different brush setups were normalized using their value at $Wi = 1$ they collapsed on a single curve as a function of Wi, revealing a universal scaling behavior. A similar procedure was followed by Desai et al. [119] for the case of weakly compressed brushes, with both approaches having the drawback of not being able to provide an accurate estimate of τ_s *a priori*, having to rely on the monitoring of chain stretching to set $Wi = 1$. Nevertheless, a wrong value of τ_s will not change the scaling relations deep inside the linear or nonlinear regimes, which for the case of compressed brushes are nicely summarized in Table 1 of the review by Kreer [114].

3.1.1 Changing Solvent Quality/Molecular weight

Changing the quality of the solvent from good to (near) theta or even poor has also been addressed by various studies [120, 112, 121, 122]. The common conclusion is that the lubrication properties of the brush bilayer worsen significantly as solvent quality drops. The main reason for the increased friction is the collapse of the brush towards the wall for bad solvents, which means that for the same applied normal stress the brush concentration will be higher and the

[4]For clarity, the intermediate to high compression transition is achieved when the density profile of the brushes becomes almost uniform. For semidilute brushes this is considered to occur at compressions $\sim h/h_0 = 0.5$

gap length smaller, leading to more collisions between the opposite grafted chains and a higher apparent shear rate. This situation is further amplified by the now effectively attractive interactions between the opposing brush monomers, which obviously cause the shear stresses to rise.

Similar to changing the solvent quality, increasing its molecular weight should lead to lubricity-reducing effects, at least at shear rates low enough that its non-Newtonian character is not demonstrated. To our knowledge, the only works including a polymeric solvent are those of Pastorino et al. [123, 124], who deal with isolated brushes under shear at a large range of grafting densities. Through MD simulations of unentangled coarse-grained polymers they track down the characteristics of the brush–free polymer interface and the slip properties of the grafted coating, not providing any insight on potential interactions between opposing brushes. The main observation is that at although at high grafting densities the brush–melt interface becomes increasingly smooth it still acts as a sticky boundary for the melt even at high shear rates. It would be also interesting to see if there are any changes in the shear response of the brush as free and/or grafted chains exceed the critical entanglement length, a case that to the best of our knowledge still remains unexplored.

3.2 Non-Steady Shear

Non-steady shear flows also present themselves as interesting case studies due to their prevalence in typically brush-lubricated systems such as the aforementioned case of mammalian joints. Spirin et al. [125] extended the scaling approach to the case of flow inversion assuming that the brush is initially tilted in a steady shear regime. Shortly after the inversion, the brush will temporarily assume an "upright" position before eventually tilting in the opposite direction, leading in a short-term increase of the brush height/interpenetration. This process, illustrated in fig. 3.3, could be accompanied by an increase in the friction and normal forces that will be easier to observe at inversion frequencies comparable to the characteristic time of the brush angle inversion, offering an alternative explanation to the early experiments of Klein et al. [98]. The hypothesized increase in interpenetration has been confirmed by MD simulations [126], while Doyle et

al. [103] also suggest a significant swelling of the brush. Grest [127] attributes this finding to the fact that the shear amplitude used is comparable to the distance between grafted points, which is irrelevant to experimental conditions and it most likely is monomeric resonance that leads to swelling. On the other hand, Ji & Ding [128] demonstrated that an increase in normal forces can be observed at a critical frequency without any increase in brush height, while the overshoot of the friction forces during the inversion has been confirmed by simulations [125], under the condition that an explicit description of the solvent is adopted.

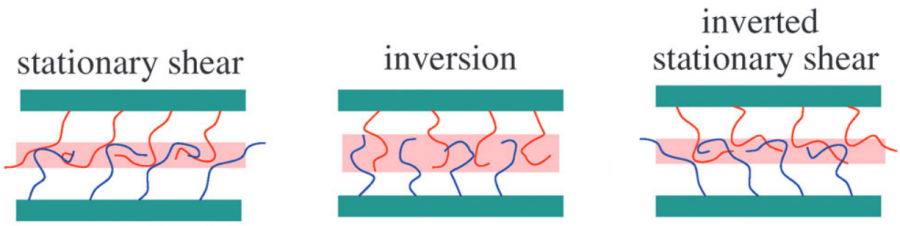

Figure 3.3. Schematic representation of the evolution of brush structure during shear flow inversion at $Wi \gg 1$. The top surface initially slides to the right (left) as evident from the chain tilt. Shortly after inversion (middle) the brush chains start changing orientation, passing through the vertical and increasing interpenetration, which is signified by the pink zone. After some time, steady shear in the opposite direction is established (right). Taken from [114].

3.3 Simulating Opposing Sheared Brushes

The methodology for simulating opposing flat brushes in relative motion is practically identical to the one described in section 1.2 before the introduction of the reservoir, which is not necessary since we are interested in the measurement of shear and not normal stresses this time. There are only two simple modifications that have to be made on the no-reservoir model to render it suitable for brushes undergoing shearing motion:

1. The walls used in our simulations are smooth and cannot transfer momentum in the shear direction. Instead, shearing motion is introduced by

imposing a steady velocity on the x-direction on the previously immobile beads representing the grafted ends. The beads will then drag the rest of the grafted chain with them, which will interact with and transfer momentum to the matrix chains, mimicking the effect of a no-slip condition on the wall surface. For a desired apparent shear rate $\dot{\gamma}$, the relative velocity between the opposing walls is $u_{rel} = \dot{\gamma} L_z$, L_z being the box size in the z direction. There are many ways to achieve that relative velocity and we choose to do it by setting $u_{top} = u_{rel}/2$ on the top and $u_{bot} = -u_{rel}/2$ on the bottom grafted ends.

2. Changes such as introducing shear that impose a velocity profile in the system can be problematic in conjunction with the use of the Langevin thermostat, as the dissipation term will act both on the thermal and the bulk constituents of the velocity vector components of the particles, resulting in an unphysical extra friction force. If the velocity field is known *a priori* it can be subtracted from the velocity appearing in the friction term of eq. (1.14) and remedy this issue. When this is not the case, like in our simulations, one can opt for the usage of a different thermostat. A typical choice is the dissipative particle dynamics (DPD) thermostat that works by applying the random and friction forces in a pairwise fashion, only accounting for the relative velocities of the particles. A simpler solution that has been shown to work just as well in cases of not too strong flows is to simply turn off the thermostat in the flow direction [129]. We opt for the second which means that only the y and z components of the white noise and the friction force terms will remain active.

3. Similarly to the previous point, the existence of a macroscopic velocity field will alter the results of stresses calculated using eq. (1.15). For fast flows the first term that corresponds to thermal motion will be artificially increased by if particle velocity due to macroscopic flow is included. Since stress calculation is a post-processing step, it is possible to first determine the steady-state velocity profile and then subtract the bulk velocity from the velocity vector of each bead depending on its position. A simpler way is to ensure that our system is well thermostatted, i.e. temperature is constant

in z-direction, in which case:

$$\sum_{k=1}^{N_V} m_k u_{k_i} u_{k_j} = \begin{cases} \frac{N k_B T}{3V}, & \text{if } i = j \\ 0, & \text{if } i \neq j \end{cases} \tag{3.1}$$

which means that the thermal contribution can be completely ignored during the calculation of shear stresses! This allows for the correct calculation of the apparent shear viscosity of the system, defined as $\eta = (P_{xz} + P_{zx})/2\dot{\gamma}$.

The choice of simulation setup is one that permits isolating the effect of grafting on rheological characteristics while all other system properties remain unaltered. For all subsequent runs we pick short chains ($N = P = 20$) that are well within the unentangled regime and use a cubic box with side size $L = 22.7$. The last choice represents a PNC being mixed at constant volume fraction with the consequence that the average distance between aggregates does not change. The effect of different degrees of matrix chain functionalization is explored by performing simulations at grafting densities in the range $[0.04, 0.38]$ and for shear rates in the range $[0.002, 0.1]$. These parameters were chosen so as to prevent overlap of the opposing brushes even at the highest grafting density, as shown in fig. 3.4. The equally — if not more — interesting case of overlapping brushes under shear will hopefully be tackled in the future. The rest of the relevant simulation parameters are set according to the values presented in section 1.2.

3.3.1 Results & Discussion

Figure 3.5 shows the velocity profiles for various grafting densities at the same apparent shear rate. The brush essentially acts as an extension of the wall upon which it is grafted, dragging the matrix material with it at the wall velocity and creating a plug flow regime near it. Predictably, the plug flow zone is thicker for higher grafting densities, immediately followed by a linear velocity profile in the interbrush zone that is populated almost exclusively by free chains. It is in this zone that shearing effectively takes place, resulting in shear rates much higher than the apparent one, signified by the black dashed line. This increase in the

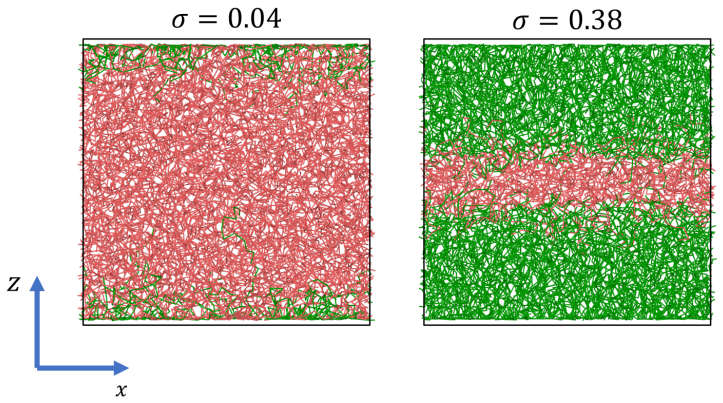

Figure 3.4. Opposing brush simulation setups used in this section. Snapshots of equilibrium configurations are presented for the minimum (left) and maximum (right) grafting densities used. Grafted chains appear in green and matrix chains in red.

shear rate within the matrix film means that systems of higher grafting density will develop higher shear stresses for the same apparent shear rate, leading to an increase in their apparent viscosity. The only exception is presented by the points corresponding to the lowest grafting density, that exhibit a small plug flow zone near the wall but then drop slightly below the no-slip prediction. Clearly, at such low grafting densities the brush is not dense enough to fully entrain the matrix chains and force them to match its speed. It should be noted that while this effect provides a nice insight on the flow state within the brush, it is "artificial" and can only be observed because of the perfectly smooth walls adopted in our simulations.

The expected increase in apparent viscosity is illustrated in fig. 3.6 where it can be seen that higher grafting density brushes will result in higher shear stresses at all examined apparent shear rates. At low grafting densities it is also possible to observe the transition from the Newtonian to the non-Newtonian shear thinning regime at $\dot{\gamma} \approx 10^{-3}$. To check the validity of this value we performed simulations of equilibrium chains of length 20 in the melt state and obtained their characteristic relaxation time, $\tau_p \approx 2 \times 10^3$, which corresponds to a critical shear rate $\dot{\gamma}_{cr} \approx 5 \times 10^{-4}$ signifying the border between the Newtonian and shear

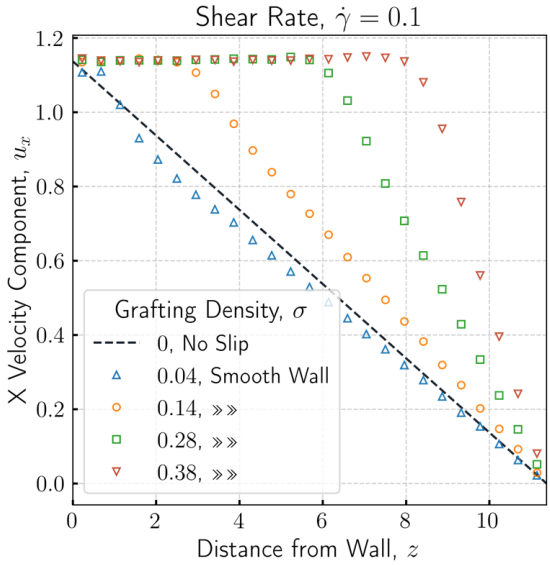

Figure 3.5. Velocity profiles of brush and matrix monomers at different grafting densities and at the prescribed shear rate. The dashed black line represents the velocity profile expected by imposing a no-slip boundary condition on the wall in the absence of grafting. The right edge of the graph where $u_x = 0$ for all grafting densities corresponds to the z coordinate midpoint.

thinning zones. The critical shear rate values predicted with the two methods are quite close, at least for the low grafting densities. At the highest grafting density the Newtonian plateau is not as easy to discern, probably due to the significant increase in the effective shear rate experienced by the matrix film in the interbrush area.

To sum up, it looks like chain grafting can also affect NPC dispersion by promoting aggregate breakup during the mixing by enhancing the transmission of shear stresses between the matrix polymer and the aggregates. Improved rupture/erosion of NP aggregates due to increased viscosity is supported by the available theoretical models and experimental data [130] but we are not yet in a position to compare our computational approach to a real life scenario. In the simulation environment going from low-medium to intermediate-high grafting densities results in just marginal increase in the mixture viscosity which may be

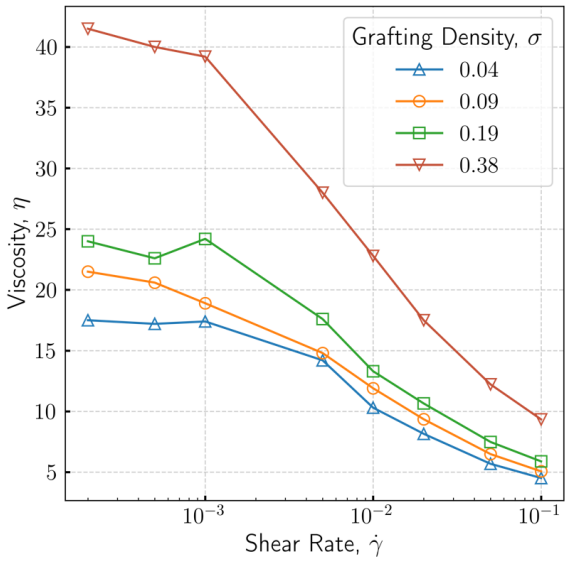

Figure 3.6. Apparent viscosity of the opposing brushes at various grafting densities as a function of the apparent shear rate.

too weak of a change to induce aggregate breakup. It is only when going to very high grafting densities that significant differences become evident. It is however at high grafting density where NP aggregation may occur due to autophobic dewetting of the surface brushes, possibly leading to an interesting optimization problem.

AVGVSTVS FRIDERICVS ROMANORVM IMPERATOR SEMPER

Conclusions

Filler phase behavior in grafted PNCs depends on the critical stage of its fabrication process, in particular the balance between mixing intensity and grafting efficiency. If optimal mixing conditions are guaranteed, the initial NP pellets will break up into small aggregates, which will form larger agglomerates after mixing stops. If all other material properties are kept the same the final agglomerate size will be determined by the grafting details, i.e. the properties of the polymer brush that forms onto the NP aggregate surface. In these conditions of quiescent assembly, interNP interactions are going to be the determining factor of the final filler morphology. We thus first focused our attention on the interactions developing between flat polymer brushes immersed in a polymeric matrix. For the most basic case, which is that of chemically identical grafted and free polymer chains of equal length, we developed a MD computational model and observed the existence of two regimes. At low grafting densities the brush is well wetted by the matrix polymer and repulsive interactions develop between overlapping brushes due to osmosis. Around a critical value ($\sigma \approx N^{-1/2}$) the matrix chains are gradually expelled from the brush as grafting density increases, marking the start of the autophobic dewetting regime. At that point the free chains will be forced to take on entropically unfavorable conformations as the two collapsed brushes are brought into contact, giving rise to depletion-like attractive forces. These brush-induced forces act cumulatively to the pre-existing NP dispersion and electrostatic interactions and it is from their sum that the final structure of the filler NPs emerges. The same methodology can be used to study in depth

alternative scenarios involving other important parameters such as the free to grafted chain length ratio. Of high interest is also the effect of curvature on the interbrush interactions, the reason being that many PNCs are fabricated with NPs whose size is comparable to that of the grafted coil, leading to a drastically different layout when compared to a flat brush of equal grafting density.

The initial hypothesis that filler structure is the sole result of the modified interparticle interactions due to the presence of grafted chains was tested through simulations of "Lennard-Jones-like" particles in an implicit solvent. By altering the attraction parameter of the interaction potential we obtained the various filler morphologies that have also been observed through TEM and SAXS experiments on industrial PNCs. This would not have been possible to achieve if the "simulation" NPs were not first organized into realistic small rigid aggregates, mimicking their state right after rigorous mixing with the matrix polymer. It is this inhomogeneous state of the post-mixing aggregates that allowed us to capture the filler structure with just a simple pairwise interparticle potential, unlike cases of lab-grown PNCs where NPs are dispersed at the individual level. In this state the growing clusters are very sensitive to the changes in the brush shape during particle adhesion, emphasizing the effects of asymmetric multi-body interactions and leading to orderly aggregate geometries.

In the opposite scenario where grafting is optimized, any post-mixing flocculation is suppressed and mixing becomes the determining stage. Stress measurements on the interface between grafted surfaces through means of MD simulations revealed an increased apparent interface viscosity at higher grafting densities. This serves as an indication that polymer grafting may also contribute in NP dispersion by facilitating the transmission of stresses and thus promote the breakup of aggregates during mixing, but the magnitude of the effect does not allow for any clear conclusions on the matter. Further work on this topic could include the study of sheared opposing brushes in significantly higher compressions or even the role of grafting in preventing surface contact during the approach of NPs in dynamic conditions, acting similar to the block copolymers used for the compatibilization of polymer blends that suppress the coalescence of the dispersed phase [131].

Bibliography

[1] Idrees Khan et al. "Polymer nanocomposites: an overview". en. In: *Smart Polymer Nanocomposites*. Elsevier, 2023, pp. 167–184. ISBN: 978-0-323-91611-0. DOI: 10.1016/B978-0-323-91611-0.00017-7. URL: https://linkinghub.elsevier.com/retrieve/pii/B9780323916110000177 (visited on 10/20/2025).

[2] S. Kangishwar et al. "A comprehensive review on polymer matrix composites: material selection, fabrication, and application". en. In: *Polymer Bulletin* 80.1 (Jan. 2023), pp. 47–87. ISSN: 0170-0839, 1436-2449. DOI: 10.1007/s00289-022-04087-4. URL: https://link.springer.com/10.1007/s00289-022-04087-4 (visited on 10/20/2025).

[3] Suschem. *Polymer Composites Circularity*. White Paper. 2018, p. 40. URL: https://baxcompany.com/wp-content/uploads/2025/02/Suschem_composites_circularity_pages.pdf (visited on 12/02/2025).

[4] Abdulrahman Adeiza Musa et al. "Nano-Enhanced Polymer Composite Materials: A Review of Current Advancements and Challenges". en. In: *Polymers* 17.7 (Mar. 2025), p. 893. ISSN: 2073-4360. DOI: 10.3390/polym17070893. URL: https://www.mdpi.com/2073-4360/17/7/893 (visited on 10/20/2025).

[5] Liangliang Qu et al. "Contribution of silica–rubber interactions on the viscoelastic behaviors of modified solution polymerized styrene butadiene rubbers (M-S-SBRs) filled with silica". en. In: *RSC Adv.* 4.109 (2014), pp. 64354–64363. ISSN: 2046-2069. DOI: 10.1039/C4RA09492A. URL: https://xlink.rsc.org/?DOI=C4RA09492A (visited on 10/20/2025).

[6] Udo Goerl et al. "Investigations into the Silica/Silane Reaction System". In: *Rubber Chemistry and Technology* 70.4 (Sept. 1997), pp. 608–623. ISSN: 1943-4804, 0035-9475. DOI: 10.5254/1.3538447. URL: https://rct.

kglmeridian.com/view/journals/rcat/70/4/article-p608.xml (visited on 10/20/2025).

[7] Stavros X. Drakopoulos et al. "Polymer nanocomposites: Interfacial properties and capacitive energy storage". en. In: *Progress in Polymer Science* 156 (Sept. 2024), p. 101870. ISSN: 00796700. DOI: 10.1016/j.progpolymsci.2024.101870. URL: https://linkinghub.elsevier.com/retrieve/pii/S007967002400087X (visited on 10/10/2025).

[8] Sanat K. Kumar et al. "Nanocomposites with Polymer Grafted Nanoparticles". en. In: *Macromolecules* 46.9 (May 2013), pp. 3199–3214. ISSN: 0024-9297, 1520-5835. DOI: 10.1021/ma4001385. URL: https://pubs.acs.org/doi/10.1021/ma4001385 (visited on 06/23/2023).

[9] Peter F. Green. "The structure of chain end-grafted nanoparticle/homopolymer nanocomposites". en. In: *Soft Matter* 7.18 (2011), p. 7914. ISSN: 1744-683X, 1744-6848. DOI: 10.1039/c1sm05076a. URL: https://xlink.rsc.org/?DOI=c1sm05076a (visited on 10/10/2025).

[10] Micaela Macchione, Catalina Biglione, and Miriam Strumia. "Design, Synthesis and Architectures of Hybrid Nanomaterials for Therapy and Diagnosis Applications". en. In: *Polymers* 10.5 (May 2018), p. 527. ISSN: 2073-4360. DOI: 10.3390/polym10050527. URL: https://www.mdpi.com/2073-4360/10/5/527 (visited on 10/20/2025).

[11] S. Alexander. "Adsorption of chain molecules with a polar head a scaling description". In: *Journal de Physique* 38.8 (1977), pp. 983–987. ISSN: 0302-0738. DOI: 10.1051/jphys:01977003808098300. URL: http://www.edpsciences.org/10.1051/jphys:01977003808098300 (visited on 10/03/2023).

[12] P. G. De Gennes. "Conformations of Polymers Attached to an Interface". en. In: *Macromolecules* 13.5 (Sept. 1980), pp. 1069–1075. ISSN: 0024-9297, 1520-5835. DOI: 10.1021/ma60077a009. URL: https://pubs.acs.org/doi/abs/10.1021/ma60077a009 (visited on 10/03/2023).

[13] Richard A. L. Jones and Randal W. Richards. *Polymers at Surfaces and Interfaces*. 1st ed. Cambridge University Press, Apr. 1999. ISBN: 978-0-521-47440-5 978-0-521-47965-3 978-0-511-62319-6. DOI: 10.1017/CBO9780511623196. URL: https://www.cambridge.org/core/product/identifier/9780511623196/type/book (visited on 10/16/2023).

[14] Georges. Hadziioannou et al. "Forces between surfaces of block copolymers adsorbed on mica". en. In: *Journal of the American Chemical Society* 108.11 (May 1986), pp. 2869–2876. ISSN: 0002-7863, 1520-5126. DOI: 10.1021/ja00271a014. URL: https://pubs.acs.org/doi/abs/10.1021/ja00271a014 (visited on 03/22/2024).

[15] Hillary J. Taunton et al. “Forces between surfaces bearing terminally anchored polymer chains in good solvents”. en. In: *Nature* 332.6166 (Apr. 1988), pp. 712–714. ISSN: 0028-0836, 1476-4687. DOI: 10.1038/332712a0. URL: https://www.nature.com/articles/332712a0 (visited on 10/30/2023).

[16] Hillary J. Taunton et al. “Interactions between surfaces bearing end-adsorbed chains in a good solvent”. en. In: *Macromolecules* 23.2 (Jan. 1990), pp. 571–580. ISSN: 0024-9297, 1520-5835. DOI: 10.1021/ma00204a033. URL: https://pubs.acs.org/doi/abs/10.1021/ma00204a033 (visited on 01/29/2024).

[17] P. Auroy, L. Auvray, and L. Léger. “Characterization of the brush regime for grafted polymer layers at the solid-liquid interface”. en. In: *Physical Review Letters* 66.6 (Feb. 1991). Publisher: American Physical Society (APS), pp. 719–722. ISSN: 0031-9007. DOI: 10.1103/physrevlett.66.719. URL: https://link.aps.org/doi/10.1103/PhysRevLett.66.719 (visited on 07/24/2025).

[18] P. G. De Gennes. “Stabilité de films polymère/solvant”. fr. In: *Comptes rendus de l’Académie des sciences. Série 2, Mécanique, physique, chimie, sciences de l’univers, sciences de la terre* 300 (1985), pp. 839–843.

[19] Sanjay Patel, Matthew Tirrell, and Georges Hadziioannou. “A simple model for forces between surfaces bearing grafted polymers applied to data on adsorbed block copolymers”. en. In: *Colloids and Surfaces* 31 (Jan. 1988), pp. 157–179. ISSN: 01666622. DOI: 10.1016/0166-6622(88)80191-4. URL: https://linkinghub.elsevier.com/retrieve/pii/0166662288801914 (visited on 03/22/2024).

[20] Lee R White. “On the deryaguin approximation for the interaction of macrobodies”. en. In: *Journal of Colloid and Interface Science* 95.1 (Sept. 1983), pp. 286–288. ISSN: 00219797. DOI: 10.1016/0021-9797(83)90103-0. URL: https://linkinghub.elsevier.com/retrieve/pii/0021979783901030 (visited on 02/14/2025).

[21] S. T. Milner, T. A. Witten, and M. E. Cates. “Theory of the grafted polymer brush”. en. In: *Macromolecules* 21.8 (Aug. 1988), pp. 2610–2619. ISSN: 0024-9297, 1520-5835. DOI: 10.1021/ma00186a051. URL: https://pubs.acs.org/doi/abs/10.1021/ma00186a051 (visited on 03/20/2024).

[22] Terence Cosgrove et al. “Neutron reflectivity studies of polymers adsorbed on mica from solution”. en. In: *Macromolecules* 24.1 (Jan. 1991). Publisher: American Chemical Society (ACS), pp. 94–98. ISSN: 0024-9297, 1520-5835. DOI: 10.1021/ma00001a015. URL: https://pubs.acs.org/doi/abs/10.1021/ma00001a015 (visited on 07/26/2025).

[23] J. B. Field et al. “Determination of end-adsorbed polymer density profiles by neutron reflectometry”. en. In: *Macromolecules* 25.1 (Jan. 1992). Publisher: American Chemical Society (ACS), pp. 434–439. ISSN: 0024-9297, 1520-5835. DOI: 10.1021/ma00027a067. URL: https://pubs.acs.org/doi/abs/10.1021/ma00027a067 (visited on 07/26/2025).

[24] P. Auroy, Y. Mir, and L. Auvray. “Local structure and density profile of polymer brushes”. en. In: *Physical Review Letters* 69.1 (July 1992). Publisher: American Physical Society (APS), pp. 93–95. ISSN: 0031-9007. DOI: 10.1103/physrevlett.69.93. URL: https://link.aps.org/doi/10.1103/PhysRevLett.69.93 (visited on 07/26/2025).

[25] C. M. Wijmans, J. M. H. M. Scheutjens, and E. B. Zhulina. “Self-consistent field theories for polymer brushes: lattice calculations and an asymptotic analytical description”. en. In: *Macromolecules* 25.10 (May 1992). Publisher: American Chemical Society (ACS), pp. 2657–2665. ISSN: 0024-9297, 1520-5835. DOI: 10.1021/ma00036a016. URL: https://pubs.acs.org/doi/abs/10.1021/ma00036a016 (visited on 07/26/2025).

[26] Amitabha Chakrabarti and Raul Toral. “Density profile of terminally anchored polymer chains: a Monte Carlo study”. en. In: *Macromolecules* 23.7 (Apr. 1990), pp. 2016–2021. ISSN: 0024-9297, 1520-5835. DOI: 10.1021/ma00209a023. URL: https://pubs.acs.org/doi/abs/10.1021/ma00209a023 (visited on 07/28/2025).

[27] Michael Murat and Gary S. Grest. “Structure of a grafted polymer brush: a molecular dynamics simulation”. en. In: *Macromolecules* 22.10 (Oct. 1989), pp. 4054–4059. ISSN: 0024-9297, 1520-5835. DOI: 10.1021/ma00200a041. URL: https://pubs.acs.org/doi/abs/10.1021/ma00200a041 (visited on 09/12/2023).

[28] Michael Rubinstein and Ralph H. Colby. *Polymer physics*. Oxford ; New York: Oxford University Press, 2003. ISBN: 978-0-19-852059-7.

[29] S. T Milner. “Compressing Polymer “Brushes”: a Quantitative Comparison of Theory and Experiment”. In: *Europhysics Letters (EPL)* 7.8 (Dec. 1988), pp. 695–699. ISSN: 0295-5075, 1286-4854. DOI: 10.1209/0295-5075/7/8/005. URL: https://iopscience.iop.org/article/10.1209/0295-5075/7/8/005 (visited on 03/22/2024).

[30] Hiroshi Watanabe and Matthew Tirrell. “Measurement of forces in symmetric and asymmetric interactions between diblock copolymer layers adsorbed on mica”. en. In: *Macromolecules* 26.24 (Nov. 1993), pp. 6455–6466. ISSN: 0024-9297, 1520-5835. DOI: 10.1021/ma00076a023. URL: https://pubs.acs.org/doi/abs/10.1021/ma00076a023 (visited on 03/19/2024).

[31] Michael Murat and Gary S. Grest. “Interaction between grafted polymeric brushes: A molecular-dynamics study”. en. In: *Physical Review Letters* 63.10 (Sept. 1989), pp. 1074–1077. ISSN: 0031-9007. DOI: 10.1103/PhysRevLett.63.1074. URL: https://link.aps.org/doi/10.1103/PhysRevLett.63.1074 (visited on 10/30/2023).

[32] Ronald Dickman and Pearl E. Anderson. “Force between grafted polymer brushes”. en. In: *The Journal of Chemical Physics* 99.4 (Aug. 1993), pp. 3112–3118. ISSN: 0021-9606, 1089-7690. DOI: 10.1063/1.465164. URL: https://pubs.aip.org/jcp/article/99/4/3112/860515/Force-between-grafted-polymer-brushes (visited on 03/22/2024).

[33] Florent Goujon, Patrice Malfreyt, and Dominic J. Tildesley. “Dissipative Particle Dynamics Simulations in the Grand Canonical Ensemble: Applications to Polymer Brushes”. en. In: *ChemPhysChem* 5.4 (Apr. 2004), pp. 457–464. ISSN: 1439-4235, 1439-7641. DOI: 10.1002/cphc.200300901. URL: https://chemistry-europe.onlinelibrary.wiley.com/doi/10.1002/cphc.200300901 (visited on 03/20/2024).

[34] Ian G. Elliott, Tonya L. Kuhl, and Roland Faller. “A Molecular Dynamics Technique to Extract Forces in Soft Matter Systems Under Compression With Constant Solvent Chemical Potential”. en. In: *Journal of Chemical Theory and Computation* 8.3 (Mar. 2012), pp. 1072–1077. ISSN: 1549-9618, 1549-9626. DOI: 10.1021/ct2005984. URL: https://pubs.acs.org/doi/10.1021/ct2005984 (visited on 03/20/2024).

[35] Ian G. Elliott, Tonya L. Kuhl, and Roland Faller. “Compression of High Grafting Density Opposing Polymer Brushes Using Molecular Dynamics Simulations in Explicit Solvent”. en. In: *The Journal of Physical Chemistry B* 117.15 (Apr. 2013), pp. 4134–4141. ISSN: 1520-6106, 1520-5207. DOI: 10.1021/jp3118117. URL: https://pubs.acs.org/doi/10.1021/jp3118117 (visited on 03/19/2024).

[36] Suzanne M. Balko et al. “Polymer Brushes under High Load”. en. In: *PLoS ONE* 8.3 (Mar. 2013). Ed. by Yang Gan, e58392. ISSN: 1932-6203. DOI: 10.1371/journal.pone.0058392. URL: https://dx.plos.org/10.1371/journal.pone.0058392 (visited on 03/19/2024).

[37] T. Kreer and S.M. Balko. “Scaling Theory for Compressed Polymer-Brush Bilayers”. en. In: *ACS Macro Letters* 2.10 (Oct. 2013), pp. 944–947. ISSN: 2161-1653, 2161-1653. DOI: 10.1021/mz4004387. URL: https://pubs.acs.org/doi/10.1021/mz4004387 (visited on 06/23/2025).

[38] Cangyi Chen et al. “Excluded volume effects in compressed polymer brushes: A density functional theory”. en. In: *The Journal of Chemical Physics* 142.12 (Mar. 2015), p. 124904. ISSN: 0021-9606, 1089-7690. DOI: 10.1063/1.4916133. URL: https://pubs.aip.org/jcp/article/142/12/124904/901448/Excluded-volume-effects-in-compressed-polymer (visited on 06/23/2025).

[39] A. Karim et al. “Neutron Reflectivity Study of the Density Profile of a Model End-Grafted Polymer Brush: Influence of Solvent Quality”. en. In: *Physical Review Letters* 73.25 (Dec. 1994), pp. 3407–3410. ISSN: 0031-9007. DOI: 10.1103/PhysRevLett.73.3407. URL: https://link.aps.org/doi/10.1103/PhysRevLett.73.3407 (visited on 08/01/2025).

[40] E. B. Zhulina et al. “Coil-globule type transitions in polymers. 1. Collapse of layers of grafted polymer chains”. en. In: *Macromolecules* 24.1 (Jan. 1991), pp. 140–149. ISSN: 0024-9297, 1520-5835. DOI: 10.1021/ma00001a023. URL: https://pubs.acs.org/doi/abs/10.1021/ma00001a023 (visited on 08/01/2025).

[41] Pik-Yin Lai and Kurt Binder. “Structure and dynamics of polymer brushes near the Θ point: A Monte Carlo simulation”. en. In: *The Journal of Chemical Physics* 97.1 (July 1992), pp. 586–595. ISSN: 0021-9606, 1089-7690. DOI: 10.1063/1.463554. URL: https://pubs.aip.org/jcp/article/97/1/586/691777/Structure-and-dynamics-of-polymer-brushes-near-the (visited on 08/01/2025).

[42] Gary S. Grest and Michael Murat. “Structure of grafted polymeric brushes in solvents of varying quality: a molecular dynamics study”. en. In: *Macromolecules* 26.12 (June 1993), pp. 3108–3117. ISSN: 0024-9297, 1520-5835. DOI: 10.1021/ma00064a019. URL: https://pubs.acs.org/doi/abs/10.1021/ma00064a019 (visited on 08/01/2025).

[43] D. I. Dimitrov, A. Milchev, and K. Binder. “Polymer brushes in solvents of variable quality: Molecular dynamics simulations using explicit solvent”. en. In: *The Journal of Chemical Physics* 127.8 (Aug. 2007), p. 084905. ISSN: 0021-9606, 1089-7690. DOI: 10.1063/1.2768525. URL: https://pubs.aip.org/jcp/article/127/8/084905/919088/Polymer-brushes-in-solvents-of-variable-quality (visited on 04/24/2024).

[44] Richard A. Frazier et al. “High-Resolution Atomic Force Microscopy of Dextran Monolayer Hydration”. en. In: *Langmuir* 13.18 (Sept. 1997), pp. 4795–4798. ISSN: 0743-7463, 1520-5827. DOI: 10.1021/la970288e. URL: https://pubs.acs.org/doi/10.1021/la970288e (visited on 08/01/2025).

[45] Miguel Aubouy and Elie Raphaël. "Surface-tethered polymers in polymeric matrices". In: *Journal de Physique II* 3.4 (Apr. 1993), pp. 443–448. ISSN: 1155-4312, 1286-4870. DOI: 10.1051/jp2:1993142. URL: http://jp2.journaldephysique.org/10.1051/jp2:1993142 (visited on 12/05/2025).

[46] M. Aubouy et al. "End-Tethered Chains in Polymeric Matrixes". en. In: *Macromolecules* 28.8 (Apr. 1995), pp. 2979–2981. ISSN: 0024-9297, 1520-5835. DOI: 10.1021/ma00112a051. URL: https://pubs.acs.org/doi/abs/10.1021/ma00112a051 (visited on 10/26/2023).

[47] C. J. Clarke et al. "The Structure of Grafted Polystyrene Layers in a Range of Matrix Polymers". en. In: *Macromolecules* 28.6 (Mar. 1995), pp. 2042–2049. ISSN: 0024-9297, 1520-5835. DOI: 10.1021/ma00110a043. URL: https://pubs.acs.org/doi/abs/10.1021/ma00110a043 (visited on 08/07/2025).

[48] Kenneth R. Shull. "Theory of end-adsorbed polymer brushes in polymeric matrices". en. In: *The Journal of Chemical Physics* 94.8 (Apr. 1991), pp. 5723–5738. ISSN: 0021-9606, 1089-7690. DOI: 10.1063/1.460456. URL: https://pubs.aip.org/jcp/article/94/8/5723/441571/Theory-of-end-adsorbed-polymer-brushes-in (visited on 03/24/2024).

[49] Gary S. Grest. "Grafted polymer brushes in polymeric matrices". en. In: *The Journal of Chemical Physics* 105.13 (Oct. 1996), pp. 5532–5541. ISSN: 0021-9606, 1089-7690. DOI: 10.1063/1.472395. URL: https://pubs.aip.org/jcp/article/105/13/5532/478450/Grafted-polymer-brushes-in-polymeric-matrices (visited on 09/19/2023).

[50] Ryuichi Hasegawa, Yuji Aoki, and Masao Doi. "Optimum Graft Density for Dispersing Particles in Polymer Melts". en. In: *Macromolecules* 29.20 (Jan. 1996), pp. 6656–6662. ISSN: 0024-9297, 1520-5835. DOI: 10.1021/ma960365x. URL: https://pubs.acs.org/doi/10.1021/ma960365x (visited on 03/24/2024).

[51] Kurt Kremer and Gary S. Grest. "Dynamics of entangled linear polymer melts: A molecular-dynamics simulation". en. In: *The Journal of Chemical Physics* 92.8 (Apr. 1990), pp. 5057–5086. ISSN: 0021-9606, 1089-7690. DOI: 10.1063/1.458541. URL: https://pubs.aip.org/jcp/article/92/8/5057/220968/Dynamics-of-entangled-linear-polymer-melts-A (visited on 09/12/2023).

[52] Burkhard Dünweg and Wolfgang Paul. "BROWNIAN DYNAMICS SIMULATIONS WITHOUT GAUSSIAN RANDOM NUMBERS". en. In: *International Journal of Modern Physics C* 02.03 (Sept. 1991), pp. 817–827. ISSN: 0129-1831, 1793-6586. DOI: 10.1142/S0129183191001037. URL:

https://www.worldscientific.com/doi/abs/10.1142/S0129183191001037 (visited on 10/28/2025).

[53] Takeshi Aoyagi, Jun-ichi Takimoto, and Masao Doi. "Molecular dynamics study of polymer melt confined between walls". en. In: *The Journal of Chemical Physics* 115.1 (July 2001), pp. 552–559. ISSN: 0021-9606, 1089-7690. DOI: 10.1063/1.1377015. URL: https://pubs.aip.org/jcp/article/115/1/552/464723/Molecular-dynamics-study-of-polymer-melt-confined (visited on 02/26/2024).

[54] S. P. Obukhov and A. N. Semenov. "Long-Range Interactions in Polymer Melts: The Anti-Casimir Effect". en. In: *Physical Review Letters* 95.3 (July 2005), p. 038305. ISSN: 0031-9007, 1079-7114. DOI: 10.1103/PhysRevLett.95.038305. URL: https://link.aps.org/doi/10.1103/PhysRevLett.95.038305 (visited on 08/29/2025).

[55] David L. Green and Jan Mewis. "Connecting the Wetting and Rheological Behaviors of Poly(dimethylsiloxane)-Grafted Silica Spheres in Poly(dimethylsiloxane) Melts". en. In: *Langmuir* 22.23 (Nov. 2006), pp. 9546–9553. ISSN: 0743-7463, 1520-5827. DOI: 10.1021/la061136z. URL: https://pubs.acs.org/doi/10.1021/la061136z (visited on 10/02/2025).

[56] J. H. Maas et al. "Wetting of a Polymer Brush by a Chemically Identical Polymer Melt: Phase Diagram and Film Stability". en. In: *Langmuir* 18.23 (Nov. 2002), pp. 8871–8880. ISSN: 0743-7463, 1520-5827. DOI: 10.1021/la020430y. URL: https://pubs.acs.org/doi/10.1021/la020430y (visited on 10/22/2025).

[57] James M. Hart et al. "Spontaneous Nanoparticle Dispersal in Polybutadiene by Brush-Forming End-Functional Polymers". en. In: *Macromolecules* 49.4 (Feb. 2016), pp. 1434–1443. ISSN: 0024-9297, 1520-5835. DOI: 10.1021/acs.macromol.5b02318. URL: https://pubs.acs.org/doi/10.1021/acs.macromol.5b02318 (visited on 10/14/2025).

[58] Clement Koh, Gary S. Grest, and Sanat K. Kumar. "Assembly of Polymer-Grafted Nanoparticles in Polymer Matrices". en. In: *ACS Nano* 14.10 (Oct. 2020), pp. 13491–13499. ISSN: 1936-0851, 1936-086X. DOI: 10.1021/acsnano.0c05495. URL: https://pubs.acs.org/doi/10.1021/acsnano.0c05495 (visited on 10/24/2023).

[59] Qiang Lan, Lorraine F. Francis, and Frank S. Bates. "Silica nanoparticle dispersions in homopolymer versus block copolymer". en. In: *Journal of Polymer Science Part B: Polymer Physics* 45.16 (Aug. 2007), pp. 2284–2299. ISSN: 0887-6266, 1099-0488. DOI: 10.1002/polb.21251. URL: https://onlinelibrary.wiley.com/doi/10.1002/polb.21251 (visited on 10/10/2025).

[60] Chen Xu et al. “Dispersion of polymer-grafted magnetic nanoparticles in homopolymers and block copolymers”. en. In: *Polymer* 49.16 (July 2008), pp. 3568–3577. ISSN: 00323861. DOI: 10.1016/j.polymer.2008.05.040. URL: https://linkinghub.elsevier.com/retrieve/pii/S0032386108004874 (visited on 09/30/2025).

[61] Luciana Meli, Abraham Arceo, and Peter F. Green. “Control of the entropic interactions and phase behavior of athermal nanoparticle/homopolymer thin film mixtures”. en. In: *Soft Matter* 5.3 (2009), pp. 533–537. ISSN: 1744-683X, 1744-6848. DOI: 10.1039/B814714K. URL: https://xlink.rsc.org/?DOI=B814714K (visited on 10/14/2025).

[62] Chloé Chevigny et al. “Polymer-Grafted-Nanoparticles Nanocomposites: Dispersion, Grafted Chain Conformation, and Rheological Behavior”. en. In: *Macromolecules* 44.1 (Jan. 2011), pp. 122–133. ISSN: 0024-9297, 1520-5835. DOI: 10.1021/ma101332s. URL: https://pubs.acs.org/doi/10.1021/ma101332s (visited on 05/13/2025).

[63] Anne-Sophie Robbes et al. “Polymer-Grafted Magnetic Nanoparticles in Nanocomposites: Curvature Effects, Conformation of Grafted Chain, and Bimodal Nanotriggering of Filler Organization by Combination of Chain Grafting and Magnetic Field”. en. In: *Macromolecules* 45.22 (Nov. 2012), pp. 9220–9231. ISSN: 0024-9297, 1520-5835. DOI: 10.1021/ma301927e. URL: https://pubs.acs.org/doi/10.1021/ma301927e (visited on 10/10/2025).

[64] Samanvaya Srivastava, Praveen Agarwal, and Lynden A. Archer. “Tethered Nanoparticle–Polymer Composites: Phase Stability and Curvature”. en. In: *Langmuir* 28.15 (Apr. 2012), pp. 6276–6281. ISSN: 0743-7463, 1520-5827. DOI: 10.1021/la2049234. URL: https://pubs.acs.org/doi/10.1021/la2049234 (visited on 11/03/2023).

[65] Daniel Sunday, Jan Ilavsky, and David L. Green. “A Phase Diagram for Polymer-Grafted Nanoparticles in Homopolymer Matrices”. en. In: *Macromolecules* 45.9 (May 2012), pp. 4007–4011. ISSN: 0024-9297, 1520-5835. DOI: 10.1021/ma300438g. URL: https://pubs.acs.org/doi/10.1021/ma300438g (visited on 10/10/2025).

[66] Shane E. Harton and Sanat K. Kumar. “Mean-field theoretical analysis of brush-coated nanoparticle dispersion in polymer matrices”. en. In: *Journal of Polymer Science Part B: Polymer Physics* 46.4 (Feb. 2008), pp. 351–358. ISSN: 0887-6266, 1099-0488. DOI: 10.1002/polb.21346. URL: https://onlinelibrary.wiley.com/doi/10.1002/polb.21346 (visited on 10/30/2023).

[67] Dmitry Bedrov, Grant D. Smith, and James S. Smith. "Matrix-induced nanoparticle interactions in a polymer melt: A molecular dynamics simulation study". en. In: *The Journal of Chemical Physics* 119.19 (Nov. 2003), pp. 10438–10447. ISSN: 0021-9606, 1089-7690. DOI: 10.1063/1.1615965. URL: https://pubs.aip.org/jcp/article/119/19/10438/965103/Matrix-induced-nanoparticle-interactions-in-a (visited on 10/10/2025).

[68] Grant D. Smith and Dmitry Bedrov. "Dispersing Nanoparticles in a Polymer Matrix: Are Long, Dense Polymer Tethers Really Necessary?" en. In: *Langmuir* 25.19 (Oct. 2009), pp. 11239–11243. ISSN: 0743-7463, 1520-5827. DOI: 10.1021/la902329v. URL: https://pubs.acs.org/doi/10.1021/la902329v (visited on 07/05/2023).

[69] Dong Meng et al. "Effective interactions between grafted nanoparticles in a polymer matrix". en. In: *Soft Matter* 8.18 (2012), p. 5002. ISSN: 1744-683X, 1744-6848. DOI: 10.1039/c2sm07395a. URL: https://xlink.rsc.org/?DOI=c2sm07395a (visited on 10/02/2025).

[70] Gianmarco Munaò et al. "Molecular structure and multi-body potential of mean force in silica-polystyrene nanocomposites". en. In: *Nanoscale* 10.46 (2018), pp. 21656–21670. ISSN: 2040-3364, 2040-3372. DOI: 10.1039/C8NR05135F. URL: https://xlink.rsc.org/?DOI=C8NR05135F (visited on 10/16/2025).

[71] Arthi Jayaraman and Kenneth S. Schweizer. "Effective Interactions and Self-Assembly of Hybrid Polymer Grafted Nanoparticles in a Homopolymer Matrix". en. In: *Macromolecules* 42.21 (Nov. 2009), pp. 8423–8434. ISSN: 0024-9297, 1520-5835. DOI: 10.1021/ma901631x. URL: https://pubs.acs.org/doi/10.1021/ma901631x (visited on 10/10/2025).

[72] David M. Trombly and Venkat Ganesan. "Curvature effects upon interactions of polymer-grafted nanoparticles in chemically identical polymer matrices". en. In: *The Journal of Chemical Physics* 133.15 (Oct. 2010), p. 154904. ISSN: 0021-9606, 1089-7690. DOI: 10.1063/1.3493330. URL: https://pubs.aip.org/jcp/article/133/15/154904/190322/Curvature-effects-upon-interactions-of-polymer (visited on 10/02/2025).

[73] Pinar Akcora et al. "Anisotropic self-assembly of spherical polymer-grafted nanoparticles". en. In: *Nature Materials* 8.4 (Apr. 2009), pp. 354–359. ISSN: 1476-1122, 1476-4660. DOI: 10.1038/nmat2404. URL: https://www.nature.com/articles/nmat2404 (visited on 06/24/2023).

[74] Victor Pryamtisyn et al. “Modeling the anisotropic self-assembly of spherical polymer-grafted nanoparticles”. en. In: *The Journal of Chemical Physics* 131.22 (Dec. 2009), p. 221102. ISSN: 0021-9606, 1089-7690. DOI: 10.1063/1.3267729. URL: https://pubs.aip.org/jcp/article/131/22/221102/949496/Modeling-the-anisotropic-self-assembly-of (visited on 10/02/2025).

[75] Yung-Lung Lin et al. “Self-Assembled Superstructures of Polymer-Grafted Nanoparticles: Effects of Particle Shape and Matrix Polymer”. en. In: *The Journal of Physical Chemistry C* 115.13 (Apr. 2011), pp. 5566–5577. ISSN: 1932-7447, 1932-7455. DOI: 10.1021/jp112088x. URL: https://pubs.acs.org/doi/10.1021/jp112088x (visited on 10/10/2025).

[76] Rabi Inoubli et al. “Nanostructure and Mechanical Properties of Polybutylacrylate Filled with Grafted Silica Particles”. en. In: *Langmuir* 22.15 (July 2006), pp. 6683–6689. ISSN: 0743-7463, 1520-5827. DOI: 10.1021/la0607003. URL: https://pubs.acs.org/doi/10.1021/la0607003 (visited on 10/10/2025).

[77] Tsung-Yeh Tang and Gaurav Arya. “Anisotropic Three-Particle Interactions between Spherical Polymer-Grafted Nanoparticles in a Polymer Matrix”. en. In: *Macromolecules* 50.3 (Feb. 2017), pp. 1167–1183. ISSN: 0024-9297, 1520-5835. DOI: 10.1021/acs.macromol.6b01936. URL: https://pubs.acs.org/doi/10.1021/acs.macromol.6b01936 (visited on 10/25/2025).

[78] Guilhem P. Baeza et al. “Multiscale Filler Structure in Simplified Industrial Nanocomposite Silica/SBR Systems Studied by SAXS and TEM”. en. In: *Macromolecules* 46.1 (Jan. 2013), pp. 317–329. ISSN: 0024-9297, 1520-5835. DOI: 10.1021/ma302248p. URL: https://pubs.acs.org/doi/10.1021/ma302248p (visited on 06/23/2023).

[79] Guilhem P. Baeza et al. “Effect of Grafting on Rheology and Structure of a Simplified Industrial Nanocomposite Silica/SBR”. en. In: *Macromolecules* 46.16 (Aug. 2013), pp. 6621–6633. ISSN: 0024-9297, 1520-5835. DOI: 10.1021/ma401016d. URL: https://pubs.acs.org/doi/10.1021/ma401016d (visited on 06/23/2023).

[80] Guilhem P. Baeza et al. “Mechanism of aggregate formation in simplified industrial silica styrene–butadiene nanocomposites: effect of chain mass and grafting on rheology and structure”. en. In: *Soft Matter* 10.35 (2014), pp. 6686–6695. ISSN: 1744-683X, 1744-6848. DOI: 10.1039/C4SM01095G. URL: http://xlink.rsc.org/?DOI=C4SM01095G (visited on 06/23/2023).

[81] Guilhem P. Baeza et al. “Studying Twin Samples Provides Evidence for a Unique Structure-Determining Parameter in Simplifed Industrial Nanocomposites”. en. In: *ACS Macro Letters* 3.5 (May 2014), pp. 448–452. ISSN: 2161-1653, 2161-1653. DOI: 10.1021/mz500137e. URL: https://pubs.acs.org/doi/10.1021/mz500137e (visited on 10/14/2025).

[82] Yang Wang et al. “Implicit Medium Model for Fractal Aggregate Polymer Nanocomposites: Linear Viscoelastic Properties”. en. In: *Macromolecules* 52.5 (Mar. 2019), pp. 2021–2032. ISSN: 0024-9297, 1520-5835. DOI: 10.1021/acs.macromol.8b02455. URL: https://pubs.acs.org/doi/10.1021/acs.macromol.8b02455 (visited on 06/23/2023).

[83] H.C. Hamaker. “The London—van der Waals attraction between spherical particles”. en. In: *Physica* 4.10 (Oct. 1937), pp. 1058–1072. ISSN: 00318914. DOI: 10.1016/S0031-8914(37)80203-7. URL: https://linkinghub.elsevier.com/retrieve/pii/S0031891437802037 (visited on 06/26/2023).

[84] T. A. Witten and L. M. Sander. “Diffusion-Limited Aggregation, a Kinetic Critical Phenomenon”. en. In: *Physical Review Letters* 47.19 (Nov. 1981), pp. 1400–1403. ISSN: 0031-9007. DOI: 10.1103/PhysRevLett.47.1400. URL: https://link.aps.org/doi/10.1103/PhysRevLett.47.1400 (visited on 06/23/2023).

[85] Murray Eden. “A two-dimensional growth process”. In: *Proceedings of the Fourth Berkeley Symposium on Mathematical Statistics and Probability, Volume 4: Contributions to Biology and Problems of Medicine*. Ed. by Jerzy Neyman. Vol. 4.4. 1961, pp. 223–239.

[86] E. Guesnet et al. “A growth model for the generation of particle aggregates with tunable fractal dimension”. en. In: *Physica A: Statistical Mechanics and its Applications* 513 (Jan. 2019), pp. 63–73. ISSN: 03784371. DOI: 10.1016/j.physa.2018.07.061. URL: https://linkinghub.elsevier.com/retrieve/pii/S0378437118309336 (visited on 06/23/2023).

[87] Belynda Benane et al. “Multiscale structure of super insulation nanofumed silicas studied by SAXS, tomography and porosimetry”. en. In: *Acta Materialia* 168 (Apr. 2019), pp. 401–410. ISSN: 13596454. DOI: 10.1016/j.actamat.2019.02.024. URL: https://linkinghub.elsevier.com/retrieve/pii/S1359645419301107 (visited on 12/07/2025).

[88] Tiong-Seng Tay and Walter Whiteley. “Generating Isostatic Frameworks”. In: *Structural Topology* 11 (1985).

[89] Kai Zhang. *On the Concept of Static Structure Factor*. Version Number: 2. 2016. DOI: 10.48550/ARXIV.1606.03610. URL: https://arxiv.org/abs/1606.03610 (visited on 10/28/2025).

[90] Andre Guinier and Gerard Fournet. *Small-Angle Scattering of X-Rays*. English. New York: John Wiley & Sons, 1955. ISBN: 978-0-598-66993-3.

[91] Guilhem P. Baeza. *Personal Communication*. Nov. 2025.

[92] Yilong Zhou et al. "Many-body potential for simulating the self-assembly of polymer-grafted nanoparticles in a polymer matrix". en. In: *npj Computational Materials* 9.1 (Dec. 2023), p. 224. ISSN: 2057-3960. DOI: 10.1038/s41524-023-01166-6. URL: https://www.nature.com/articles/s41524-023-01166-6 (visited on 10/09/2025).

[93] Chigusa Yamada et al. "Influence of functionalized S–SBR on silica–filled rubber compound properties". en. In: *Functional Composite Materials* 3.1 (Oct. 2022), p. 6. ISSN: 2522-5774. DOI: 10.1186/s42252-022-00034-8. URL: https://functionalcompositematerials.springeropen.com/articles/10.1186/s42252-022-00034-8 (visited on 10/28/2025).

[94] Jean Louis Barrat. "A possible mechanism for swelling of polymer brushes under shear". en. In: *Macromolecules* 25.2 (Jan. 1992), pp. 832–834. ISSN: 0024-9297, 1520-5835. DOI: 10.1021/ma00028a050. URL: https://pubs.acs.org/doi/abs/10.1021/ma00028a050 (visited on 09/04/2025).

[95] V. Kumaran. "Hydrodynamic interactions in flow past grafted polymers". en. In: *Macromolecules* 26.10 (May 1993), pp. 2464–2469. ISSN: 0024-9297, 1520-5835. DOI: 10.1021/ma00062a011. URL: https://pubs.acs.org/doi/abs/10.1021/ma00062a011 (visited on 09/04/2025).

[96] M. Aubouy, J.L Harden, and M. E. Cates. "Shear-Induced Deformation and Desorption of Grafted Polymer Layers". In: *Journal de Physique II* 6.7 (July 1996), pp. 969–984. ISSN: 1155-4312, 1286-4870. DOI: 10.1051/jp2:1996111. URL: http://www.edpsciences.org/10.1051/jp2:1996111 (visited on 09/04/2025).

[97] Y Rabin and S Alexander. "Stretching of Grafted Polymer Layers". In: *Europhysics Letters (EPL)* 13.1 (Sept. 1990), pp. 49–54. ISSN: 0295-5075, 1286-4854. DOI: 10.1209/0295-5075/13/1/009. URL: https://iopscience.iop.org/article/10.1209/0295-5075/13/1/009 (visited on 07/25/2024).

[98] Jacob Klein, Dvora Perahia, and Sharon Warburg. "Forces between polymer-bearing surfaces undergoing shear". en. In: *Nature* 352.6331 (July 1991), pp. 143–145. ISSN: 0028-0836, 1476-4687. DOI: 10.1038/352143a0. URL: https://www.nature.com/articles/352143a0 (visited on 07/09/2024).

[99] Pik-Yin Lai and Kurt Binder. "Grafted polymer layers under shear: A Monte Carlo simulation". en. In: *The Journal of Chemical Physics* 98.3 (Feb. 1993), pp. 2366–2375. ISSN: 0021-9606, 1089-7690. DOI: 10.1063/1.464164. URL: https://pubs.aip.org/jcp/article/98/3/2366/

662836/Grafted-polymer-layers-under-shear-A-Monte-Carlo (visited on 09/04/2025).

[100] Pik-Yin Lai and Chee-Yuen Lai. "Polymer brush under strong shear". en. In: *Physical Review E* 54.6 (Dec. 1996), pp. 6958–6961. ISSN: 1063-651X, 1095-3787. DOI: 10.1103/PhysRevE.54.6958. URL: https://link.aps.org/doi/10.1103/PhysRevE.54.6958 (visited on 09/04/2025).

[101] Ling Miao, Hong Guo, and Martin J. Zuckermann. "Conformation of Polymer Brushes under Shear: Chain Tilting and Stretching". en. In: *Macromolecules* 29.6 (Jan. 1996), pp. 2289–2297. ISSN: 0024-9297, 1520-5835. DOI: 10.1021/ma951071z. URL: https://pubs.acs.org/doi/10.1021/ma951071z (visited on 09/05/2025).

[102] Igor M. Neelov, Oleg V. Borisov, and Kurt Binder. "Stochastic dynamics simulation of grafted polymer brushes under shear deformation". en. In: *Macromolecular Theory and Simulations* 7.1 (Jan. 1998), pp. 141–156. ISSN: 1022-1344, 1521-3919. DOI: 10.1002/(SICI)1521-3919(19980101)7:1<141::AID-MATS141>3.0.CO;2-5. URL: https://onlinelibrary.wiley.com/doi/10.1002/(SICI)1521-3919(19980101)7:1%3C141::AID-MATS141%3E3.0.CO;2-5 (visited on 09/05/2025).

[103] Patrick S. Doyle, Eric S. G. Shaqfeh, and Alice P. Gast. "Rheology of Polymer Brushes: A Brownian Dynamics Study". en. In: *Macromolecules* 31.16 (Aug. 1998), pp. 5474–5486. ISSN: 0024-9297, 1520-5835. DOI: 10.1021/ma970821x. URL: https://pubs.acs.org/doi/10.1021/ma970821x (visited on 07/25/2024).

[104] Marina G. Saphiannikova, Victor A. Pryamitsyn, and Terence Cosgrove. "Self-Consistent Brownian Dynamics Simulation of Polymer Brushes under Shear". en. In: *Macromolecules* 31.19 (Sept. 1998), pp. 6662–6668. ISSN: 0024-9297, 1520-5835. DOI: 10.1021/ma971808f. URL: https://pubs.acs.org/doi/10.1021/ma971808f (visited on 09/18/2025).

[105] G. H. Peters and D. J. Tildesley. "Computer simulation of the rheology of grafted chains under shear". en. In: *Physical Review E* 52.2 (Aug. 1995), pp. 1882–1890. ISSN: 1063-651X, 1095-3787. DOI: 10.1103/PhysRevE.52.1882. URL: https://link.aps.org/doi/10.1103/PhysRevE.52.1882 (visited on 09/05/2025).

[106] Gary S. Grest. "Polymer Brushes in Strong Shear Flow". en. In: *MRS Proceedings* 464 (1996), p. 71. ISSN: 0272-9172, 1946-4274. DOI: 10.1557/PROC-464-71. URL: http://link.springer.com/10.1557/PROC-464-71 (visited on 09/04/2025).

[107] Richard M. Webber, John L. Anderson, and Myung S. Jhon. "Hydrodynamic studies of adsorbed diblock copolymers in porous membranes". en. In: *Macromolecules* 23.4 (Feb. 1990), pp. 1026–1034. ISSN: 0024-9297, 1520-5835. DOI: 10.1021/ma00206a020. URL: https://pubs.acs.org/doi/abs/10.1021/ma00206a020 (visited on 09/05/2025).

[108] D. Nguyen et al. "Investigation of Polymer Brushes and Adsorbed Layers under Shear". In: *Journal of Applied Crystallography* 30.5 (Oct. 1997), pp. 680–683. ISSN: 0021-8898. DOI: 10.1107/S0021889897001532. URL: https://scripts.iucr.org/cgi-bin/paper?S0021889897001532 (visited on 07/30/2024).

[109] S. M. Baker et al. "Structure of Polymer Brushes under Shear Flow in a Good Solvent". en. In: *Macromolecules* 33.4 (Feb. 2000), pp. 1120–1122. ISSN: 0024-9297, 1520-5835. DOI: 10.1021/ma991499o. URL: https://pubs.acs.org/doi/10.1021/ma991499o (visited on 07/28/2024).

[110] Sabrina Jahn, Jasmine Seror, and Jacob Klein. "Lubrication of Articular Cartilage". en. In: *Annual Review of Biomedical Engineering* 18.1 (July 2016), pp. 235–258. ISSN: 1523-9829, 1545-4274. DOI: 10.1146/annurev-bioeng-081514-123305. URL: https://www.annualreviews.org/doi/10.1146/annurev-bioeng-081514-123305 (visited on 09/08/2025).

[111] Jacob Klein et al. "Reduction of frictional forces between solid surfaces bearing polymer brushes". en. In: *Nature* 370.6491 (Aug. 1994), pp. 634–636. ISSN: 0028-0836, 1476-4687. DOI: 10.1038/370634a0. URL: https://www.nature.com/articles/370634a0 (visited on 07/25/2024).

[112] Phillip A. Schorr et al. "Shear Forces between Tethered Polymer Chains as a Function of Compression, Sliding Velocity, and Solvent Quality". en. In: *Macromolecules* 36.2 (Jan. 2003), pp. 389–398. ISSN: 0024-9297, 1520-5835. DOI: 10.1021/ma011207v. URL: https://pubs.acs.org/doi/10.1021/ma011207v (visited on 07/07/2024).

[113] F. Goujon, P. Malfreyt *, and D. J. Tildesley. "The compression of polymer brushes under shear: the friction coefficient as a function of compression, shear rate and the properties of the solvent". en. In: *Molecular Physics* 103.19 (Oct. 2005), pp. 2675–2285. ISSN: 0026-8976, 1362-3028. DOI: 10.1080/00268970500134706. URL: http://www.tandfonline.com/doi/abs/10.1080/00268970500134706 (visited on 07/07/2024).

[114] T. Kreer. "Polymer-brush lubrication: a review of recent theoretical advances". en. In: *Soft Matter* 12.15 (2016), pp. 3479–3501. ISSN: 1744-683X, 1744-6848. DOI: 10.1039/C5SM02919H. URL: http://xlink.rsc.org/?DOI=C5SM02919H (visited on 03/19/2024).

[115] J Klein. “Shear, Friction, and Lubrication Forces Between Polymer-Bearing Surfaces”. en. In: *Annual Review of Materials Science* 26.1 (Aug. 1996), pp. 581–612. ISSN: 0084-6600. DOI: 10.1146/annurev.ms.26.080196.003053. URL: https://www.annualreviews.org/doi/10.1146/annurev.ms.26.080196.003053 (visited on 07/06/2024).

[116] Alexander N. Semenov. “Rheology of Polymer Brushes: Rouse Model”. en. In: *Langmuir* 11.9 (Sept. 1995), pp. 3560–3564. ISSN: 0743-7463, 1520-5827. DOI: 10.1021/la00009a045. URL: https://pubs.acs.org/doi/abs/10.1021/la00009a045 (visited on 09/18/2025).

[117] A. Galuschko et al. “Frictional Forces between Strongly Compressed, Nonentangled Polymer Brushes: Molecular Dynamics Simulations and Scaling Theory”. en. In: *Langmuir* 26.9 (May 2010), pp. 6418–6429. ISSN: 0743-7463, 1520-5827. DOI: 10.1021/la904119c. URL: https://pubs.acs.org/doi/10.1021/la904119c (visited on 07/07/2024).

[118] L. Spirin et al. “Polymer-brush lubrication in the limit of strong compression”. en. In: *The European Physical Journal E* 33.4 (Dec. 2010), pp. 307–311. ISSN: 1292-8941, 1292-895X. DOI: 10.1140/epje/i2010-10674-3. URL: http://link.springer.com/10.1140/epje/i2010-10674-3 (visited on 07/07/2024).

[119] Parth Rakesh Desai and Siddhartha Das. “Lubrication in polymer-brush bilayers in the weak interpenetration regime: Molecular dynamics simulations and scaling theories”. en. In: *Physical Review E* 98.2 (Aug. 2018), p. 022503. ISSN: 2470-0045, 2470-0053. DOI: 10.1103/PhysRevE.98.022503. URL: https://link.aps.org/doi/10.1103/PhysRevE.98.022503 (visited on 09/09/2025).

[120] S. M. Kilbey, P. Schorr, and M. Tirrell. “Effect of Solvent Condition on the Dynamic Response of Polymer Brushes”. en. In: *MRS Proceedings* 543 (1998), p. 181. ISSN: 0272-9172, 1946-4274. DOI: 10.1557/PROC-543-181. URL: http://link.springer.com/10.1557/PROC-543-181 (visited on 09/07/2025).

[121] T. Kreer et al. “Frictional Drag Mechanisms between Polymer-Bearing Surfaces”. en. In: *Langmuir* 17.25 (Dec. 2001), pp. 7804–7813. ISSN: 0743-7463, 1520-5827. DOI: 10.1021/la010807k. URL: https://pubs.acs.org/doi/10.1021/la010807k (visited on 07/07/2024).

[122] Danial Irfachsyad, Dominic Tildesley, and Patrice Malfreyt. “Dissipative particle dynamics simulation of grafted polymer brushes under shear”. In: *Physical Chemistry Chemical Physics* 4.13 (June 2002), pp. 3008–3015. ISSN: 14639076, 14639084. DOI: 10.1039/b110738k. URL: https://xlink.rsc.org/?DOI=b110738k (visited on 07/07/2024).

[123] C. Pastorino et al. “Static and dynamic properties of the interface between a polymer brush and a melt of identical chains”. en. In: *The Journal of Chemical Physics* 124.6 (Feb. 2006), p. 064902. ISSN: 0021-9606, 1089-7690. DOI: 10.1063/1.2162883. URL: https://pubs.aip.org/jcp/article/124/6/064902/903991/Static-and-dynamic-properties-of-the-interface (visited on 07/04/2024).

[124] C. Pastorino, K. Binder, and M. Müller. “Coarse-Grained Description of a Brush-Melt Interface in Equilibrium and under Flow”. en. In: *Macromolecules* 42.1 (Jan. 2009), pp. 401–410. ISSN: 0024-9297, 1520-5835. DOI: 10.1021/ma8015757. URL: https://pubs.acs.org/doi/10.1021/ma8015757 (visited on 07/06/2024).

[125] L. Spirin, A. Galuschko, and T. Kreer. “Response to Shear Inversion of Polymer Brushes with Embedded Colloids”. en. In: *Macromolecules* 44.23 (Dec. 2011), pp. 9399–9410. ISSN: 0024-9297, 1520-5835. DOI: 10.1021/ma2014029. URL: https://pubs.acs.org/doi/10.1021/ma2014029 (visited on 09/14/2025).

[126] Torsten Kreer, Kurt Binder, and Martin H. Müser. “Friction between Polymer Brushes in Good Solvent Conditions: Steady-State Sliding versus Transient Behavior”. en. In: *Langmuir* 19.18 (Sept. 2003), pp. 7551–7559. ISSN: 0743-7463, 1520-5827. DOI: 10.1021/la030008x. URL: https://pubs.acs.org/doi/10.1021/la030008x (visited on 09/14/2025).

[127] Gary S. Grest. “Normal and Shear Forces Between Polymer Brushes”. en. In: *Polymers in Confined Environments*. Ed. by Akihiro Abe et al. Vol. 138. Series Title: Advances in Polymer Science. Berlin, Heidelberg: Springer Berlin Heidelberg, 1999, pp. 149–183. ISBN: 978-3-540-64266-4 978-3-540-69711-4. DOI: 10.1007/3-540-69711-X_4. URL: http://link.springer.com/10.1007/3-540-69711-X_4 (visited on 09/13/2023).

[128] Shichen Ji and Jiandong Ding. “Rheology of polymer brush under oscillatory shear flow studied by nonequilibrium Monte Carlo simulation”. en. In: *The Journal of Chemical Physics* 123.14 (Oct. 2005), p. 144904. ISSN: 0021-9606, 1089-7690. DOI: 10.1063/1.2018630. URL: https://pubs.aip.org/jcp/article/123/14/144904/905377/Rheology-of-polymer-brush-under-oscillatory-shear (visited on 07/09/2024).

[129] C. Pastorino et al. “Comparison of dissipative particle dynamics and Langevin thermostats for out-of-equilibrium simulations of polymeric systems”. en. In: *Physical Review E* 76.2 (Aug. 2007), p. 026706. ISSN: 1539-3755, 1550-2376. DOI: 10.1103/PhysRevE.76.026706. URL: https://link.aps.org/doi/10.1103/PhysRevE.76.026706 (visited on 08/25/2025).

[130] Véronique Collin, Innocent Boudimbou, and Edith Peuvrel-Disdier. "New insights in dispersion mechanisms of carbon black in a polymer matrix under shear by rheo-optics". en. In: *Journal of Applied Polymer Science* 127.3 (Feb. 2013), pp. 2121–2131. ISSN: 0021-8995, 1097-4628. DOI: 10.1002/app.37769. URL: https://onlinelibrary.wiley.com/doi/10.1002/app.37769 (visited on 12/08/2025).

[131] Scott T. Milner and Haowen Xi. "How copolymers promote mixing of immiscible homopolymers". en. In: *Journal of Rheology* 40.4 (July 1996), pp. 663–687. ISSN: 0148-6055, 1520-8516. DOI: 10.1122/1.550731. URL: https://pubs.aip.org/sor/jor/article/40/4/663-687/239000 (visited on 03/16/2025).